Hydrodynamic Study of a Suction Stabilized Float (SSF)

by

Susheelkumar Cherangara Subramanian

A Thesis Presented in Partial Fulfillment
Of the Requirements for the Degree
Master of Science

Approved August 2014 by the
Graduate Supervisory Committee:

Sangram Redkar, Chair
Bradley Rogers
John Rajadas

ARIZONA STATE UNIVERSITY

December 2014

ABSTRACT

In this work, the hydrodynamics of Suction Stabilization is studied. Suction stabilization was found to stabilize floating platforms/floats in a much better way as compared to the conventional methods. This was achieved by an effective increment in the metacentric height due to the Inverse Slack Tank (IST) effect. The study involves the analysis of the existing designs and optimizing its performance. This research investigates the stability of such floats and the hydrodynamic forces acting on the same for offshore applications, such as wind turbines. A simple mathematical model for the condition of parametric resonance is developed and the results are verified, both analytically and experimentally.

ACKNOWLEDGEMENTS

I sincerely thank my advisor, Professor Sangram Redkar, for providing me an opportunity to work with him. And also for his incessant support and help in each and every mode of my project work. I would have never completed this work, without his help. He has not only helped me in my project, but guided my coursework in the best possible way.

I would like to thank Mr. James Montgomery, to support financially and with all other requirements for my research work and also for believing in me that I could contribute to his idea. I would also like to thank Professor Bradley Rogers and Professor John Rajadas for taking some time from their busy schedule to be a part of my supervisory committee. I would like to thank Professor Thomas Schildgen for his efforts to help me present my work in a suitable format.

I would like to thank the instrument shop supervisor, Mr. Osama Jameel, for his persistent help in conducting my experiments and allowing me to use the facilities as per my convenience. I would also like to thank Alvaro Vargas Clara, for his continuous efforts in strengthening my software knowledge required for my research work. I would also like to thank Govind Goyal, for his moral support and helping me present my thesis work in a timely manner.

Finally I would like to thank all my friends and family for all their help and support.

TABLE OF CONTENTS

CHAPTER Page

APPENDIX Page

LIST OF FIGURES

Figure Page

Figure Page

Figure Page

Figure Page

LIST OF TABLES

Table Page

Chapter 1
INTRODUCTION

Need of the Project

In the present scenario of energy crisis, renewable sources of energy are preferred to the conventional ones. Among them, wind is the most prominent source. It is abundantly available in the far off coast, where the water depth is greater than 30 meters. Current technologies, based on fixed bottom, are limited to water depths of 20 m. But as per the advancement in technology, studies in wind turbines on floating structure for greater water depth are under development. Such floating structures need to have sufficient buoyancy and capability to resist the hydrodynamic forces, aerodynamic forces and also the dynamic forces due to rotating mass.

Significance of the Project

The current technologies in the field of offshore wind turbines platforms have a fixed base to the seabed, so they have a limitation of water depth for installation. The other developing technologies, with a floating base, are complicated in design and also difficult to install in offshore. This research has led to the development of a very simple, efficient and economical design for a floating base, using suction stabilization, for offshore wind turbines.

A Suction-Stabilized Floating platform, or Suction-Stabilized Float, is one such option that may prove well suited for offshore wind applications. A SSF is designed with an internal void to trap water above the water plane. This trapped water acts as ballast with a moving center of gravity that acts further from the center of floatation with

increased roll angle. This ballast will increase the restoring force of the float and aid in the resistance of roll and pitch motions (Montomery, 2011), (Redkar, 2012)

Statement of Problem

This research deals with the design and development of a floating structure, using suction stabilization. The project aims at formulating a simple mathematical model representing the hydrodynamic forces acting on the structure. The study also involves defining the limiting operating conditions. This includes defining the condition of parametric roll resonance. And verify the results experimentally, by testing the same using a scaled model.

Limitations of the Study

The condition of offshore can be replicated only to some extent. The conditions of the sea vary to a large extent. Moreover the natural forces exerted by the sea waves also change as per the climatic conditions. So the natural forces exerted are approximated on the scaled model for the study. So the response of the wind turbine to the natural forces in offshore are predicted using the response observed on the scaled model, during the experiment.

Definition of Terms

The following terms are used in the report:-

Suction Stabilized Float (SSF): The SSF is a float that has a buoyant portion and a chamber portion that traps liquid within an internal volume above the interface, or waterline, of the surrounding fluid (Montomery, 2011).

Roll motion: When a ship is heeled to a certain angle, the hydrostatic restoring moment acts in the opposite direction of heeling and tends to return the ship back to the stable upright position. But due to inertia, the ship does not stop heeling at the instant when the equilibrium angle is reached but continues to roll to at a progressively slower velocity until a maximum roll angle is reached. Again the excess restoring moment in the opposite direction causes the ship to come back to the stable position. Once upright, inertia causes the ship to continue to roll. As before, the restoring moment works against further motion and it stops at some roll angle (ABS, 2004). This continuous tilting of ship is known as roll motion of the ship. The period of the oscillations of the roll motion is the natural roll period of the ship.

Parametric Roll Resonance: Parametric roll resonance is defined as the amplification of roll motion is head or following seas. This occurs when the ships wave encounter frequency is approximately twice the natural roll frequency of the ship, and the ship's damping is insufficient to dissipate parametric roll energy resulting in a resonant condition (ABS, 2004).

Metacenter: The metacenter is the intersection of the line of action of the buoyant force when the ship is upright and the line of action of the buoyant force when the ship heels to a certain angle (Biran, 2003).

Metacentric Height: Metacentric height is the vertical distance between the center of gravity of the ship and the metacenter.

Righting Lever/Righting Arm: The horizontal distance between the center of buoyancy and center of gravity of the ship is called righting lever (Biran, 2003).

Restoring Torque/Righting Moment: The righting moment is defined as the product of the righting lever and the weight of the ship (Biran, 2003).

Inverse Slack Tank (IST) effect: The internal volume, when not enclosed on all four sides, inside a floating platform or a ship is known as a slack tank. This slack-tank results in lowering the metacentric height through a phenomena known as the 'free surface effect' (Biran, 2003, pp. 137-142). However, in the case of the SSF, the internal tank does not open to air but rather opens to the submerging fluid. The result of this is that the internal volume acts as an inverse slack tank (IST) and raises the metacentric height rather than lower it (Redkar, 2012).

Summary

The study deals with design and development of a floating structure for offshore wind turbine applications, which works on the concept of suction stabilization. The research also involves the study of the hydrodynamic forces acting on the same and also create a mathematical model for a suction stabilized float platform with the goal of determining the stability criteria, narrowing down the factors that increase or decrease stability, and suggesting methods to increase stability.

The thesis report proceeds in the following manner:-

- The introduction of the project is described in Chapter 1, where the need and significance of the project is explained along with defining various terminology used in the report.

- The current technologies pertaining to the field of offshore platforms, suction stabilization and parametric resonance is described in detail in Chapter 2. The basics of ship stability are explained in this section.
- The various mathematical concepts utilized for the determining the stability of ships and how they are related to SSFs are explained in detail in Chapter 3. The equations utilized in the following sections are also derived in this section.
- The mathematical models utilized for defining the behavior of the SSF and also the condition of parametric roll resonance is explained and equations are derived in Chapter 4.
- The dynamics of offshore wind turbines with application of SSF as its base platform and the equations are derived and explained in Chapter 5.
- The experimental data and results obtained are shown in Chapter 6.
- The thesis report is concluded in Chapter 7 along with discussions about various applications of SSF and also suggestions for future work.

Chapter 2
LITERATURE REVIEW

Though the concept of offshore floating wind turbines was introduced by Professor William Heronemus in 1972, it was not commercialized until 1990's (Butterfield S. J. J., 2007). The earlier technologies were based on a fixed bottom designs. But there was a limitation of water depth of 20 meters, in which such wind turbines could be installed. This limitation was mainly due to the economic infeasibility of the fixed bottom designs for water depth greater than 20 meters. But resources of wind, for more than 1TW power is estimated in the far off coast of United States, at water depth greater than 30 meters (Butterfield S. J. J., 2006)

Therefore deployment of wind turbines on floating platforms, provides the ultimate solution for greater water depths. A platform can float on the sea water due to the buoyant force exerted on it, by the sea (Cheung, 2000). But in case of a floating wind turbine, it is also required to resist the hydrodynamic forces, influencing the heave, pitch and roll motions, exerted by the sea waves. It also needs to resist the aerodynamic forces, exerted on the blades of the wind turbine due to the high velocity of wind and also the dynamic forces due to the functioning of the wind turbines (Butterfield S. J. J., 2007).

Ship Coordinates

A ship can be considered as a rigid body, experiencing similar wave forces as that of a floating platform. The kinematics of a ship can be expressed in its 6 degrees of freedom. This include 3 types of displacement motions as heave, sway and surge. And also 3 angular motions as yaw, pitch and roll, as shown in Figure 1 (R.A. Ibrahim, 2009).

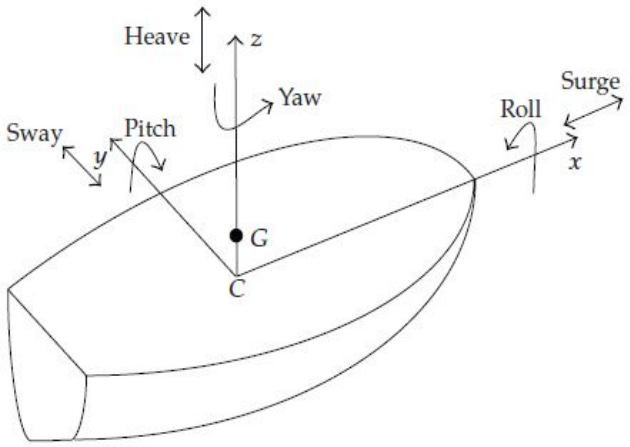

Figure 1. Ship Coordinates (R.A. Ibrahim, 2009)

Classification

In general floating platforms can be classified as: ballast, buoyancy, and mooring lines, as shown in Figure 2. Though the platform can be stabilized as per the above classification, they all have their own drawbacks (Butterfield S. J. J., 2007).

The most common among them was using mooring lines, also known as Tension Leg Platform (TLP). But when the platform is located at regions with greater water depth, the use of mooring lines was found to be expensive and also difficult for onsite installation (Butterfield S. J. J., 2007).

The other type of stabilizing platform is the Ballast type floating platform, wherein a ballast tank or ballast weight in suspended beneath the platform to resist the roll motion and improve its stability. They are less expensive as compared to TLPs and they face less problems in onsite installation and maintenance. But the suspended ballast is designed to work in higher water depths, so there would be difficulty in load out of the

platform from the port. Though the cost of ballast type platforms are less compared to TLPs, they are still expensive (Butterfield S. J. J., 2007).

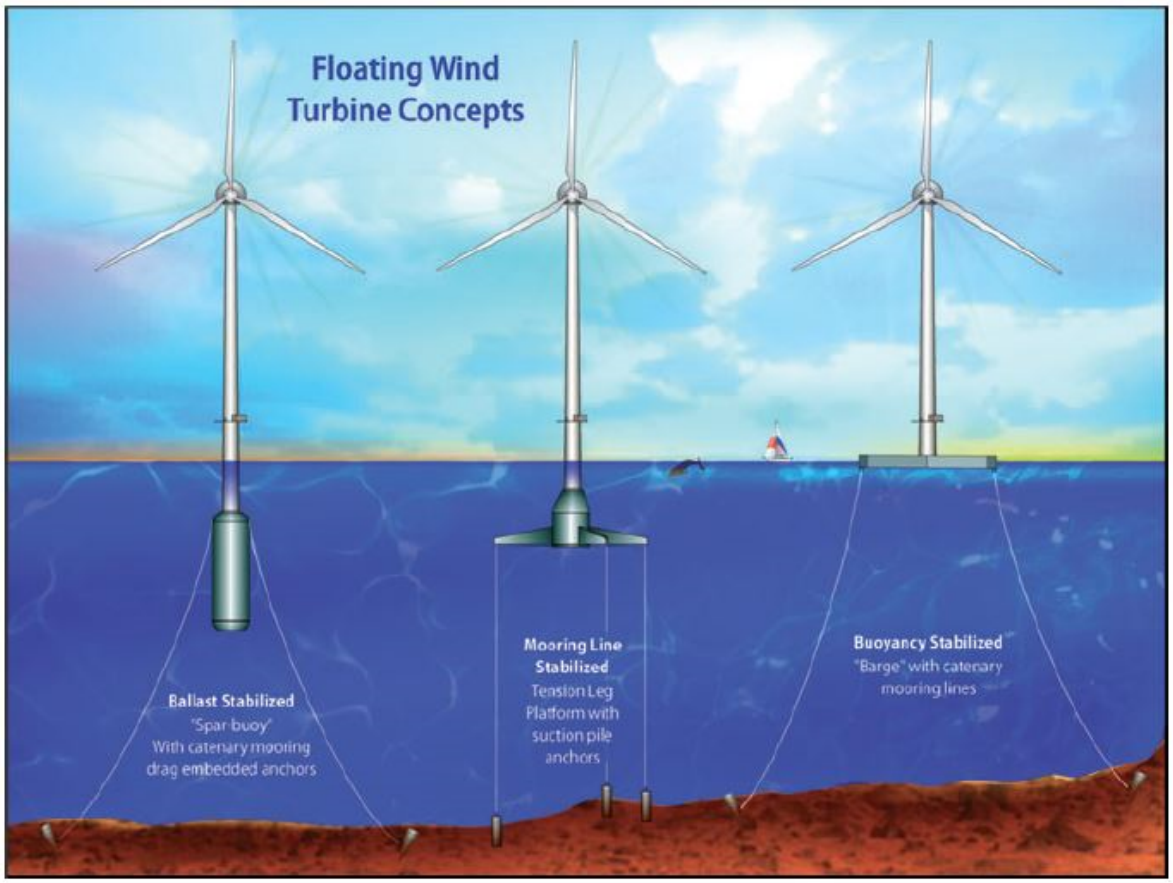

Figure 2. Classification of Floating Wind Turbine concepts (Jonkman, 2009)

The third type is the buoyant type platforms, where a weighted water plane area is used for improving the stability. A barge operates on such a principle and it is independent of water depth. So there are no problems in float-out of such a platform from the port. But to keep the platform in a specific location, it needs to be anchored (Butterfield S. J. J., 2007).

In addition to these three types of floating platforms, there are many 'add-on techniques' that are used for improving the stability of the floating platform. Many of

these are also utilized in ships. These techniques create a restoring torque, which helps in the righting moment against the roll motion, thereby increasing the stability of the ship (Biran, 2003).

Bilge Keel: A bilge keel is an appendage protruding from the bottom edge of the ship or floating platform, in the longitudinal direction. This help in resisting the roll motion, by increasing the surface area, thereby increasing the friction (Utsonomiya T., 2010). It also creates vortices thereby increasing the viscous damping against the roll direction (Biran, 2003, p. 286) .

Roll Fins: Roll fins are wing shaped appendages protruding from the ship body in the transverse direction. They resist the roll as motion as the forward velocity of the ship increases. But in case of a platform, it would not contribute much, as the forward velocity is absent (Biran, 2003, p. 286).

Anti –Roll Tank: An anti-roll tank utilizes a tank filled with water as a ballast, within the ship or a platform. They can be designed in several ways, but the principle is to provide a torque, which adds to the righting moment and thereby increasing the resistance in the roll motion (Biran, 2003, pp. 287-288).

Pneumatic Floating Platform: Pneumatic floating platforms have an open bottom, wherein it utilizes trapped air that acts as a spring and damper system. This displaces the water and help in stabilizing the platform (Cheung, 2000).

The method of analyzing the stability of a ship is fully described in the textbook of ‘Ship Hydrostatics and Stability’ (Biran, 2003). The two important parameters that are

used to determine the stability are the metacentric height and the righting lever. As long as the metacenter is vertically above the center of gravity of the ship, it is stable.

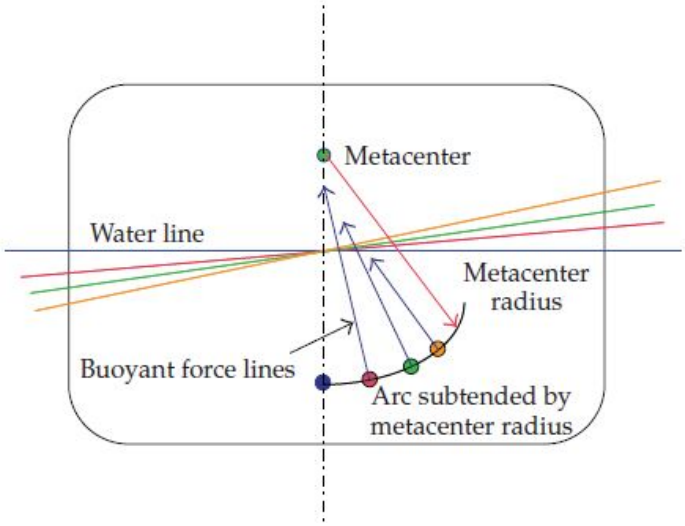

Figure 3. Variation of location of Metacenter (R.A. Ibrahim, 2009)

But for larger heel angles this criterion would not be dependable as the inclined waterlines no longer intersects the centerline. And the position of metacenter keeps changing (Perunovic, 2011), as shown in Figure 3 (R.A. Ibrahim, 2009). So for higher heel angles, stability of the ship is determined by righting moment, which is obtained from the couple generated due to the weight of the ship and the buoyant force acting on the ship. This couple of forces creates a restoring torque or moment, bringing the ship back to its stable position (Kliava, 2010).

The righting moment of a ship is expressed as,

$$M_R = W_{ship} \times \overline{GZ} \tag{2.1}$$

where W_{ship} is the weight of the ship, M_R is the righting moment, and $\overline{GZ}$ is the horizontal distance between center of gravity of the ship and center of buoyancy of the ship (Biran, 2003, p. 112), as shown in Figure 4 (R.A. Ibrahim, 2009).

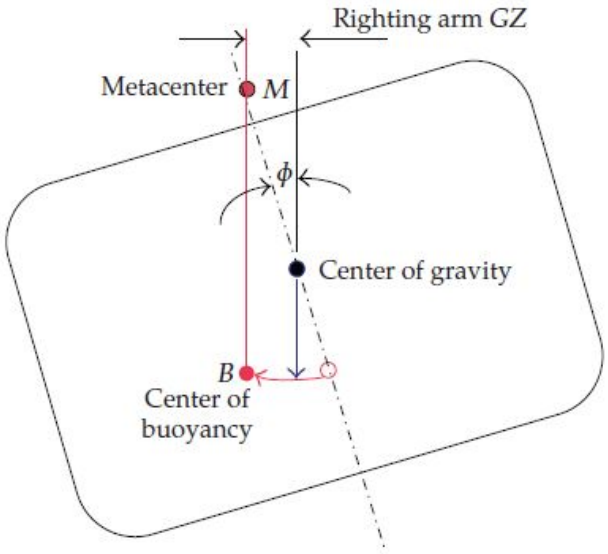

Figure 4. Righting arm (R.A. Ibrahim, 2009)

The value of righting moment mainly depends on $\overline{GZ}$, which can be further expressed as,

$$\overline{GZ} = l_k - \overline{KG}\sin\phi \tag{2.2}$$

where l_k is the value of stability cross-curves and $\overline{KG}$ is the vertical distance between the bottom-most point on the ship and center of gravity of the ship and ϕ is the heel angle. But for small heel angles, the righting lever is calculated using the metacentric height (Biran, 2003, pp. 112-114).

$$\overline{GZ} = \overline{GM}\sin\phi \tag{2.3}$$

The equations mentioned above are for ships and not for platforms. But by considering the geometry of the SSF, the above equations can be utilized. A modified version of the anti-roll tanks are utilized in the mechanism of a suction stabilized float (SSF). The fluid trapped above the waterline creates a downward force that adds to the restoring moment of the SSF (Montomery, 2011). The patent application deals with a general description of a SSF and the study utilizes one among the embodiments defined in the patent application.

In case of a SSF, due to the IST effect, roll motion appears in an opposite way. When the float heels to a direction, the fluid in the internal ballast chamber changes in shape. Consider the float experiencing a roll motion towards its port side, in a stable waterline. The volume of ballast water in the port side reduces and at the same time that of starboard side is increased. For small heel angles, the mass of the trapped fluid remains constant. So the volume of fluid subtracted from the port side adds up to that on the starboard side, resulting in a change of the center of gravity of the ballast fluid towards the starboard side. This creates a righting moment opposite to the heel direction, thereby trying to bring the SSF back to a stable position. The IST effect acting in the opposite direction raises the metacentric height and thereby improving the stability (Redkar, 2012)

.

The functioning of SSF is effectively achieved only when the internal ballast chamber is completely filled with fluid, leaving no space for air and isolated from atmosphere. Once the internal volume is open to the atmosphere and air is allowed to enter, water no longer fills the entire internal volume of the SSF. This negates the IST

effect and causes the trapped water to act as a standard slack tank and lowers the effective metacentric height rather than increasing it.

Parametric Roll Resonance

In late 1998, APL China, a post- Panamax container ship, experienced severe roll motions (approximately 35-40 degrees) in the sea, and out of 1300 containers on deck, they lost about 300 cargos and damaged another 400 of them and also the ship faced severe damage, costing APL more than USD 50 million (Holden, 2011).

Figure 5. APL China Incident (Holden, 2011)

Figure 6. Maersk Incident (Holden, 2011)

In a similar incident in January 2001, Maersk Carolina carried 2280 cargo containers from Spain to Canada. They experienced heavy roll motions in the sea, tilting the ship to an angle of approximately 47 degrees, costing a loss of USD 4 million, by losing 133 containers and damaging 40 another containers and the ship, in the sea (Holden, 2011).

These incidents led to the revelation of the phenomenon of parametric roll resonance and was investigated further. When the ship follows the head sea, there is no roll motions directly developed in the ship. It was found that the vertical plane motions of heave were the only ones excited, in such a condition. This affected the water plane area of the submerged part of the ship as shown in Figure 7 (Holden, 2011). It was found that the when the ship, is a wave trough, the water plane area is larger as compared to when the ship is in a wave crest. So the periodic variation of submerged hull geometry, due to

the wave action results in a periodic variation of the water plane area. And the water plane area is directly related to the metacentric height, *GM*.

So the periodic variation of the metacentric height can be expressed as

$$GM(t) = \overline{GM} + GM_a \cos(\omega_e \, t) \tag{2.4}$$

where $\overline{GM}$ is the average metacentric height of the ship in clam water, GM_a is the amplitude of variation of metacentric height and ω_e is the wave encounter frequency of the ship. But for smaller angles the restoring torque $\tau_\phi(t)$ can be approximated as

$$\tau_\phi(t) \approx \rho g \nabla GM(t) \phi(t) \tag{2.5}$$

where ∇ is the displaced volume of water, $\phi(t)$ is the heel angle for the instant *t*, g is the acceleration due to gravity and ρ is the density of sea water. This further affects the stability of the ship, as it is largely dependent on the metacentric height, *GM*, which is also shown in Figure 8 (Kassteen, 2010).

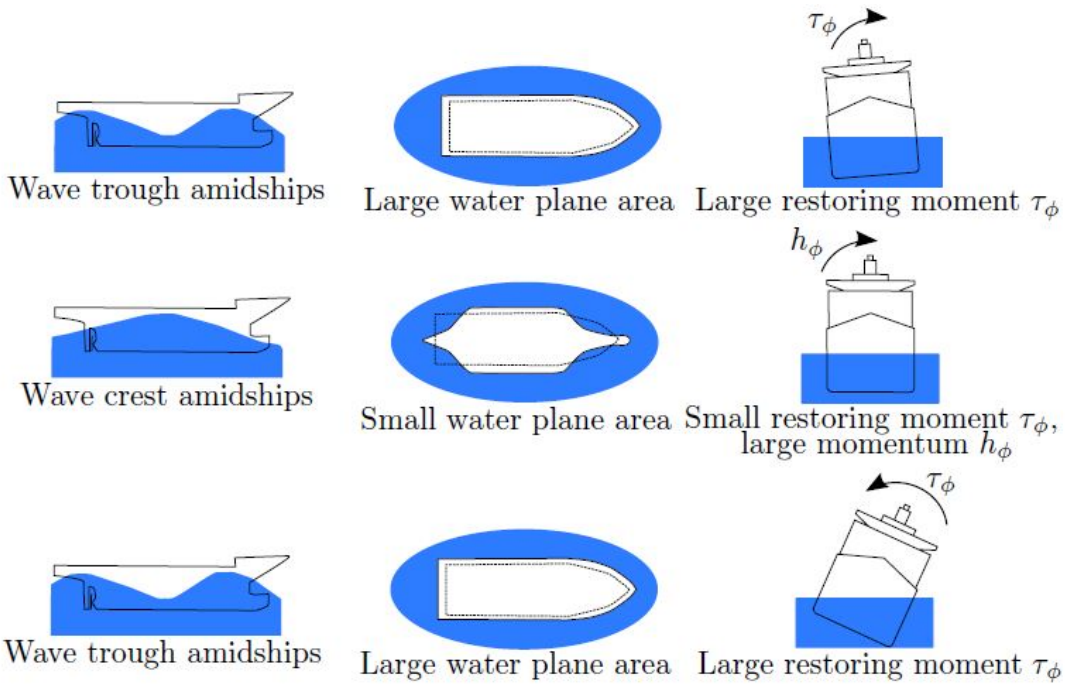

Figure 7. Variation of Water Plane area and Restoring Torques on Ships (Holden, 2011)

A detailed explanation of parametric roll resonance is shown in Figure 8 (Kassteen, 2010). It is observed that the roll behavior of the ship in sea waves is shown in red line. And it different from that of in a clam water due to free rolling, shown in green line. When the wave trough is amidship, the ship rolls to an angle $\Delta\phi_1$ greater than its free roll, due to the change in water plane area as compared to that in calm water. The ship gains its restoring torque and tries to stabilize itself. But as the wave crest is amidship, the water plane area is reduced, thereby reducing the ships stability and the inertia of the ship tends to roll it further by an angle of $\Delta\phi_2$ greater than its free roll behavior. This sequence of events is repeated, thereby increasing the roll angles constantly, even when the waves are not directly exciting the ship roll motion. This leads to a resonance condition when the wave encounter frequency is twice the natural roll frequency of the ship, which is termed as parametric roll resonance.

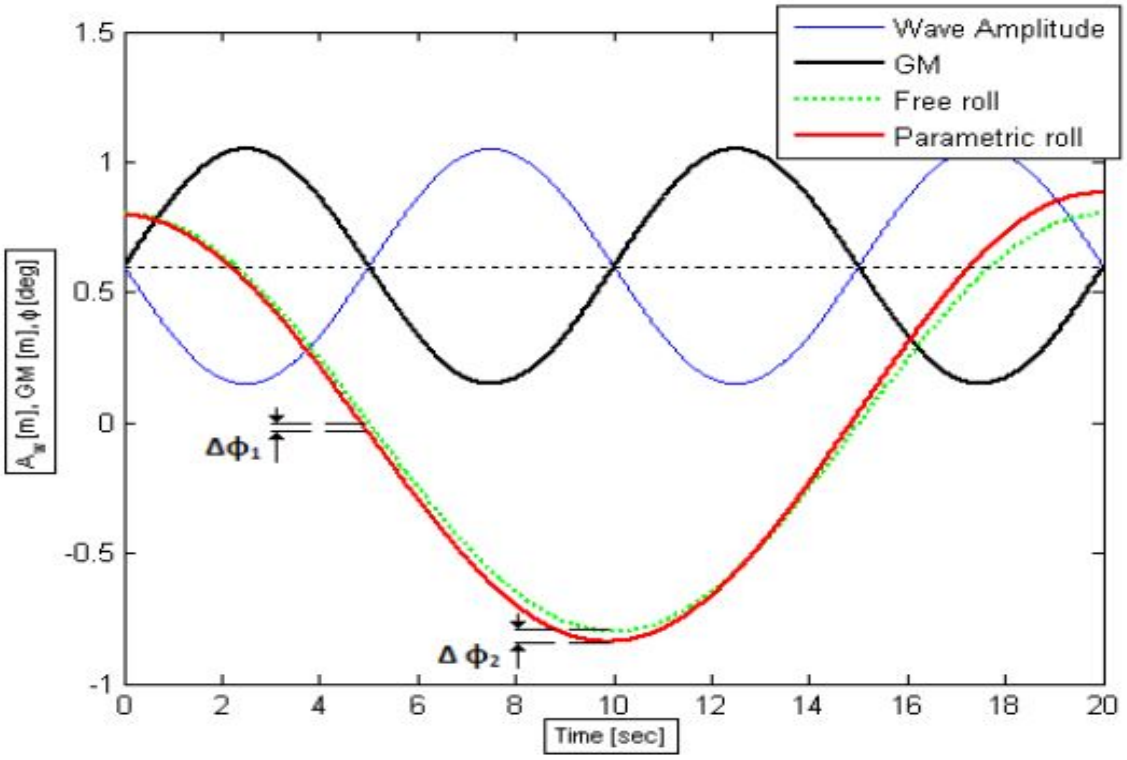

Figure 8. Parametric Roll Resonance (Kassteen, 2010)

Chapter 3
MATHEMATICAL BACKGROUND

The system of dynamics of SSF can be considered as a periodically time varying system. Since the system is parametrically excited, the governing differential equations are having periodic coefficients. The system is primarily analyzed using single degree of freedom initially and then the complex dynamics is incorporated on later stages. The boundary conditions of stability of SSF is determined by a classic Hill-Mathieu equation and the general solution of the system of SSF is determined by using Floquet theory.

Floquet theory

Floquet theory is one of the most important tool used to predict the stability and response of a homogenous system with periodic coefficients. The condition of stability is determined by the characteristic exponents of the Floquet Transition Matrix (FTM). FTM is the state transition matrix (STM) evaluated at the end of the principal period. And STM is a fundamental matrix following the given system.

A general linear periodic system is given as

$$\dot{x}(t) = A(t)x(t) \tag{3.1}$$

Where $x(t)$ is a n vector and $A(t)$ is an $n \times n$ periodic matrix with a principal period T such that $A(t+T)=A(t)$.

Let $P(t)$ be the STM of Eq. (3.1) and $P(0) = I$, identity matrix. So it can be expressed as

$$\dot{P}(t) = A(t)P(t) \tag{3.2}$$

And

$$P(t+T) = P(t)F \tag{3.3}$$

where F is a constant matrix called the Floquet Transition Matrix (FTM) and is given by $F=P(T)$

The general solution of the system in Eq. (3.1) can be also given as

$$x(t) = P(t)x(0) \tag{3.4}$$

for all $t \epsilon [0, T]$. For times greater than the principal time, the STM is given by

$$P(t+nT) = P(t)P(T)^n \tag{3.5}$$

where n=1,2,3… The stability of Eq. (3.1), is dependent on the eigenvalues (υ) of FTM, which are known as characteristic multipliers (Ramalingam, 1994). The stability criteria are:-

a) If absolute value of eigenvalues of FTM, $|eig(FTM)| < 1$, system is asymptotically stable.
b) If absolute value of eigenvalues of FTM, $|eig(FTM)| = 1$, system is simply stable.
c) If absolute value of eigenvalues of FTM, $|eig(FTM)| > 1$, system is unstable.

But generally, the characteristic multipliers can be positive, negative, real or complex. By considering it as complex, it can be expressed as

$$\upsilon = \upsilon_R + i\upsilon_I \tag{3.6}$$

And the characteristic exponents *($\lambda=a_c+ib_c$)* of the system can be related to the characteristic multipliers as

$$\upsilon = e^{\lambda T} \tag{3.7}$$

Therefore a_c and b_c can be expressed as

$$a_c = \frac{1}{T}\ln|\upsilon| \tag{3.8}$$

$$b_c = \frac{1}{T}\tan^{-1}\left(\frac{\upsilon_I}{\upsilon_R}\right) \tag{3.9}$$

The stability criteria by using the characteristic exponents of the system at the end of the principal period are (Ramalingam, 1994):-

a) The system is asymptotically stable when the values of the real part of the characteristic exponents, $a_c < 0$.
b) The system is simply stable when the values of the real part of the characteristic exponents, $a_c = 0$.
c) The system is unstable when the values of the real part of the characteristic exponents, $a_c > 0$.

Therefore the stability of the system can be predicted from the eigenvalues of FTM and also from the real part of the characteristic exponent.

Hill-Mathieu Equation

A normal second order differential equation, with a time periodic coefficient can be expressed as

$$\ddot{x} + A(t)x = 0 \tag{3.10}$$

The above differential equation, Eq. (3.10), can be utilized to represent physical systems that are parametrically excited by substituting

$$A(t) = \delta + 2\varepsilon \cos 2t \tag{3.11}$$

Therefore Eq. (3.10) becomes

$$\ddot{x} + (\delta + 2\varepsilon \cos 2t)x = 0 \tag{3.12}$$

The Eq. (3.12) is known as Mathieu's equation, where the stability of the system is dependent on the parameters δ and ε. And it represents some of the parametrically excited systems like a pendulum, excited sinusoidally at its fixed end, as shown in Figure 9.

The state space form of Eq. (3.10) can be given as

$$\begin{pmatrix} \dot{x}_1 \\ \dot{x}_2 \end{pmatrix} = \begin{pmatrix} 0 & 1 \\ -A(t) & 0 \end{pmatrix} \begin{pmatrix} x_1 \\ x_2 \end{pmatrix} \tag{3.13}$$

where $x_1 = x$ and $x_2 = \dot{x}$. Let $X(t)$ be the STM of the system, then as per Floquet theory from Eq. (3.3), it can be expressed as

$$X(t+T) = X(t)F \tag{3.14}$$

And

$$X(t) = \begin{pmatrix} x_1 & \dot{x}_1 \\ x_2 & \dot{x}_2 \end{pmatrix} \tag{3.15}$$

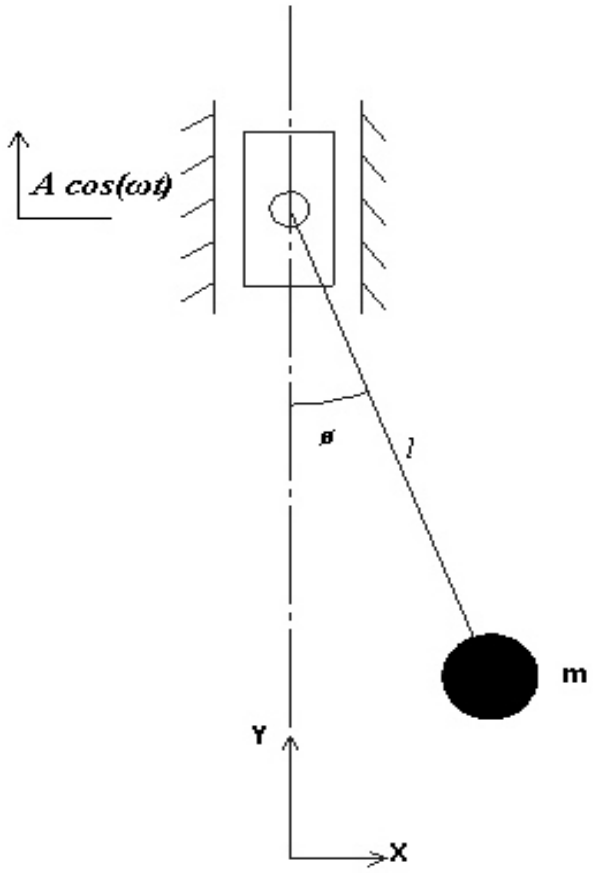

Figure 9. A Pendulum with moving base

Since x_1 and x_2 are linearly independent solutions of the Eq. (3.12), the initial condition of the system can be given as $X(0)=I$, when $t=0$. Then Eq. (3.14) becomes

$$X(T) = X(0)F \tag{3.16}$$

Therefore, the constant matrix of the system (FTM) is given by

$$F = X(0)^{-1} X(T) \tag{3.17}$$

By substituting Eq. (3.15) in Eq. (3.17), we get

$$F = \begin{pmatrix} x_1(T) & \dot{x}_1(T) \\ x_2(T) & \dot{x}_2(T) \end{pmatrix} \tag{3.18}$$

If υ denotes the eigenvalues (characteristic multipliers) and *Tr* the trace of the constant matrix, *F*, then the stability of the system can be given by

$$\upsilon^2 - 2Tr\upsilon + 1 = 0 \tag{3.19}$$

where

$$Tr = \left\{ \frac{x_1(T) + \dot{x}_2(T)}{2} \right\} \tag{3.20}$$

So finally, by solving Eq. (3.19) the characteristic multipliers can be given as

$$\upsilon_{1,2} = Tr \pm \sqrt{Tr^2 - 1} \tag{3.21}$$

As discussed earlier, the negative real part of the characteristic multipliers is supposed to represent a stable system and the positive real represents the unstable system. The trace of the matrix, *Tr*, is dependent on the parameters δ and ε, which further affects the stability of the system. And it is separated by the values which make the real part of characteristic multipliers as zero, where the system is simply stable. This results in a graph between δ and ε, as shown in Figure 10, differentiating the region of stability and instability, popularly known as Ince-Strutt diagram.

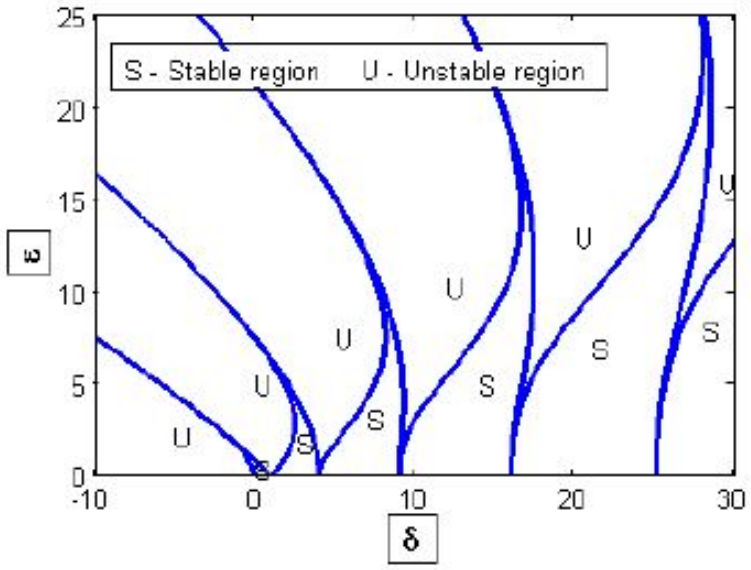

Figure 10. Ince-Strutt diagram (Kassteen, 2010)

It is observed in Figure 10 that the parameters δ and ε, divides the plane into stable and unstable regions, during parametric excitation. Along the x-axis, the system is observed to be stable for all positive values of δ and unstable for all negative values. This condition corresponds to $\varepsilon=0$ in Eq. (3.12), which becomes

$$\ddot{x}+\delta x=0 \tag{3.22}$$

Eq. (3.22), represents the equation of a linear harmonic oscillator. Consider the system to be periodic with a time period ($T_0=2\pi/\sqrt{\delta}$), the general solution of the system is given by

$$x(t)=C_1\cos(\sqrt{\delta}t)+C_2\sin(\sqrt{\delta}t) \tag{3.23}$$

By substituting Eq. (3.23) in Eq. (3.15) and applying the initial condition of $X(0)=I$, we get

$$x_1(t) = \cos(\sqrt{\delta}t) \tag{3.24}$$

$$x_2(t) = \frac{\sin(\sqrt{\delta}t)}{\sqrt{\delta}} \tag{3.25}$$

By substituting Eq. (3.24) and Eq. (3.25) in Eq. (3.20) at principal period ($t=T$), we get

$$Tr = \cos\sqrt{\delta}T \tag{3.26}$$

The boundaries of stability, when $\varepsilon=0$, can be defined by

$$Tr = 1, \sqrt{\delta}T = 2k\pi \Rightarrow T = kT_0 \tag{3.27}$$

Or

$$Tr = -1, \sqrt{\delta}T = (2k+1)\pi \Rightarrow T = (2k+1)T_0 \tag{3.28}$$

where $k=0, 1, 2, 3$.....indicating the condition of parametric resonance. The condition of Tr =-1 and k=0 results in $T=2T_0$, which is called the condition of principal parametric resonance. This is the condition when the frequency of forcing waves is double the natural frequency of the system, which results in large amplitude oscillations for small forcing.

Since no system is perfect and losses associated with the system can be considered dissipating as a damping force, the equation of the system, Eq. (3.12), can be modified as

$$\ddot{x} + 2\mu\dot{x} + (\delta + 2\varepsilon\cos 2t)x = 0 \tag{3.29}$$

The stable region for such a system is further raised by the viscous damping term in Eq. (3.29), as shown in Figure 11.

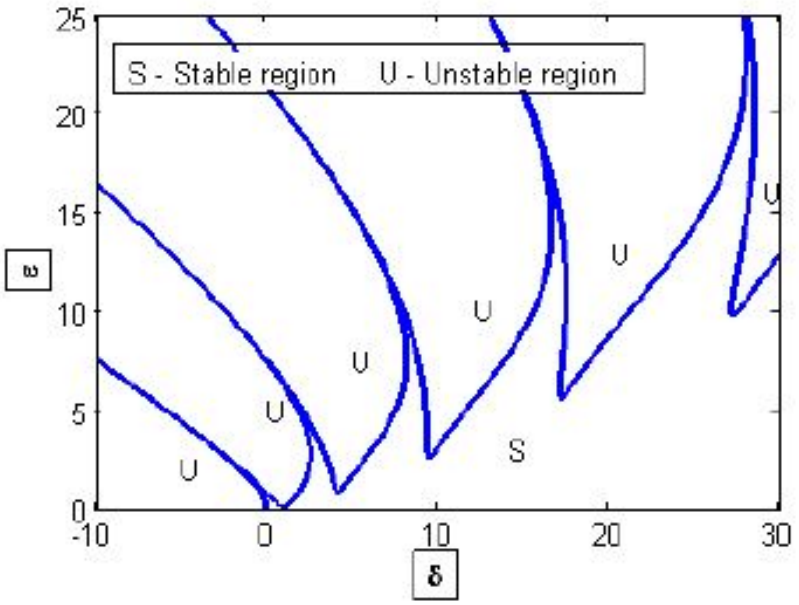

Figure 11. Ince-Strutt diagram with Viscous Damping effect (Kassteen, 2010)

Inverse Slack Tank effect

The phenomenon of inverse slack tank can be explained in three different ways. The first one by comparing that to the inverse effect of moving mass on the deck of a ship. The second way is by comparing that to the inverse effect of internal tanks in ships. The third way is by comparing the stability conditions of a float with suction stability to that without suction stabilization.

Consider a mass m, shifting a distance d, as shown in Figure 12 (Biran, 2003), on the deck of a ship, which has a displacement mass of Δ, with initial water plane as W_0L_0. And it heels to an angle ϕ, producing a water plane $W_\phi L_\phi$. A heeling moment of, $M_H = dm \cos\phi$, is generated in the direction of heel, which further heels the ship to the same

direction. This also changes the location of the center of gravity of the ship mass system from G to G_1 (Biran, 2003).

Therefore by comparing the moments in the horizontal direction it can be expressed as

$$\Delta\overline{GG_1} = dm \tag{3.30}$$

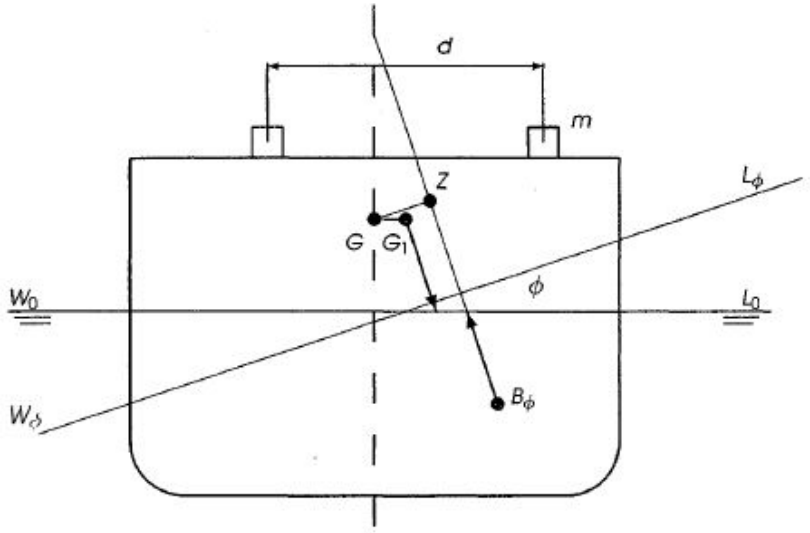

Figure 12. Shifting of mass on Ship Deck (Biran, 2003)

Rearranging which gives

$$\overline{GG_1} = \frac{dm}{\Delta} \tag{3.31}$$

A detailed change in the position of the center of center of gravity and forces are shown in the free body diagram in Figure 13 (Biran, 2003). It is shown that there is a shifting of the position of the effective center of gravity resulting in change in the effective metacentric height. The new metacentric height can be expressed as

$$\overline{GM}_{effective} = \overline{GM} - \overline{GG}_v \tag{3.32}$$

But from Figure 13, we get that

$$\overline{GG}_v = \frac{\overline{GG}_1}{\tan\phi} \tag{3.33}$$

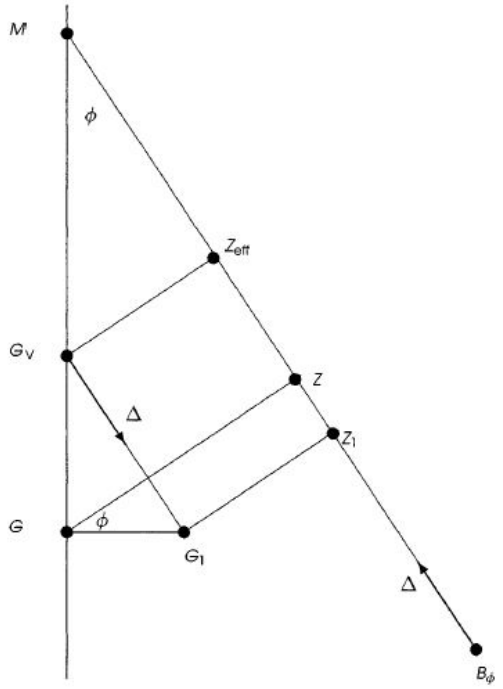

Figure 13. Free body diagram of Shifting of mass on Ship Deck (Biran, 2003)

By substituting Eq. (3.33) in Eq. (3.32), we get

$$\overline{GM}_{effective} = \overline{GM} - \frac{\overline{GG}_1}{\tan\phi} \tag{3.34}$$

By substituting Eq. (3.31) in Eq. (3.34), we get

$$\overline{GM}_{effective} = \overline{GM} - \frac{dm}{\Delta \tan\phi} \tag{3.35}$$

Therefore from Eq. (2.3), the righting lever can be expressed as

$$\overline{GZ}_{effective} = \overline{GZ} - \frac{dm\cos\phi}{\Delta} \tag{3.36}$$

The mass here can be compared to that of the mass of ballast water above the water plane in case of SSF and the distance as the breadth or diameter of the inner chamber. But the mass in SSF creates a righting moment in the opposite direction to the heel because it displaces in the opposite direction as compared to the mass on the deck of the ship, as shown in Figure 14. Moreover in case of a SSF the weight of the fluid increases, in the opposite end, as the heel angle increases. So the value of righting moment keeps increasing, trying to stabilize the SSF, instead of destabilizing action as in case of a mass on the ship deck.

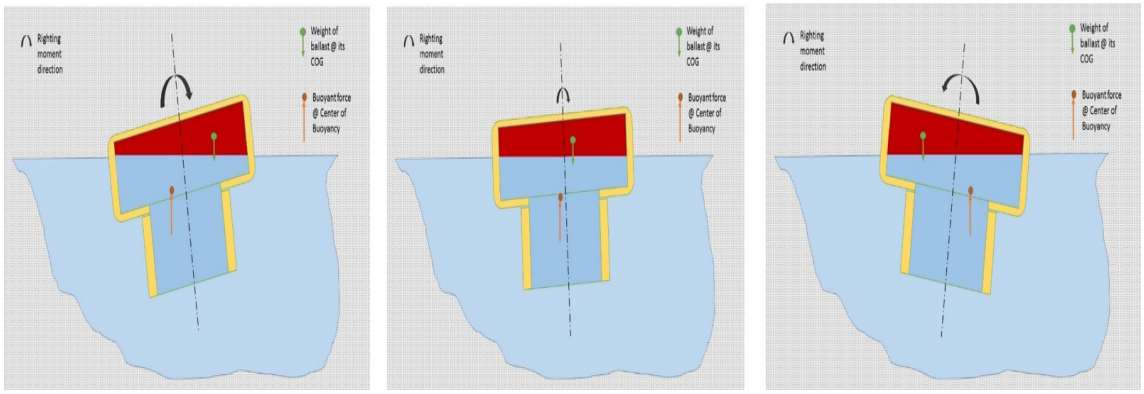

Figure 14. Shifting of mass in SSF

So instead of reducing the metacentric height and the righting lever, the equations for SSF can be modified as

$$\overline{GM}_{effective,SSF} = \overline{GM} + \frac{dm}{\Delta\tan\phi} \tag{3.37}$$

$$\overline{GZ}_{effective,SSF} = \overline{GZ} + \frac{dm\cos\phi}{\Delta} \tag{3.38}$$

But a more accurate approximation for the working of SSF done by comparing it to the change in metacentric height, due to motion of fluid in slack tanks in the ship. Slack tanks are partially filled tanks in a ship or a vessel, usually used to transport liquid cargo or fuel.

Consider a hull, in a ship as shown in Figure 15, partially filled with a fluid of density, ρ. Let the fluid in the tank be of volume, v, which has a different water plane. The initial location of buoyant center of the fluid filled in the slack tank is indicated by b_0. And as the ship heels to an angle, ø, the position of buoyant center shifts to b_ϕ. And the center of gravity of the whole system of the ship changes as shown in Figure 13 (Biran, 2003).

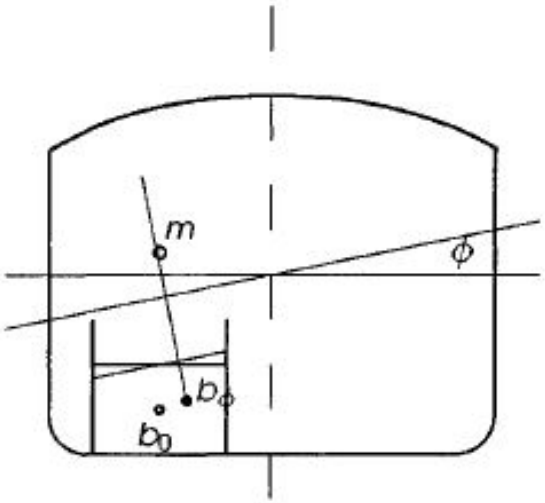

Figure 15. Slack Tank effect in Ships (Biran, 2003)

The horizontal distance between the points of the center of buoyancy for the slack tank is given by (Biran, 2003)

$$\overline{b_0 b_\phi} = \overline{b_0 m} \tan\phi \tag{3.39}$$

Where $\overline{b_0 m}$ is the metacentric radius of the fluid in the slack tank, which can be further expressed as (Biran, 2003)

$$\overline{b_0 m} = \frac{i_s}{v} \tag{3.40}$$

Where i_s, is the moment of inertia of the water plane area of the fluid in the slack tank. And by substituting Eq. (3.40) in Eq. (3.39) we get

$$\overline{b_0 b_\phi} = \frac{i_s}{v} \tan\phi \tag{3.41}$$

Therefore the moment caused due to the free surface effect in the slack tank in the horizontal direction is given by

$$M_s = \rho v \overline{b_0 b_\phi} \tag{3.42}$$

By substituting Eq. (3.41) in Eq. (3.42), we get

$$M_s = \rho i_S \tan\phi \tag{3.43}$$

The horizontal distance of change in center of gravity of the ship in Eq. (3.31) is given as (Biran, 2003)

$$\overline{GG_1} = \frac{\rho i_S}{\Delta} \tan\phi \tag{3.44}$$

Therefore by substituting Eq. (3.44) in Eq. (3.34) and we get the effective metacentric height as

$$\overline{GM}_{effective} = \overline{GM} - \frac{\rho i_S}{\Delta} \tag{3.45}$$

The working of SSF is very similar to the process of slack tank. The inner chamber in SSF acts as a slack tank, but with an opposite effect. Consider the fluid in the slack tank heeling in the opposite direction to the heel angle of the vessel. The moment due to the fluid in the slack tank acts as a righting moment, thereby increasing the effective metacentric height of the whole system. This phenomena is termed as 'inverse slack tank effect'. So Eq. (3.45) can be modified as

$$\overline{GM}_{effective,SSF} = \overline{GM} + \frac{\rho i_S}{\Delta} \tag{3.46}$$

But in case of SSF the fluid column is continuous and it is same as the fluid surrounding it. So the factor $\frac{\rho}{\Delta}$ represents the inverse of the total volume of the fluid displaced due to the system $\left(\frac{1}{V_{Tdis}}\right)$. And since the ballast chamber acts as the slack tank, i_s would represent the moment of inertia of the water plane area of the inner chamber (I_{WP}). So Eq. (3.46) can be expressed as

$$\overline{GM}_{effective,SSF} = \overline{GM} + \frac{I_{WP}}{V_{Tdis}} \tag{3.47}$$

The concept of IST affecting the metacentric height of the system, can be explained in detail, by considering two floating bodies of same dimensions $l \times b \times h$, as shown in Figure 16.and Figure 17. Consider the float in Figure 16 to be with open top, with no IST effect, where the level of the water plane inside the float chamber is same as

the water plane level surrounding the float. The hatched area indicates the level of the fluid inside the body.

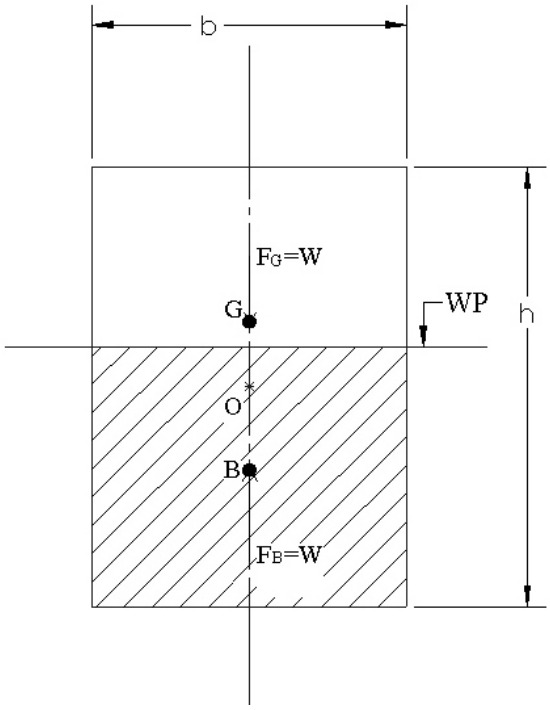

Figure 16. A Normal Float at the Water Surface

The level of the fluid inside is raised in the second float in Figure 17, because of suction stabilization and it fills up the chamber. The water until the water plane is indicated as the hatched region in the figure and the remaining chamber is also filled with water, which is indicated as the dotted region. The location of the center of gravity and center of buoyancy of the body along with the forces acting on them, in stable condition, are also shown in the same figures. It is observed the in both the floats in stable condition the total couple on the body is zero, because equal and opposite forces are acting on the same line of action.

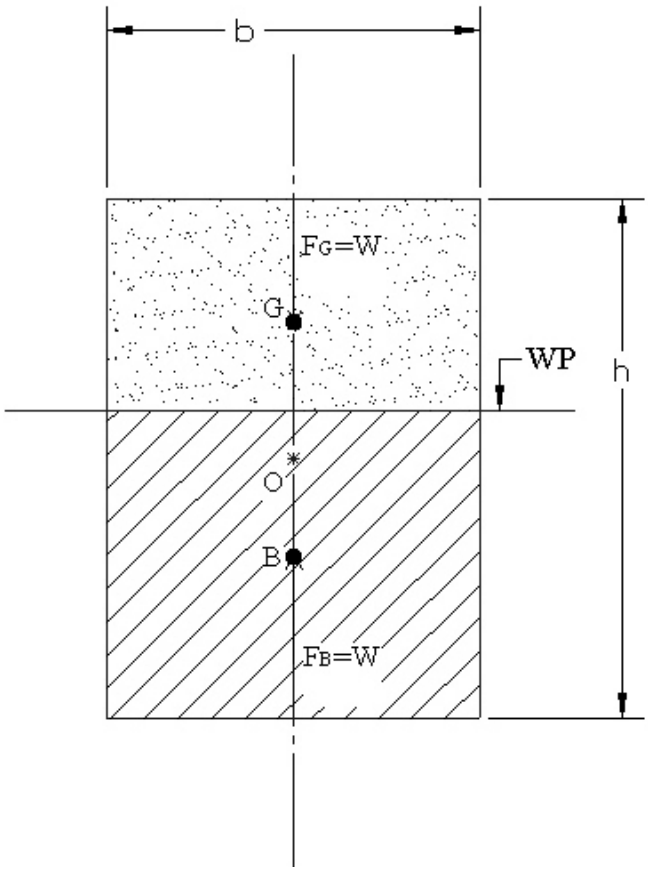

Figure 17. A Float with IST effect at the Water Surface

Now let the bodies heel to an angle ø, as shown in Figure 18 and in Figure 19. The float without suction stabilization will still have the waterplane inside the float inline with the waterplane surrounding it. Note that the location of the center of bouyancy changes as per the heel angle, from *B* to *B'*, but not the center of gravity, *G*, in this case, as shown in Figure 18. So the effective metancentric height remains *GM* and the righting lever remains *GZ*.

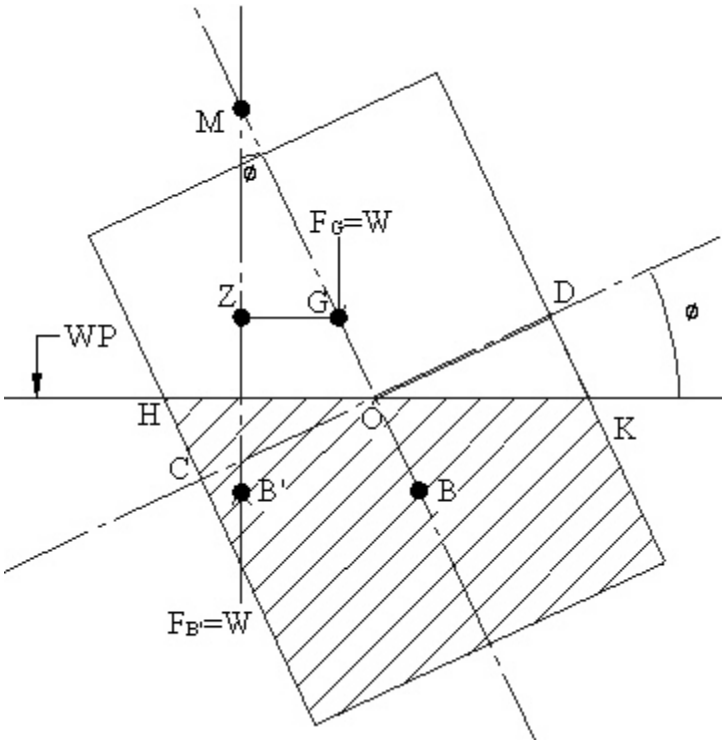

Figure 18. Heeling of an Open Top Float

But in case of the float with suction stabilization, it is observed that the level of the fluid inside the chamber of the float does not remain in level with the surrounding water plane area, as shown in Figure 19. Instead there is movement of mass of fluid and an additional wedge of section KOD is raised above the water plane area, which is absent in Figure 18. Due to the change of mass above the water plane area, there will be shift in the center of gravity of the system towards the mass of wedge, from *G* to *G'* as shown in Figure 19. But note that the volume of body below the water plane remains the same as compared to the float without suction stabilization. So the location of the center of buoyancy remains the same, *B'*, at the same heel angle. And also the buoyant force, $F_{B'}$, acting at *B'* is equal to the weight of the float with water inside, *W*.

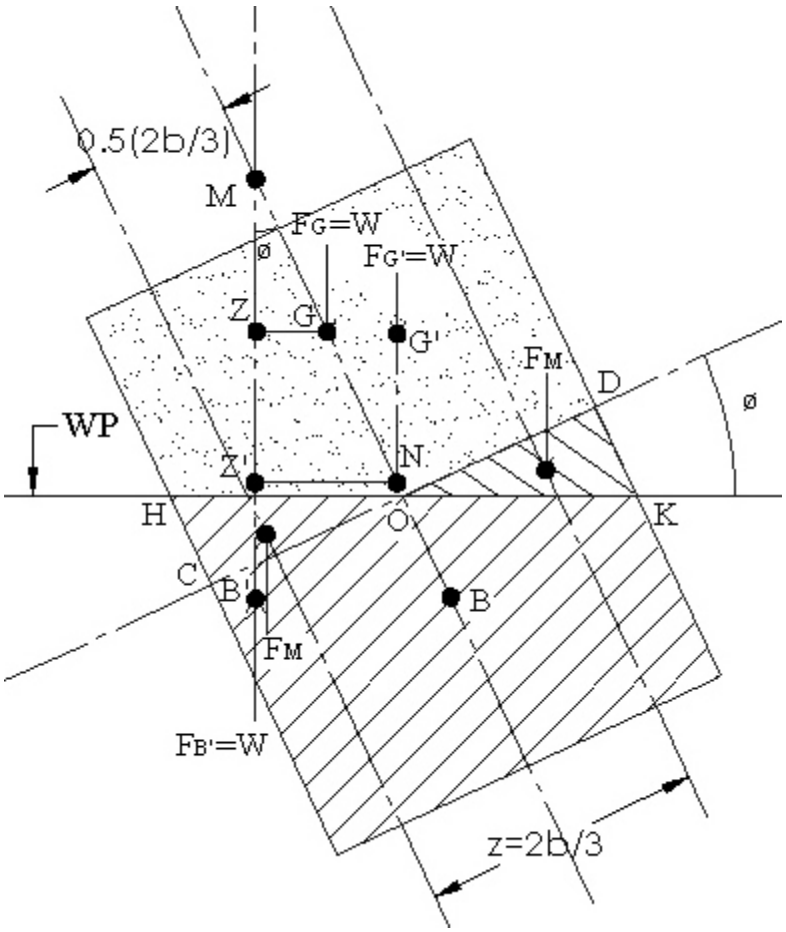

Figure 19. Heeling of Float with IST effect

When the float heels to the opposite direction, wedge HOC is going to come above water plane. So the weight of the wedge section acts at the center of gravity of the wedge section. So a restoring torque is created by the fluid wedge DOK and COH, due to the forces F_M, which is equal to the weight of the wedge section.

Volume of the wedge section is given as

$$V_M = \frac{1}{2} \times \frac{b}{2} \times \frac{b}{2} \sin\phi \times l \tag{3.48}$$

So the weight of the fluid of wedge section, F_M, can be given as

$$F_M = w \times \frac{b^2 l}{8} \times \phi \tag{3.49}$$

Where *w*, is the weight density of the fluid and for small heel angle $sin\text{ø} \approx \text{ø}$ and $cos\text{ø} \approx 1$. Therefore the couple due the water shifting can be given as (P.N. Modi, 1995)

$$M_M = F_M \times \frac{2b}{3} \tag{3.50}$$

By substituting Eq. (3.49) in Eq. (3.50), we get

$$M_M = w \times \frac{b^2 l}{8} \times \frac{2b}{3} \times \phi = w \times \frac{b^3 l}{12} \times \phi \tag{3.51}$$

But the moment of inertia of the rectangular section of the water plane section in the float in stable condition, I_M, can be expressed as

$$I_M = \frac{bl^3}{12} \tag{3.52}$$

By substituting Eq. (3.52) in Eq. (3.51), we get

$$M_M = wI_M \phi \tag{3.53}$$

Now by considering the total couple on the float body, in Figure 19, we get

$$M_T = F_{G'} \times \overline{Z'N} - F_G \times \overline{ZG} - M_M \tag{3.54}$$

By considering small angle of heel, ø, and substituting all the forces in Eq. (3.54), we get

$$M_T = W \times \overline{MN} \times \phi - W \times \overline{GM} \times \phi - wI_M \phi = 0 \tag{3.55}$$

Rearranging Eq. (3.55), we get

$$\overline{MN} = \overline{GM} + \frac{wI_M}{W} \tag{3.56}$$

Since the fluid displaced by the system is same as the fluid inside the float inner chamber, we can replace the total weight of the displaced fluid, W, as

$$\overline{MN} = \overline{GM} + \frac{wI_M}{wV_{Tdis}} = \overline{GM} + \frac{I_M}{V_{Tdis}} \tag{3.57}$$

The metacentric height, $\overline{MN}$, in Eq. (3.57), is the effective metacentric height of the SSF, given as $\overline{GM}_{effective,SSF}$ in Eq. (3.47).

Chapter 4
PARAMETRIC ROLL RESONANCE IN SSF

To evaluate the hydrodynamic forces acting on the ship and to determine the stability of the system, different models are proposed. Though the models for described ship are not the exact replica of the offshore conditions. The dynamics of the ship stability properties can be compared to a system consisting of an oscillating mass under spring damper and a rotating mass. The oscillating mass represents the heave and pitch motions of the ship, whereas the rotating mass represents the roll motion.

The three models proposed for ship are (Kassteen, 2010):-

1) Heave-Roll model
2) Heave-Pitch model
3) Heave-Pitch-Roll model

Though the above models were proposed for ships, the dynamics and stability properties of ship and SSF are comparable. The main mass of SSF and the mass of fluid inside can be compared to the oscillating under the spring-damper system. And the varying ballast mass of the fluid inside the SSF chamber is compared to the pendulum action of the rotating mass in the model.

Heave-Roll model for Ships

The dynamics of this model represents the influence of moderate longitudinal waves on the ship stability wherein the ships undergo vertical displacement (in z-direction). The effect of coupled actions of heave and roll motions are studied in this model.

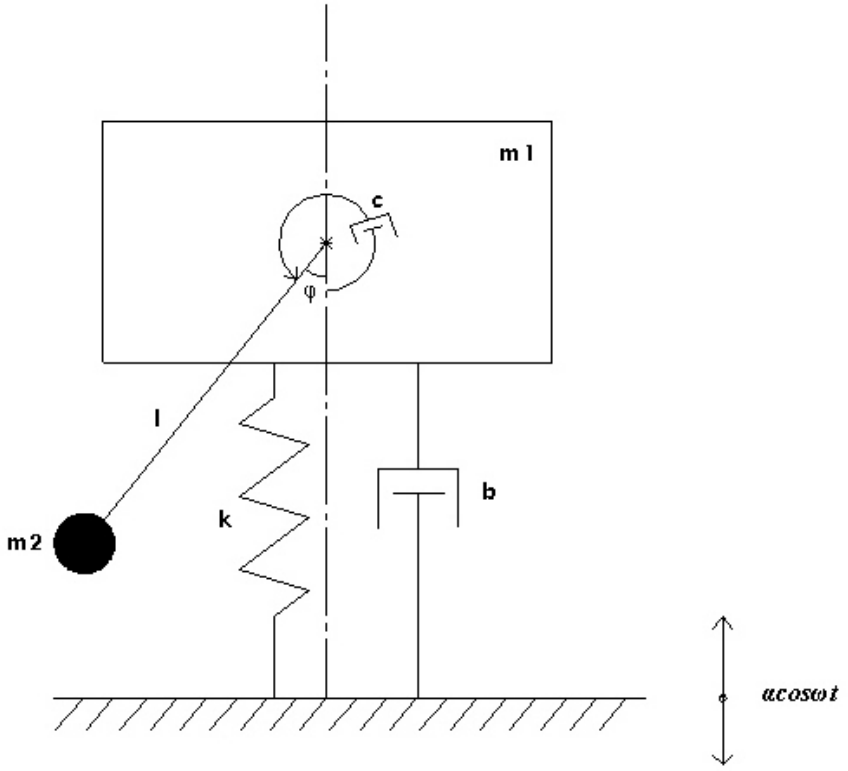

Figure 20. Heave-Roll model for Ships (Kassteen, 2010)

As shown in Figure 20 (Kassteen, 2010), the vertical motion of the mass represents the heave motion and the pendulum action of the rotating mass represents the roll motion. In Figure 20 masses m_1 and m_2 represents the vertically displacing mass and rotating mass of the ship respectively. And the constants b and c are the linear damping co-efficient and rotational damping co-efficient of the pendulum respectively. The length of the pendulum is represented by l, which rotates with an angular displacement of φ and k is the stiffness constant for the spring. The base of the system is excited by the wave motion which propagates sinusoidal as $\alpha cos\omega t$, where ω represents the frequency of wave motion.

For such a system, the equations of motion are given by the Lagrange's equation, which is given below and the detailed derivation of the expression is shown in Appendix-A (Tondl A., Autoparametric Resonance in Mechanical Systems, 2000).

$$(m_1 + m_2)\{\ddot{z} - \alpha\omega^2 \cos(\omega t)\} + b\dot{z} + kz + m_2 l\{\ddot{\varphi}\sin(\varphi) + \dot{\varphi}^2 \cos(\varphi)\} = 0 \quad (4.1)$$

$$m_2 l^2 \ddot{\varphi} + c\dot{\varphi} + m_2 gl \sin(\varphi) + m_2 l\{\ddot{z} - \alpha\omega^2 \cos(\omega t)\}\sin(\varphi) = 0 \quad (4.2)$$

It is observed that the above equations are converted to the dimensionless form as the following

$$\ddot{w} + K\dot{w} + q^2 w + \mu\{\ddot{\varphi}\sin(\varphi) + \dot{\varphi}^2 \cos(\varphi)\} = a\eta^2 \cos(\eta\tau) \quad (4.3)$$

$$\ddot{\varphi} + K_0\dot{\varphi} + \sin(\varphi) + \{\ddot{w} - a\eta^2 \cos(\eta\tau)\}\sin(\varphi) = 0 \quad (4.4)$$

The heave motions for the given system, as per Eq. (4.3) is plotted with respect time in Figure 21. It is observed that the heave motions are bounded within limits continuously as the excitation is continuous in heave direction.

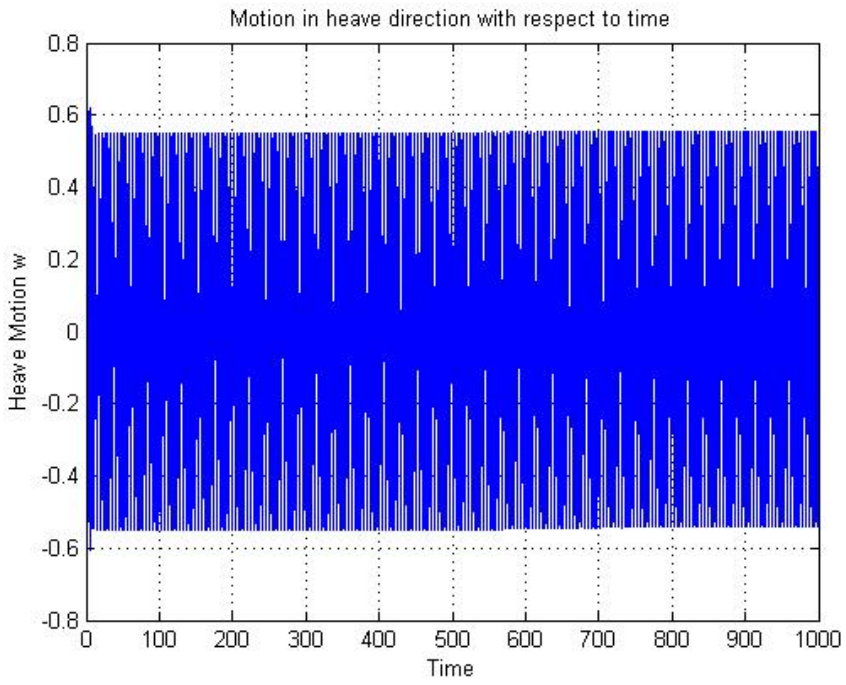

Figure 21. Motion in Heave direction with respect to Time

The roll motions for the given system, as per Eq. (4.4) is plotted with respect time in Figure 21. It is observed that the amplitude of the roll motions increases as the time proceeds. But note that roll motions are not excited directly by the wave motions. And the roll motions are developed and increasing continuously, which is due to the phenomenon of parametric roll resonance, as explained in Chapter-2.

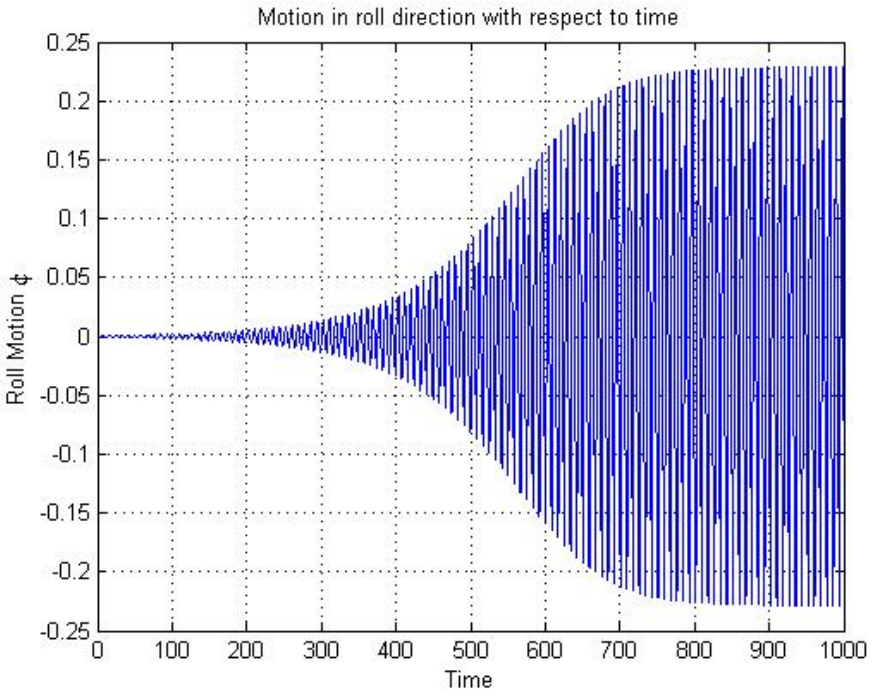

Figure 22. Motion in Roll direction with respect to Time

The semi trivial solution of Eq. (4.3) and Eq. (4.4) are given as

$$w_0(\tau) = a(\text{Acos}(\eta\tau) + \text{Bsin}(\eta\tau)) \tag{4.5}$$

$$\varphi_0(\tau) = 0 \tag{4.6}$$

Where $A = \dfrac{\eta^2(q^2-\eta^2)}{(q^2-\eta^2)^2+(K\eta)^2}$ and $B = \dfrac{K\eta^3}{(q^2-\eta^2)^2+(K\eta)^2}$. And by adding small perturbations to w and φ as

$$w = w_0 + u \tag{4.7}$$

$$\varphi = \varphi_0 + \psi \tag{4.8}$$

And with first order approximation we get the following equations

$$\ddot{u} + K\dot{u} + q^2 u = 0 \tag{4.9}$$

$$\ddot{\psi} + K_0\dot{\psi} + \psi - a\eta^2\{(1+A)\cos(\eta\tau) + \mathrm{Bsin}(\eta\tau)\}\psi = 0 \tag{4.10}$$

Eq. (4.9) is a homogenous differential equation, with constant coefficients, the solution of which is stable. But Eq. (4.10) is a classic Mathieu equation, whose stability is dependent on different parameters. For the first approximation, by substituting the Eq. (3.23) in Eq. (4.10), and solving for the non-trivial solutions for C_1 and C_2, we get the following condition

$$(1-\frac{1}{4}\eta^2)^2 + \frac{1}{4}K_0{}^2\eta^2 - \frac{1}{4}a^2\eta^2\{(1+A)^2 + B^2\} = 0 \tag{4.11}$$

The value of a_c here represents the critical value of wave amplitude above which resonance occurs, which can be expressed as

$$a_c = \sqrt{\frac{4}{\eta^4}\left[\frac{\left(\left(1-\frac{\eta^2}{4}\right)^2 + \frac{\eta^2 K_0^2}{4}\right)}{(1+A)^2 + B^2}\right]} \tag{4.12}$$

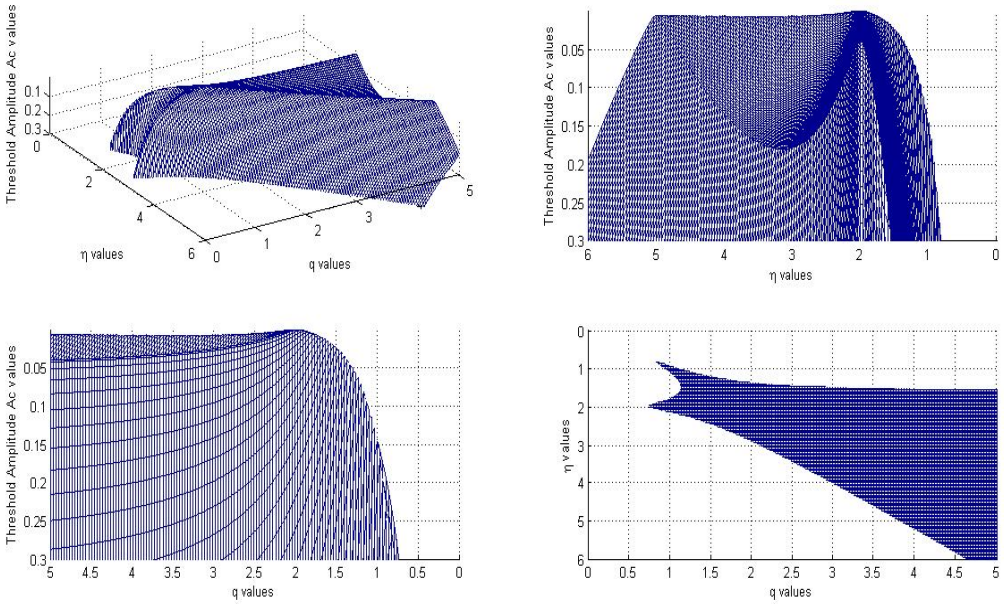

Figure 23. Variation of Threshold Amplitude with η and q values

The expression in Eq. (4.12) is plotted in Figure 23. Note that the z-axis with a_c values and the y-axis with η values have been inverted. So the highest point in the graph indicates the minimum value of threshold amplitude for parametric excitation. Hence the white region in the graph indicates comparatively stable regions of the system, because the threshold amplitude values are too high for such areas, in the graph. It is observed that the system is more stable at lower values of η and q. And later the minimum value of threshold amplitude, a_c, is observed for the condition of $\eta = q$.

Energy Transfer for Heave-Roll model for Ships

The whole system can be divided into two system as primary and secondary system. Primary system is encounters the base excitation continuously, thereby deals with the energy possessed due to heave motions in the model. And the secondary system is the part of the system, on which no forces are directly applied, but still possess energy. This

energy is observed in the form of roll motions. So there appears to be a transfer of energy form in the whole system.

To observe the energy transfer phenomenon mathematically, the energy equations are derived and plotted. By neglecting the nonlinear factors, the energy possessed by primary system, in heave direction, is given as

$$E_{Heave} = \frac{1}{2}(m_1 + m_2)\dot{w}^2 \tag{4.13}$$

The expression in Eq. (4.13) is plotted in Figure 24. It is observed that the energy in the primary system remains almost constant with time, as the base is constantly excited with wave action.

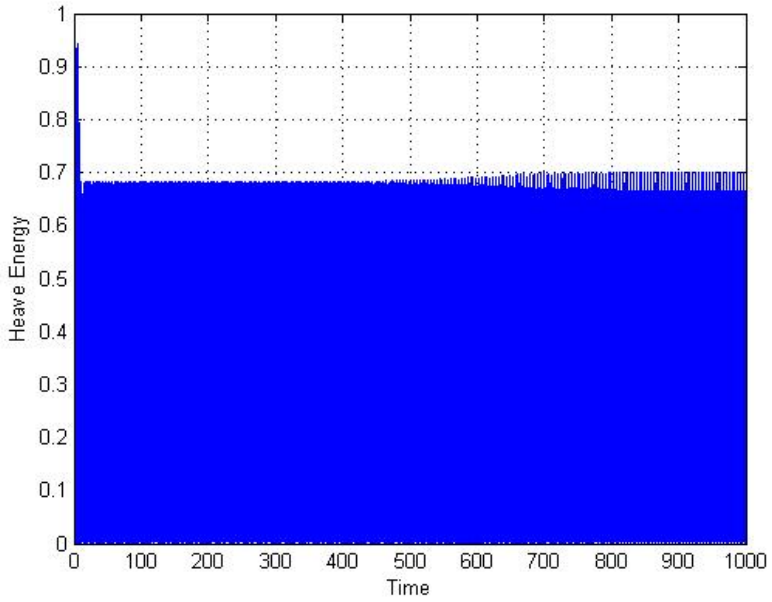

Figure 24. Variation of Heave Energy with respect to Time

Similarly the energy possessed by the secondary system, in roll direction, is given as

$$E_{Roll} = m_2\left(\frac{1}{2}l^2\dot{\varphi}^2 + gl(1-\cos\varphi)\right) \tag{4.14}$$

The expression in Eq. (4.14) is plotted in Figure 25. It is observed that the energy in the secondary system increases with time, even without any forces acting directly on them. Therefore it can be established that the primary system is excited by the wave action and the energy level is saturated. And there is spillover of energy from the primary system to the secondary system, resulting in development of roll motions, without any external forces acting on it. So the energy possessed by the secondary system is due to the phenomenon of parametrically roll resonance.

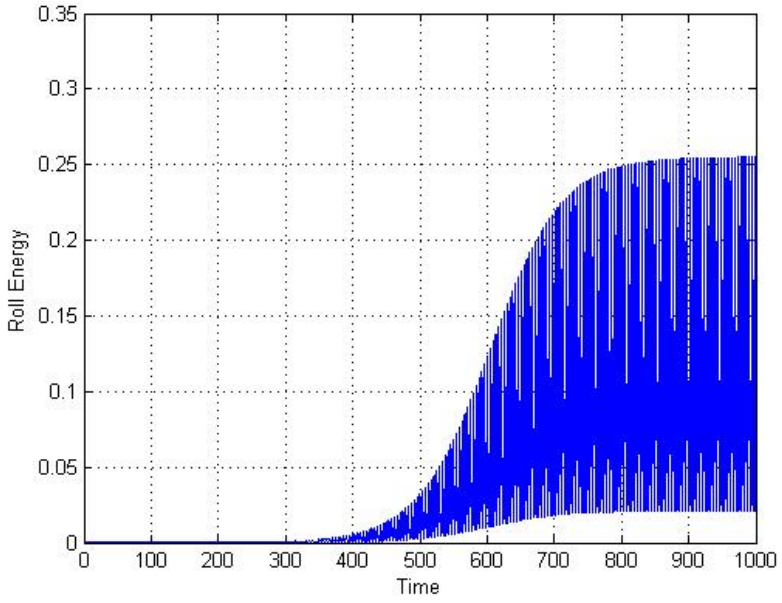

Figure 25. Variation of Roll Energy with respect to Time

Heave-Roll model for SSF

The above mentioned ship model be modified and is utilized for the dynamic study of SSF.

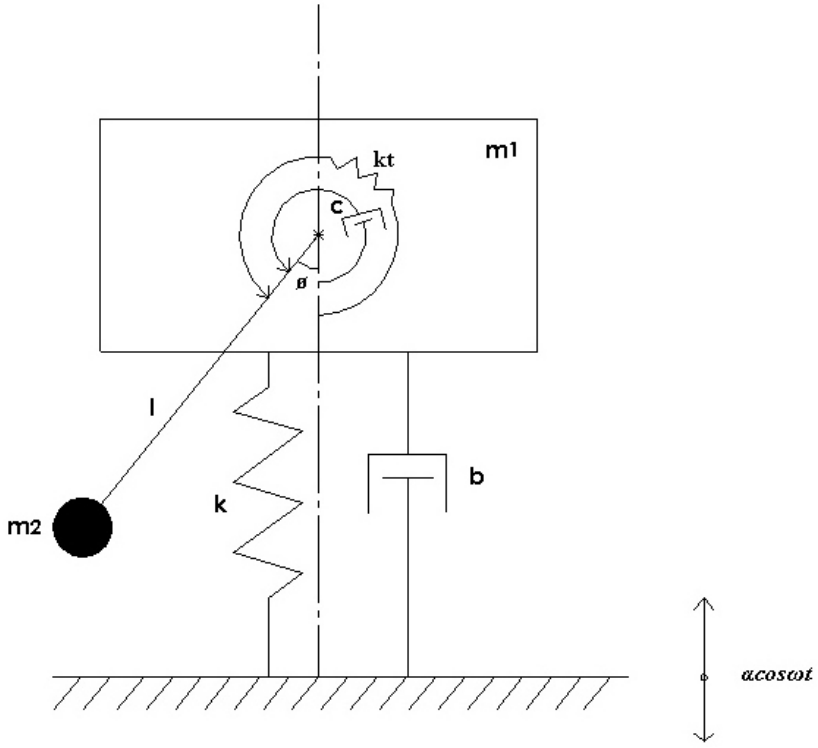

Figure 26. Heave-Roll model for SSF

In Figure 26, a modified version of heave-roll model is described, which would represent the dynamic study of SSF. The SSF working is considered equivalent to a mass-spring-damper system. Similar to the ship model, m_1 represents the total mass of the SSF and m_2 represents the mass of the fluid inside the inner chamber in stable condition of SSF. The mass m_1 is mounted on a linear spring, with spring constant k and a dashpot, with a linear damping coefficient of b. And the mass m_2, attached to mass m_1 by rod of length l, which would act as a pendulum. Also a rotational spring constant, k_t, is added to the system, which would add to the rotational damping coefficient c and help in

stabilizing the SSF. The SSF displaces in the vertical direction by a distance of z and rolls at an angle of ϕ.

For the system of SSF the equations of motions are given by Lagrange's equation, detailed derivation of which is shown in Appendix B.

$$(m_1 + m_2)\{\ddot{z} - \alpha\omega^2 \cos(\omega t)\} + b\dot{z} + kz + m_2 l\{\ddot{\phi}\sin(\phi) + \dot{\phi}^2 \cos(\phi)\} = 0 \quad (4.15)$$

$$m_2 l^2 \ddot{\phi} + c\dot{\phi} + k_t\phi + m_2 gl\sin(\phi) + m_2 l\{\ddot{z} - \alpha\omega^2 \cos(\omega t)\sin(\phi)\} = 0 \quad (4.16)$$

It is observed that the above equations are converted to the dimensionless form as the following

$$\ddot{x} + \bar{B}\dot{x} + q^2 x + \mu\{\ddot{\phi}\sin(\phi) + \dot{\phi}^2 \cos(\phi)\} = a\eta^2 \cos(\eta\tau) \quad (4.17)$$

$$\ddot{\phi} + \bar{C}\dot{\phi} + \sin(\phi) + q_t^2\phi + \{\ddot{x} - a\eta^2 \cos(\eta\tau)\}\sin(\phi) = 0 \quad (4.18)$$

The heave motions for the given system, as per Eq. (4.17) is plotted with respect time in Figure 27. It is observed that the heave motions are bounded within limits in heave direction, similar to the case shown in Figure 21.

The roll motions for the given system, as per Eq. (4.18) is plotted with respect time in Figure 28, for the value of $q_t = 0.1$. It is observed that the amplitude of the roll motions increases as the time proceeds, similar to the case as shown in Figure 22. But note that development of roll motions are delayed, thereby indicating better stability of the system with time. This stability is due to the effect of suction stabilization on the system. Further it is observed that maximum amplitude of roll motion for SSF is less compared to the ship model, indicating its higher damping effect and more stability.

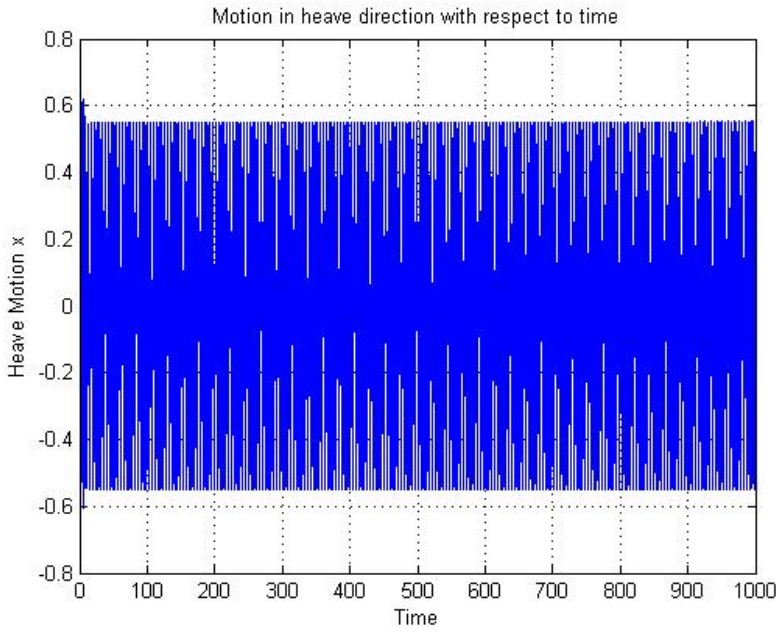

Figure 27. Motion in Heave direction with respect to Time for SSF

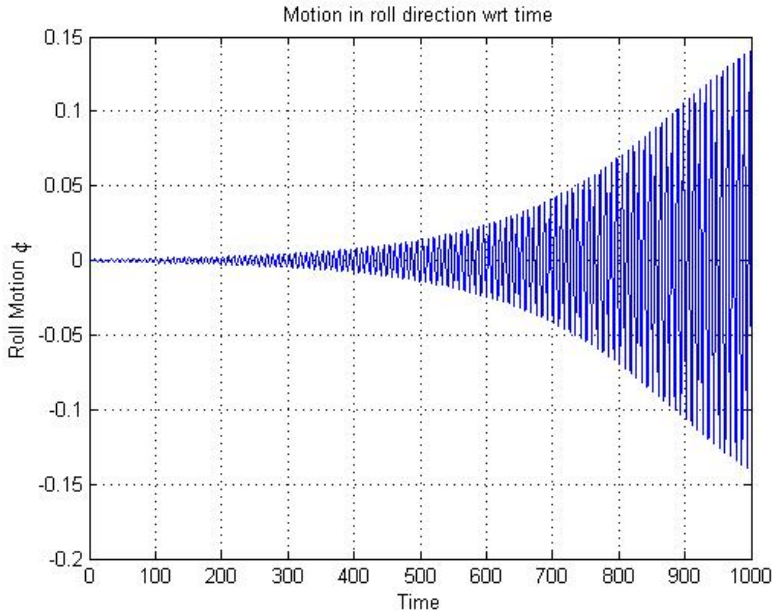

Figure 28. Motion in Roll direction with respect to Time for SSF

The semi trivial solution of the Eq. (4.17) and Eq. (4.18) are given as

$$x_0(\tau) = a(M\cos(\eta\tau) + N\sin(\eta\tau)) \tag{4.19}$$

$$\phi_0(\tau) = 0 \tag{4.20}$$

Where $M = \frac{\eta^2(q^2 - \eta^2)}{(q^2 - \eta^2)^2 + (\bar{B}\eta)^2}$ and $N = \frac{\bar{B}\eta^3}{(q^2 - \eta^2)^2 + (\bar{B}\eta)^2}$. And by adding small perturbations to x and ϕ as

$$x = x_0 + s \tag{4.21}$$

$$\phi = \phi_0 + \theta \tag{4.22}$$

And with first order approximation we get the following equations

$$\ddot{s} + \bar{B}\dot{s} + q^2 s = 0 \tag{4.23}$$

$$\ddot{\theta} + \bar{C}\dot{\theta} + (1 + q_t^2)\theta - a\eta^2\{(1 + M)\cos(\eta\tau) + N\sin(\eta\tau)\}\theta = 0 \tag{4.24}$$

Eq. (4.23) is a homogenous differential equation, with constant coefficients, the solution of which is stable. But Eq. (4.24) is a Mathieu equation, whose stability is dependent on different parameters. For the first approximation, by substituting Eq. (3.23) in Eq. (4.24) , and solving for the non-trivial solutions for C_1 and C_2, we get the following condition

$$(1 + q_t^2 - \frac{1}{4}\eta^2)^2 + \frac{1}{4}\bar{C}^2\eta^2 - \frac{1}{4}a^2\eta^2\{(1 + M)^2 + N^2\} = 0 \tag{4.25}$$

The value a_c here, represents the critical value of wave amplitude above which resonance occurs, which can be expressed as

$$a_c = \sqrt{\frac{4}{\eta^4}\left[\frac{\left(\left(1+q_t^2-\frac{\eta^2}{4}\right)^2+\frac{\eta^2\bar{C}^2}{4}\right)}{\left(1+M\right)^2+N^2}\right]} \tag{4.26}$$

The expression in Eq. (4.26) is plotted in Figure 29, when $q_t = 2$. By observing the η versus q graph of the same plot, the threshold amplitude of the system is found to have higher values, which is shown by the white region, for initial values of η and q. Therefore the system is more stable for the initial values of η and q. It is observed that the stability region is more compared to that in Figure 23. Therefore the system becomes more stable due to the q_t increament, which depicts the effect of suction stabilization.

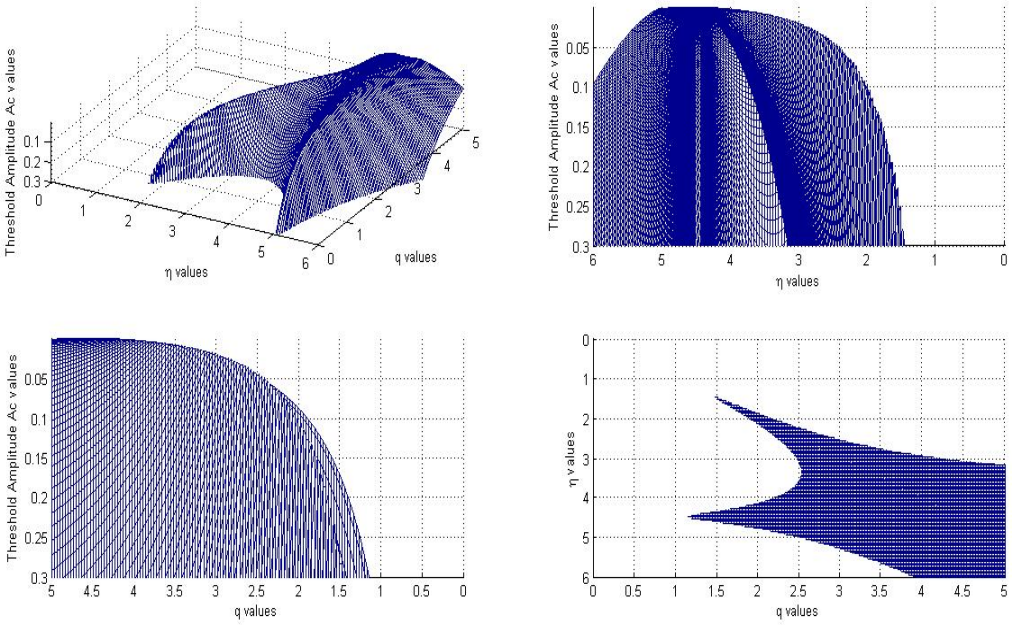

Figure 29. Variation of Threshold Amplitude with η and q values when q_t =2

The expression in Eq. (4.26) is plotted in Figure 30, when $q_t = 5$. It is observed that the stability region is more compared to that in Figure 29. So the system becomes further stable when the q_t is further increased. This proves that by increasing the suction stabilization effect in the SSF, the q_t increases thereby increasing the white region in the graph which further increases the stability of the system.

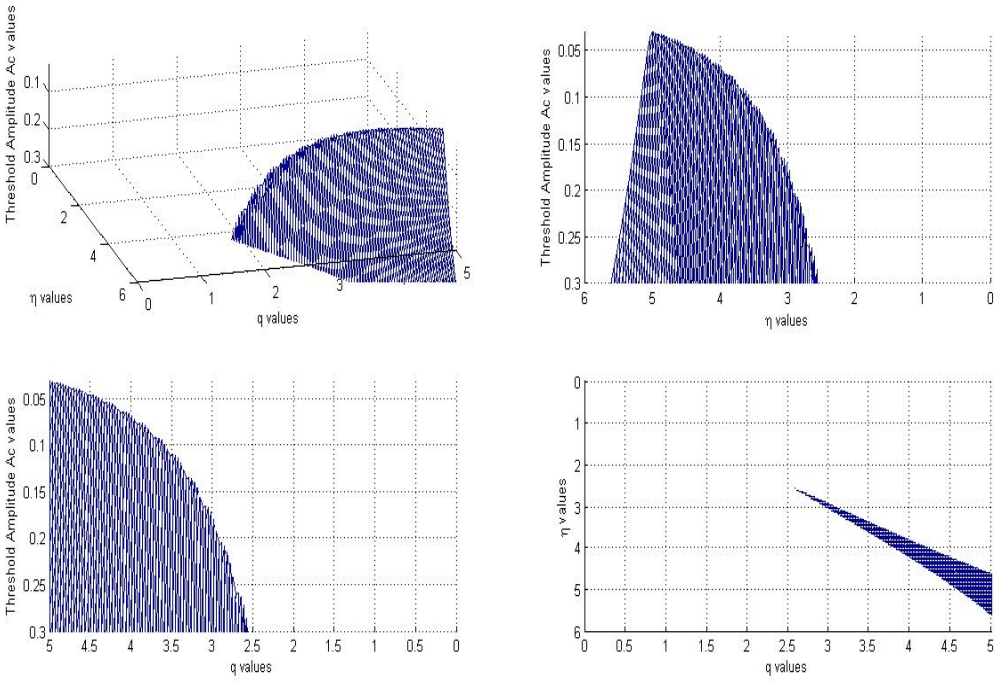

Figure 30. Variation of Threshold Amplitude with η and q values when $q_t = 5$

Energy Transfer for Heave-Roll model for SSF

The system of SSF can also be divide into primary system and secondary system, similar to the ship model. The primary system possess the energy due to the heave motions and the secondary system possess the energy due to the roll motions. The equation for energy of the primary system modifies as

$$E_{Heave} = \frac{1}{2}(m_1 + m_2)\dot{x}^2 \tag{4.27}$$

The expression in Eq. (4.27) is plotted in Figure 31. It is observed that the energy in the primary system remains almost constant with time, as the base is constantly excited with wave action, similar to the ship model in Figure 24.

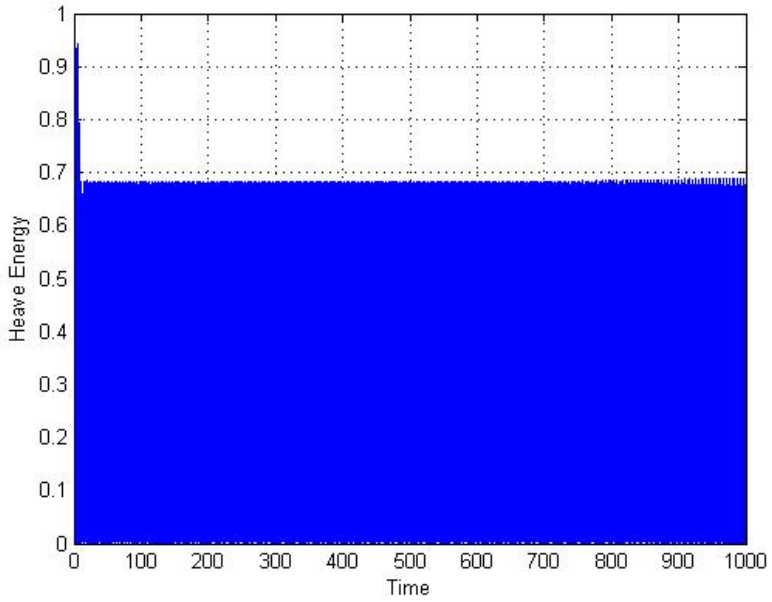

Figure 31. Variation of Heave Energy with respect to Time for SSF

Similarly the energy possessed by the secondary system, in roll direction, is modified as

$$E_{Roll} = m_2\left(\frac{1}{2}l^2\dot{\phi}^2 + gl(1-\cos\phi)\right) \tag{4.28}$$

The expression in Eq. (4.28) is plotted in Figure 32. It is observed that the energy in the secondary system increases with time, even without any forces acting directly on them, as shown in the ship model in Figure 25. In this case too, a spillover of energy is observed. But note that the energy amplitude for roll energy is much lower compared to

that of ship model. And also the development of roll energy is delayed, implying that suction stabilization reduces the roll energy and also delays the spillover of energy, thereby delaying the resonant condition. Therefore the stability of the SSF are more even, under dynamic conditions of wave action and also performs better for the condition of parametric roll resonance.

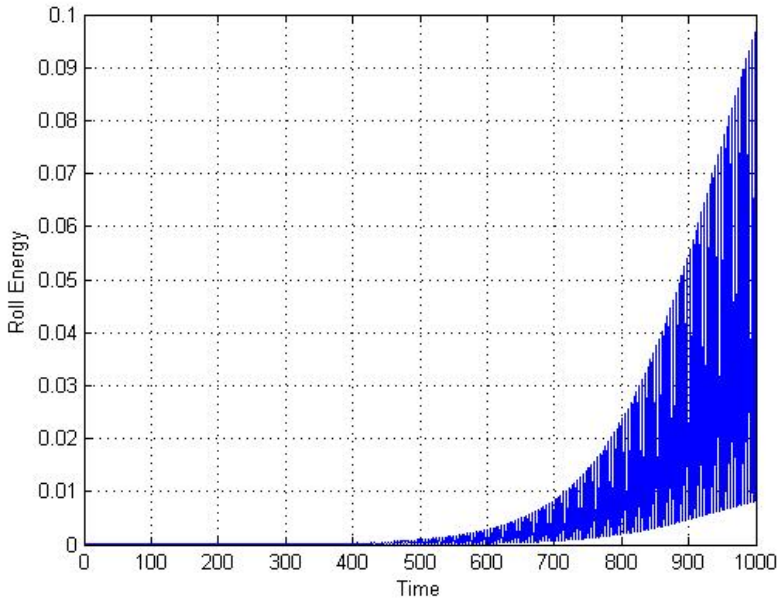

Figure 32. Variation of Roll Energy with respect to Time for SSF

Detailed Heave-Roll Model for SSF

The Heave-Roll model for SSF, explained earlier, is investigated in detail in this section. The study of SSF in this model, is restricted to the specific geometry of SSF and it is also compared to the dynamics of a spring-mass system. Consider a float of circular section, as shown in Figure 33 (Vendrell, 2013).

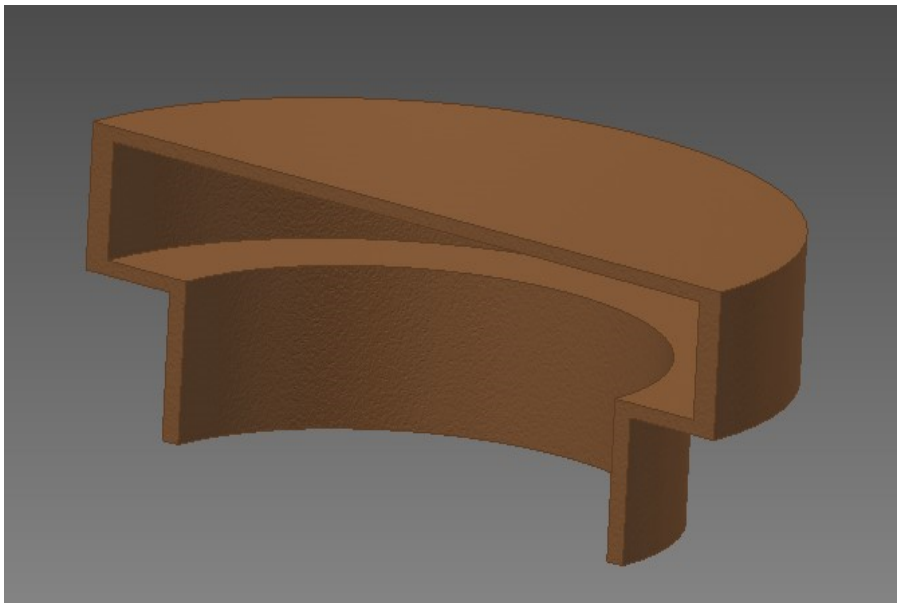

Figure 33. SSF with Cylindrical Inner Chamber (Vendrell, 2013)

The inner chamber consists of fluid due to the suction stabilization, which also heels as the float heels, as shown in Figure 34. It is observed that there is wedge formation DOK similar to the one in Figure 19. But the wedge section in Figure 34 is cylindrical in section, because the ballast chamber in the SSF is cylindrical in shape of radius, R and height, $2h$. Let the SSF heel to an angle θ about O, which is the center of the ballast chamber. The point J represents the center of gravity of the wedge section DOK at a distance of z', from the center of the ballast chamber. Let the total mass of the float with the fluid inside be denoted as m_1, the mass moment of inertia as I and the mass of the fluid of the wedge section as m_2. Consider the float to have a linear damping coefficient, b, a linear spring constant, k and a rotational damping coefficient, c. And the heave motions as considered to be acting at point O, at half the height of the ballast chamber, by a wave varying as $a\cos\omega t$.

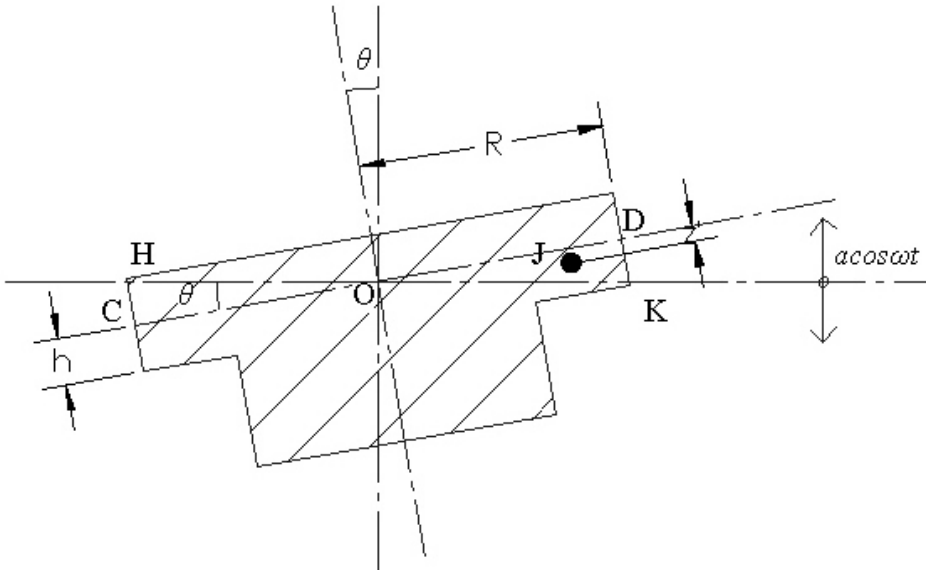

Figure 34. Heeling of SSF with Cylindrical Inner Chamber

The mass of the fluid, m_2, in the cylindrical wedge section DOK can be expressed as (P.N. Modi, 1995)

$$m_2 = \frac{2}{3} R^2 h \rho \tag{4.29}$$

Where ρ is the density of the fluid inside and outside. But the height of the wedge section can be replaced as $h = R\tan\theta$ and for smaller angles $tan\theta \approx \theta$. Therefore Eq. (4.29) becomes

$$m_2 = \frac{2}{3} \rho R^3 \theta \tag{4.30}$$

Using the above equations, the Lagrange's equations of motions are derived, which is shown in detail in Appendix-C, after linearization is

$$m_1\ddot{z} - m_1 a\omega^2 \cos\omega t - \frac{2}{3}R^3\rho\theta a\omega^2 \cos\omega t - \frac{2}{3}R^3\rho\dot{\theta}a\omega \sin\omega t + kz + ka\cos\omega t + \frac{2}{3}R^3\rho g\theta + b\dot{z} = 0$$

(4.31)

$$-\frac{2}{3}\times 0.7R^4\rho\theta a\omega^2 \cos\omega t + I\ddot{\theta} - \frac{1}{3}R^3\rho a^2\omega^2 \sin^2\omega t + \frac{2}{3}\rho R^3\dot{z}a\omega \sin\omega t + \frac{2}{3}\rho R^3 gz + \frac{2}{3}\rho R^3 ga\cos\omega t + \frac{4}{3}\times 0.7R^4\rho g\theta + c\dot{\theta} = 0$$

(4.32)

The state space form of the above equations can be expressed as

$$\frac{d}{dt}\begin{Bmatrix} z \\ \dot{z} \\ \theta \\ \dot{\theta} \end{Bmatrix} = \begin{bmatrix} 0 & 1 & 0 & 0 \\ \frac{-k}{m_1} & \frac{-b}{m_1} & \frac{-2}{3m_1}R^3\rho g & 0 \\ 0 & 0 & 0 & 1 \\ \frac{-2}{3I}R^3\rho g & 0 & \frac{-4}{3I}\times 0.7R^4\rho g & \frac{-c}{I} \end{bmatrix} \begin{Bmatrix} z \\ \dot{z} \\ \theta \\ \dot{\theta} \end{Bmatrix} + \begin{bmatrix} 0 & 0 & 0 & 0 \\ 0 & 0 & \frac{2}{3m_1}R^3\rho a\omega^2 \cos\omega t & \frac{2}{3m_1}R^3\rho a\omega \sin\omega t \\ 0 & 0 & 0 & 0 \\ 0 & \frac{-2}{3I}R^3\rho a\omega \sin\omega t & \frac{2}{3I}\times 0.7R^4\rho a\omega^2 \cos\omega t & 0 \end{bmatrix} \begin{Bmatrix} z \\ \dot{z} \\ \theta \\ \dot{\theta} \end{Bmatrix} + \begin{bmatrix} 0 \\ a\omega^2 \cos\omega t - \frac{k}{m_1}a\cos\omega t \\ 0 \\ \frac{1}{3}R^3\rho^2 a\omega^2 \sin^2\omega t - \frac{2}{3}R^3\rho g a\cos\omega t \end{bmatrix}$$

(4.33)

The above expression in Eq. (4.33) can also be expressed, in short, as

$$\dot{X} = \{A_0 + A(t)\}X + F(t) \tag{4.34}$$

Where A_0, represents the constant matrix and $A(t)$, the time varying matrix and $F(t)$, the time varying forcing matrix. Now Eq. (4.34) is similar to the Hill-Mathieu Equation and the stability boundaries are determined by applying Floquet theory, as discussed in Chapter-3. The absolute value of the eigen value of the FTM of the system of SSF is determined for varying wave amplitude and angular velocity terms, as shown in Figure 35. Similar results were obtained when the stability was determined using the characteristic exponents.

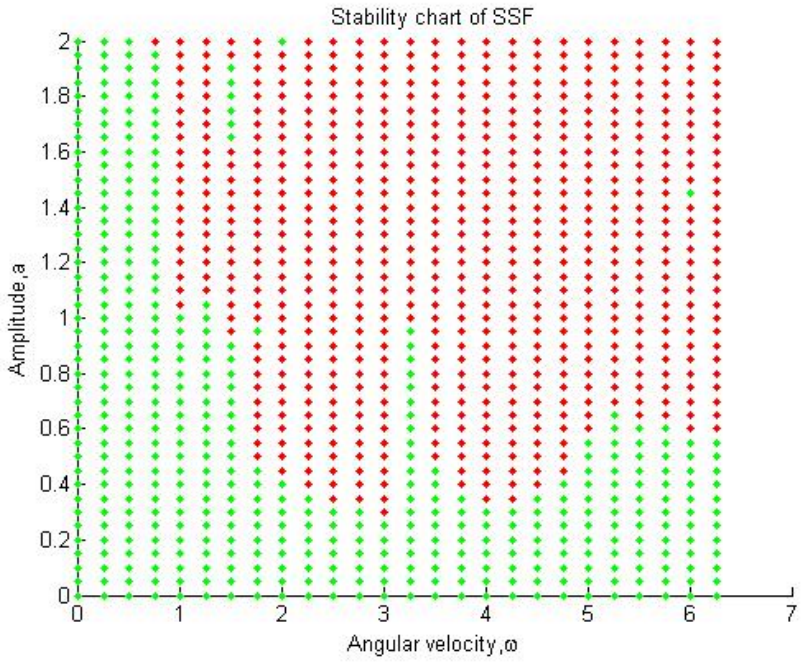

Figure 35. Stability Chart of SSF

The green dots indicate the stable region and the red dots indicate the unstable region for the system. The same was determined by varying the values of the linear damping coefficient, *b* and the rotational damping coefficient, *c*.

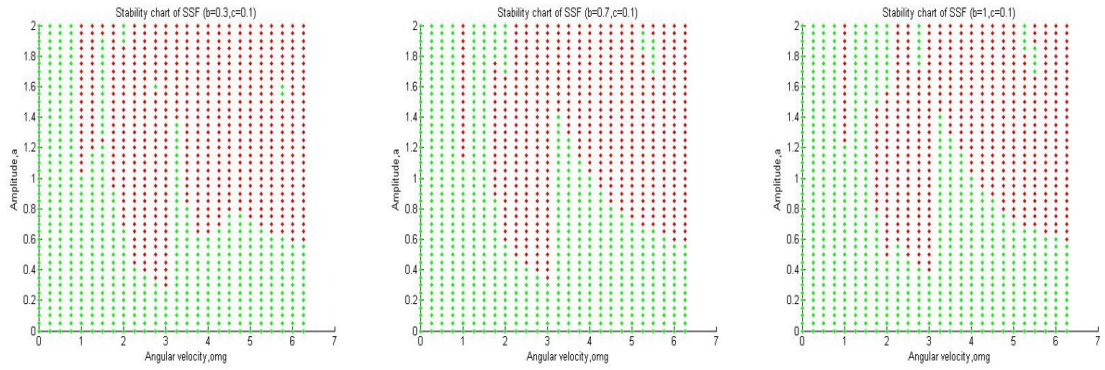

Figure 36. Stability Charts of SSF for b=0.3, 0.7, 1.0 and c=0.1

In Figure 36, the stability charts are obtained by keeping the rotational damping, c, constant and increasing the linear damping constant, b. It is observed that the stability region for the system is increased more from $\omega = \pi$ to $\omega = 2\pi$, as the linear damping increases from $b = 0.1$ to $b = 1.0$.

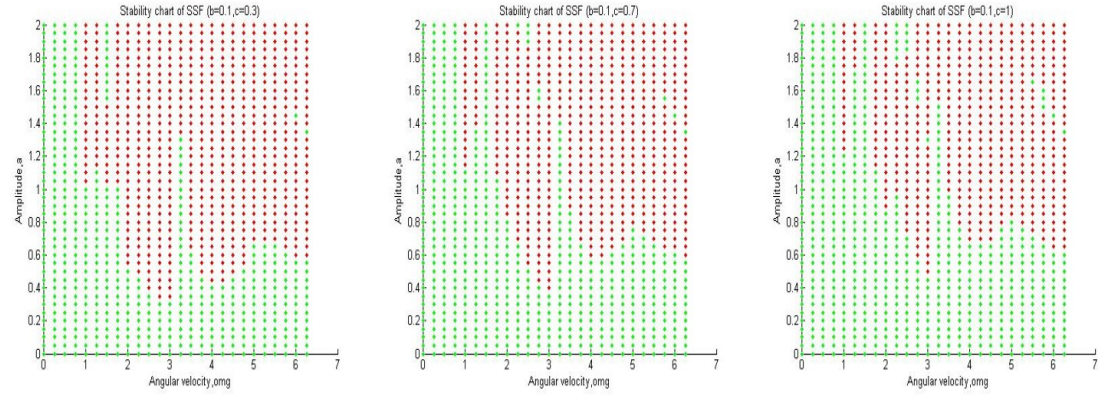

Figure 37. Stability Charts of SSF for c=0.3, 0.7, 1.0 and b=0.1

In Figure 37, the stability charts are obtained by keeping the linear damping, b, constant and increasing the rotational damping constant, c. It is observed that the stability region for the system is increased more from $\omega = 0$ to $\omega = \pi$, as the linear damping increases from $c = 0.1$ to $c = 1.0$.

Chapter 5
DYNAMICS OF SSF IN TURBINE APPLICATION

The SSF, as discussed earlier, can be employed for offshore wind turbine applications. In such an application, the floating platform will be experiencing the wave loading and the turbine part will be experiencing the wind loading. SSF can resist the roll motion, but not the horizontal wave forces, which can shift the position of the platform. In order to resist the horizontal shifting, the platforms need to be anchored to the sea bed with the help of mooring lines. So the SSF is almost towed to a fixed position, but can slide horizontally to some extent and the turbine performance and requirements can be estimated for a specific location. So the dynamics considered in this model is approximated similar to that of the gravity based wind turbine model.

Mathematical model for Turbine Application

A rigid turbine structure is mounted on a SSF in a stable position, as shown in Figure 38. And consider it is experiencing a time dependent net wind force, F, horizontally at an equivalent height, $h_{0,}$ as shown in Figure 39. The force causes the platform to displace horizontally, x and also to heel to an angle, θ, about the point O, which is in line with the water plane. The mooring lines are expected to provide a stiffness, of linear stiffness constant, k_1 and damping effect in the horizontal motion, with a linear damping coefficient, $c_{1.}$ The rotational damping, c_0 and rotational stiffness, k_0, are provided by SSF. The total weight of the turbine structure and float is considered to be acting downwards at the center of gravity of the assembly, at G. And the mass moment of inertia about G is given by J_G and about the center of heel, O, is given by J_O. The buoyant force, equivalent to the weight of the assembly, is acting in the upwards direction, at B.

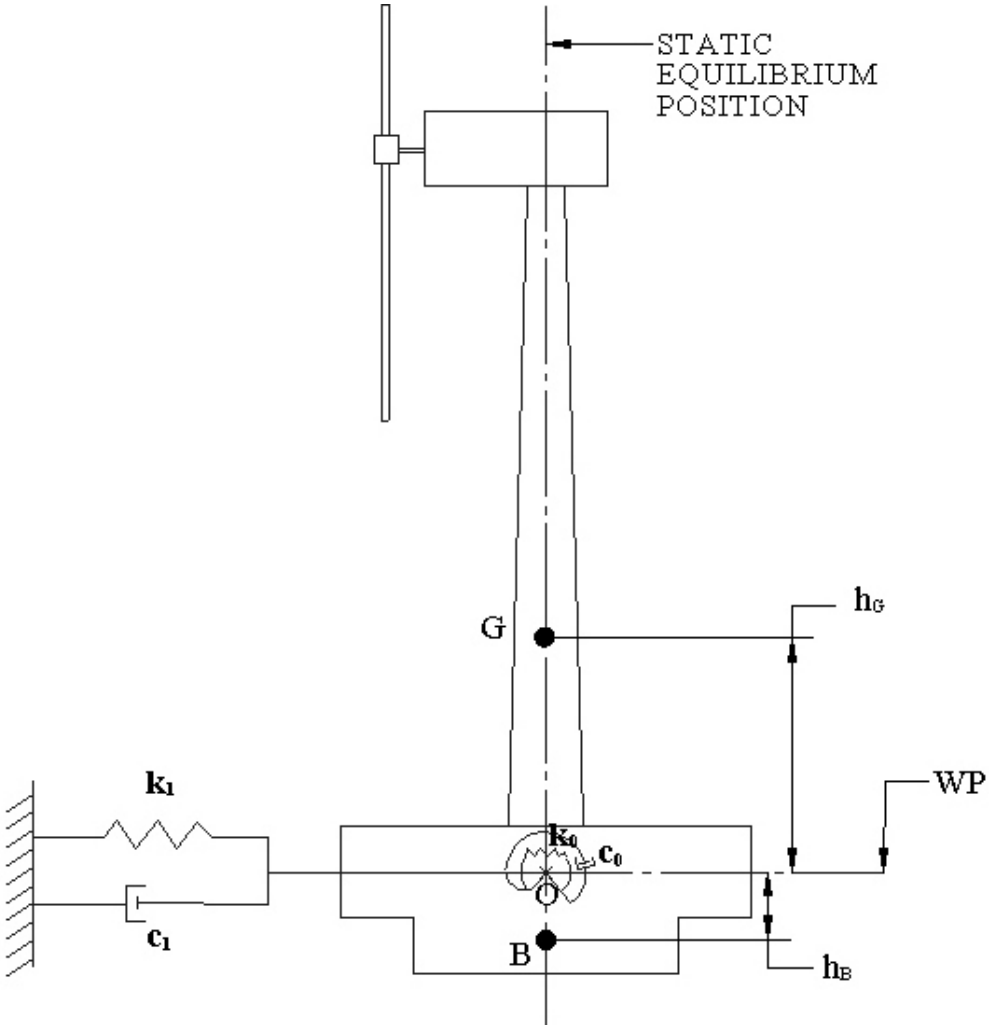

Figure 38. Wind Turbine model in Stable Position (Wilson, 2003)

The Lagrange's equations of motion, derived in detail in Appendix-D, are given as (Wilson, 2003)

$$m\ddot{x} + mh_G\ddot{\theta} + c_1\dot{x} + k_1 x = F \tag{5.1}$$

$$mh_G\ddot{x} + (J_G + mh_G^2)\ddot{\theta} + c_0\dot{\theta} + (k_0 - mgh_G - mgh_B)\theta = h_0 F + Mc \tag{5.2}$$

But by using parallel axis theorem, we get

$$J_O = J_G + mh_G^2 \tag{5.3}$$

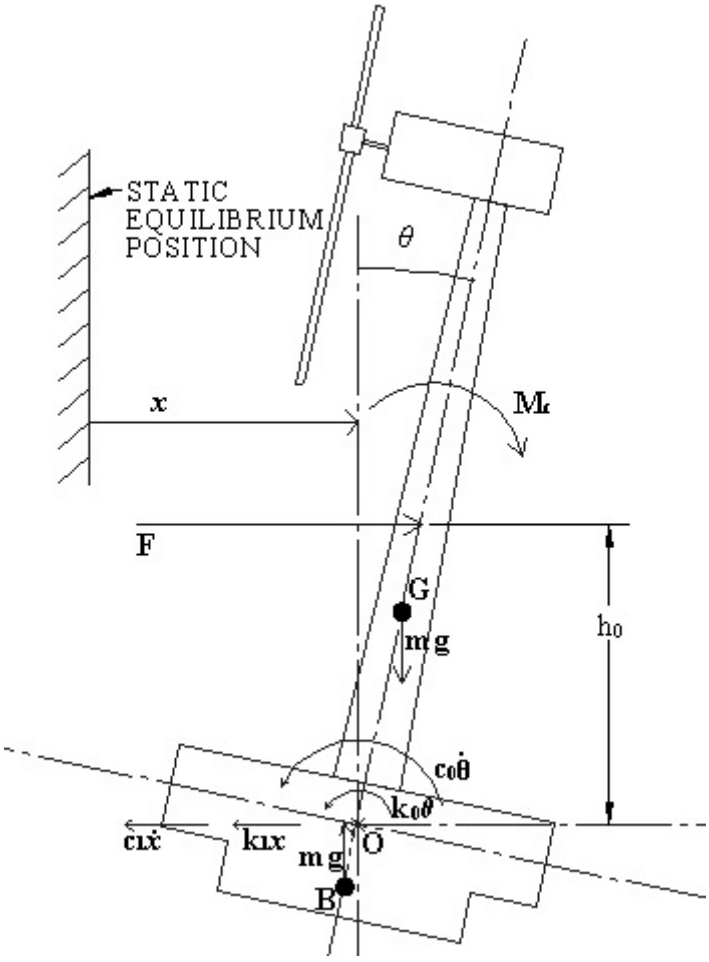

Figure 39. Heeling of Wind Turbine model with SSF

By using Eq. (5.3) in Eq. (5.2) and Eq. (5.1) and modifying them into the state space form, we get

$$\begin{bmatrix} m & 0 \\ 0 & J_G \end{bmatrix}\begin{bmatrix} \ddot{x} \\ \ddot{\theta} \end{bmatrix}+\begin{bmatrix} \frac{J_O}{J_G}c_1 & -\frac{mh_G}{J_G}c_0 \\ -h_G c_1 & c_0 \end{bmatrix}\begin{bmatrix} \dot{x} \\ \dot{\theta} \end{bmatrix}+\begin{bmatrix} \frac{J_O}{J_G}k_1 & -\frac{mh_G}{J_G}(k_O - mgh_G - mgh_{B)} \\ -h_G k_1 & (k_O - mgh_G - mgh_B) \end{bmatrix}\begin{bmatrix} x \\ \theta \end{bmatrix}$$
$$=\begin{bmatrix} \left\{1-\frac{mh_G}{J_G}(h_O - h_G)\right\}F - \frac{mh_G}{J_G}M_C \\ M_C + (h_O + h_G)F \end{bmatrix}$$

(5.4)

Considering the force, F and the moment, M_C in Eq. (5.4), as time dependent variables and by converting the equation into a non-dimensional form, the displacement of the wind turbine in horizontal direction is plotted in Figure 40. It is observed that there is movement in the horizontal direction initially, but later it becomes bounded due to the horizontal damping effect of mooring lines. Hence the shifting of the location of the turbine is restricted.

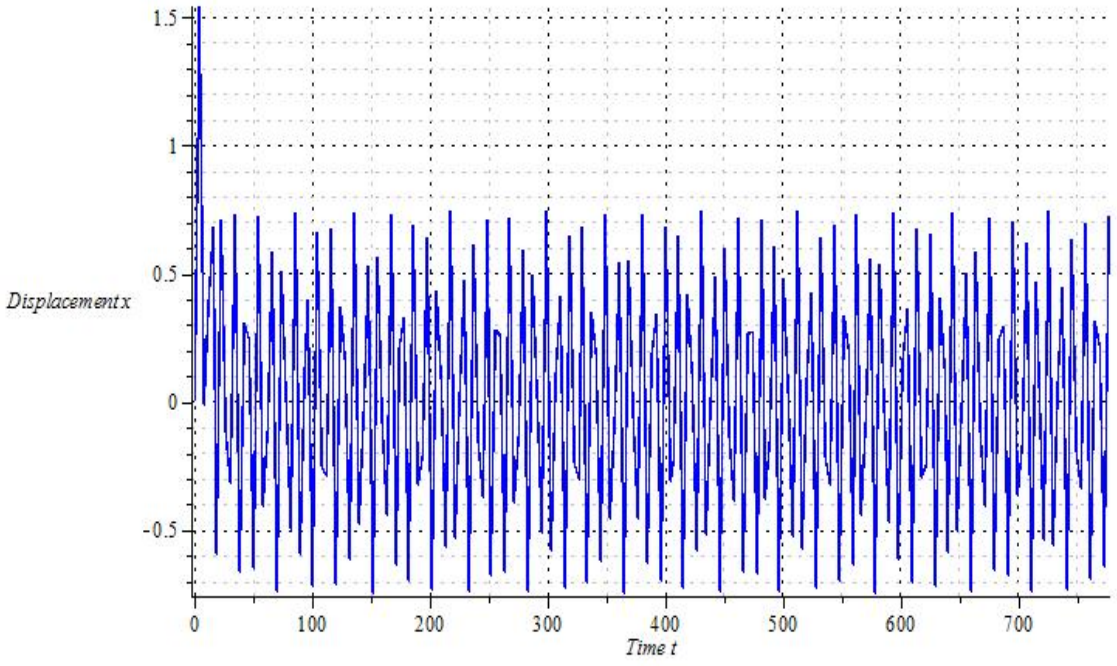

Figure 40. Variation of Horizontal Displacement of Wind Turbine with respect to Time

Using Eq. (5.4) the roll motion of the turbine assembly, about point O, is plotted in Figure 41. Consider the assembly to be initially heeled to a certain angle, due to wave and wind actions. It is observed later that the amplitude of roll motion is reduced subsequently, indicating the damping effect due to suction stabilization. And it tries to stabilize itself without any active controls.

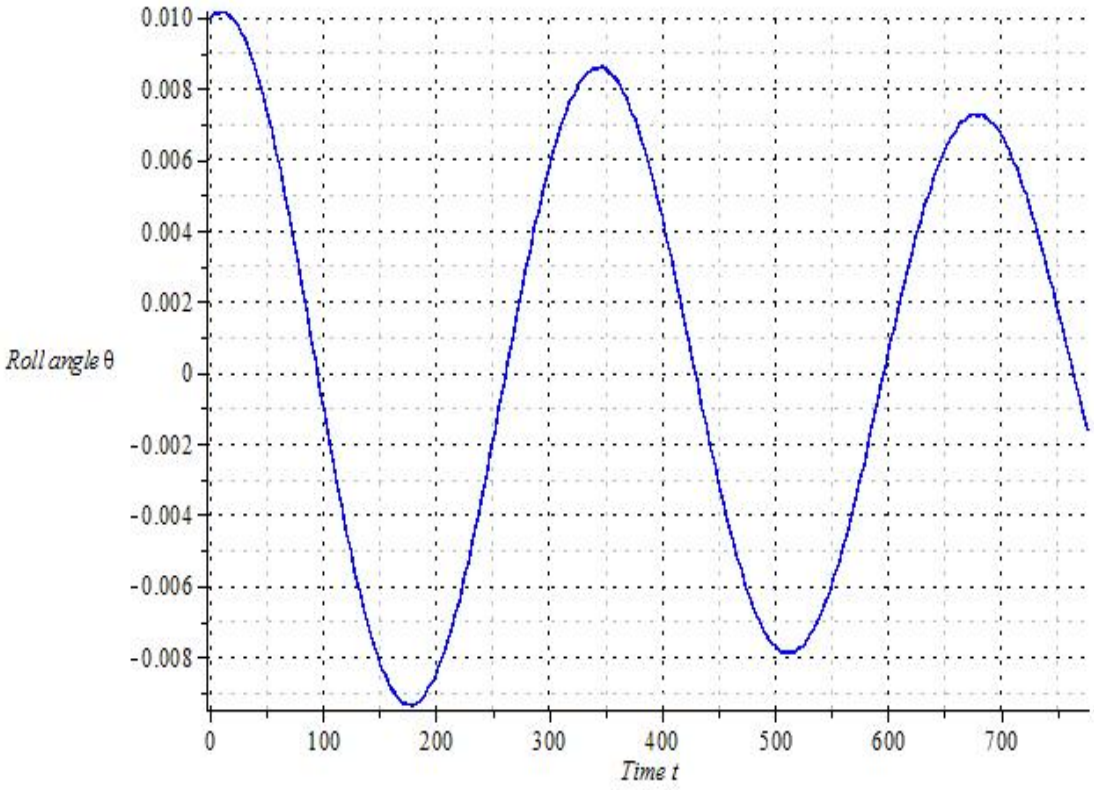

Figure 41. Variation of Heel Angle of Wind Turbine with respect to Time

Chapter 6
EXPERIMENTAL DATA AND RESULTS

The dynamics of SSF was determined analytically in the earlier chapters of the report. The same is verified experimentally using a scaled model of the float of 15 inch diameter in a water tank and also in a pool with a 32 inch diameter float. The approximate replication of wave actions are applied and the motion of the float is captured to study the dynamics.

Experimental Setup

A typical experimental setup appears to be like one shown in Figure 42. The float utilized for the experiment is a 15 inch diameter or a 32 inch diameter circular float, made of rigid foam. The top cover of the float is a transparent conical shaped cover with a hole, which can help to remove the entrapped air in the inner chamber and can be plugged using a rubber cork. In case of a 32 inch diameter float, there is valve at the side, which serves the same purpose. The conical shape provides more volume of water inside the inner chamber, providing more stability for the float, compared to a flat surface on the top. The transparent cover helps to detect the presence of air entrapped in the inner chamber and remove it through the hole. A light weight carbon fiber rod passes through the center of the float vertically and is fixed at the bottom to the float, using two rods passing through it at 90 degrees horizontally. This provides more support for the vertical carbon fiber, while heeling.

The float is immersed in a tank filled with water and the inner chamber is filled with same water, until there is no air bubbles are visible in the inner chamber. The hole

on the cover is plugged and let the SSF float to the water surface. Due to the buoyancy of the material the SSF floats to the surface. The IST effect comes in action and the float stabilizes more due to suction stabilization. The same float acts as a normal float without suction stabilization, when the hole is unplugged and left open. It is observed that the SSF raises up, when the hole is unplugged, because there is no suction pressure anymore and the water inside the inner chamber drains out. On top of the vertical carbon fiber rod, an arrangement to support and house the instrumentation is fixed temporarily. So as the float heels, the carbon fiber rod heels, which in turn tilts the instrumentation assembly too. The instrumentation box senses the motion and records and transmits the signal accordingly.

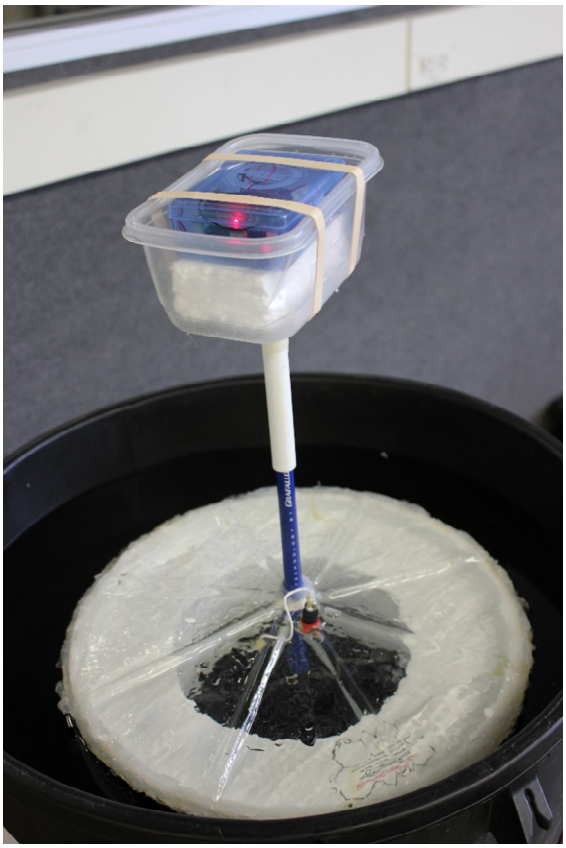

Figure 42. Experimental Setup for 15 inch diameter Float

Similar experiments were conducted with a 32 inch float in a pool. The instrumentation box had the same components, but were mounted on the topside of the cover directly, as shown in Figure 43.

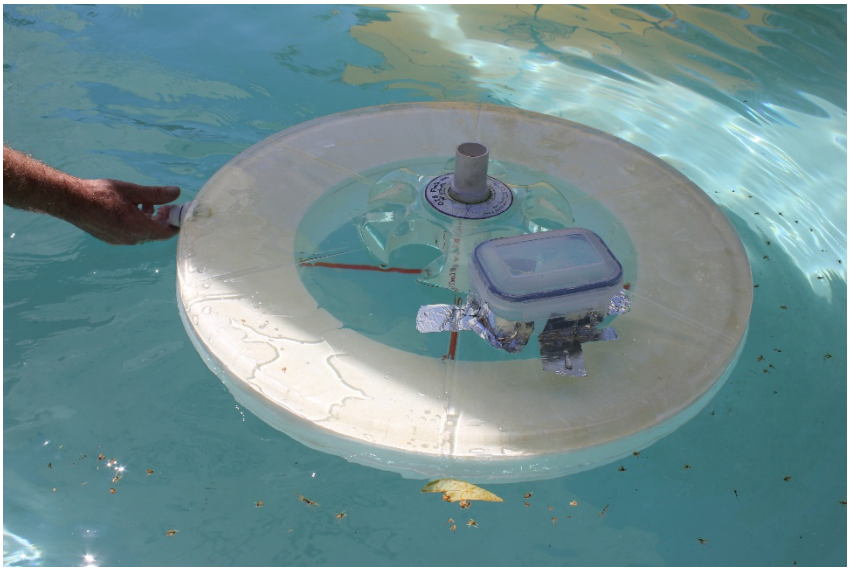

Figure 43. Experimental Setup for 32 inch diameter Float

Before the instrumentation box is mounted on top of the housing, the same is being calibrated using an analog inclinometer, as shown in Figure 44. The test were conducted both in open and closed environment.

Instrumentation

To sense and measure the motions of the float, an Inertial Measuring Unit (IMU), as shown in Figure 45, is utilized. The IMU senses the motion and the orientation and transmits the signal via bluetooth to a computer. The signal obtained is decoded into interpretable formats using MATLAB. To power the IMU, a battery assembly of 4.5 V, as shown in Figure 46, is employed. The instrumentation box, mounted on top of the

carbon fiber rod, contains both IMU and battery assembly, connected to each other, as shown in Figure 47.

Figure 44. Calibration of Setup

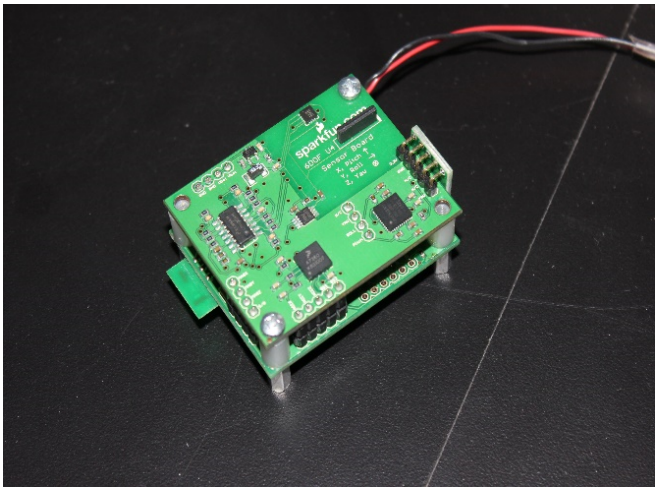

Figure 45. Inertial Measurement Unit (IMU)

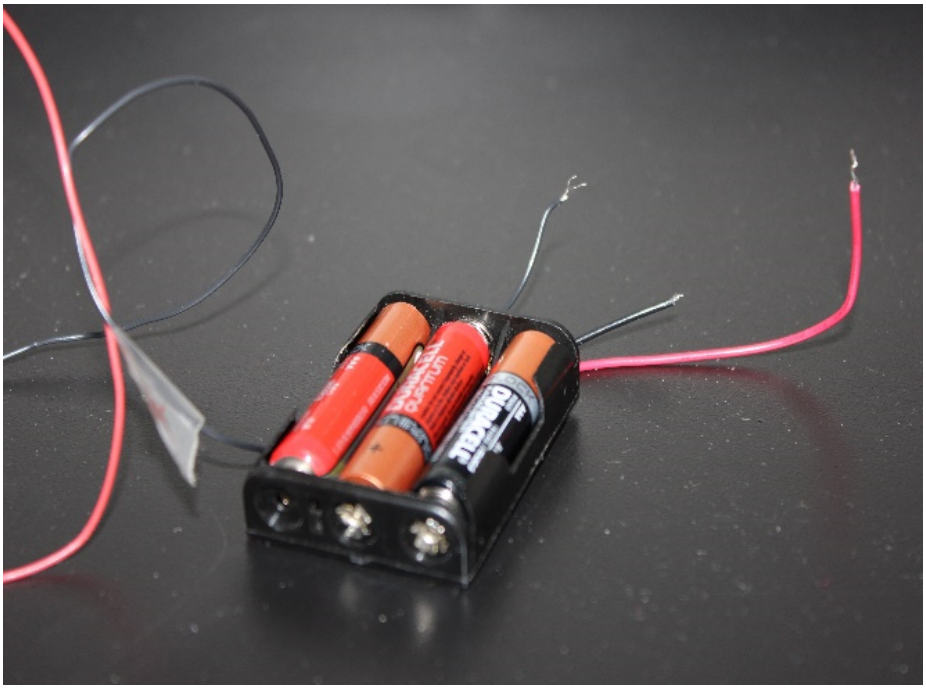

Figure 46. Battery Assembly for IMU

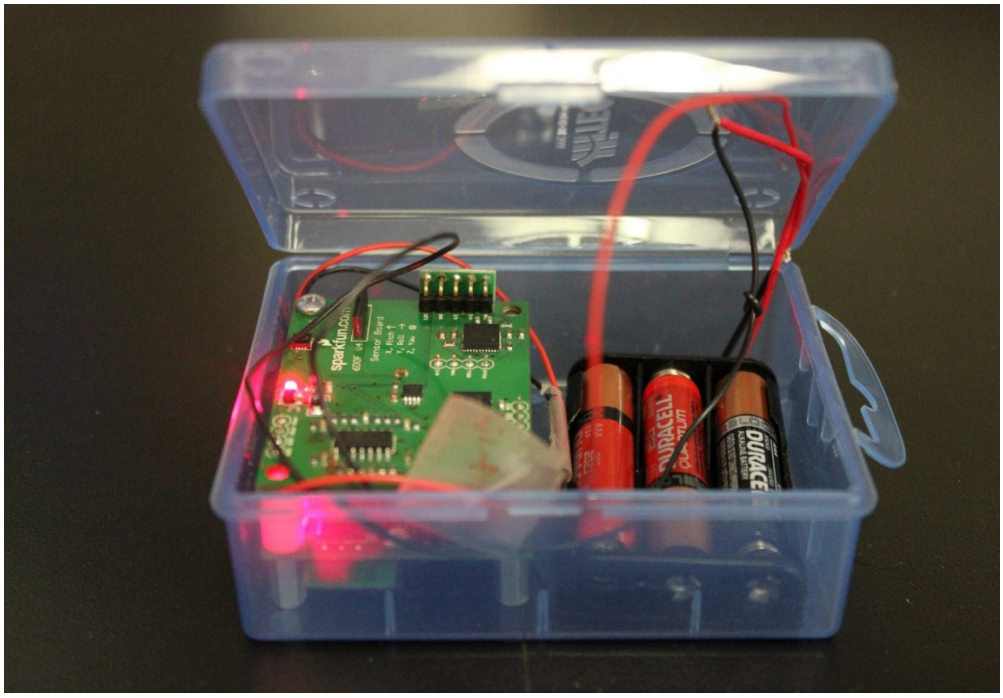

Figure 47. Instrumentation Box

Results

The experiment was conducted on the float involving the IST effect and even without involving the IST effect. So it depicted the behavior of a SSF and a normal float. The IMU was used to sense and record the yaw, pitch and roll motions along with the displacement in three directions. As the yaw motions are not considered in the modeling part and was not observed to significantly affect the dynamics of the SSF, it is not being considered. And due to symmetry in geometry, the float behaves in similar pattern for roll and pitch motions.

The tests were conducted on the 15 inch diameter float initially. The float was initially tested with the hole unplugged and open to the atmosphere, thereby behaving as a normal float, as shown in Figure 48. The motions of the float are captured using the instrumentation box and interpreted. The float was initially heeled to an angle in roll

direction, as shown in Figure 49. It is observed that though there is a damping effect due the fin structure of the float, it does not return back to its stable position. At the end of 27 seconds, the float is still oscillating. There is still amplitude variation of 0-3 degrees.

Figure 48. SSF without IST effect Activated

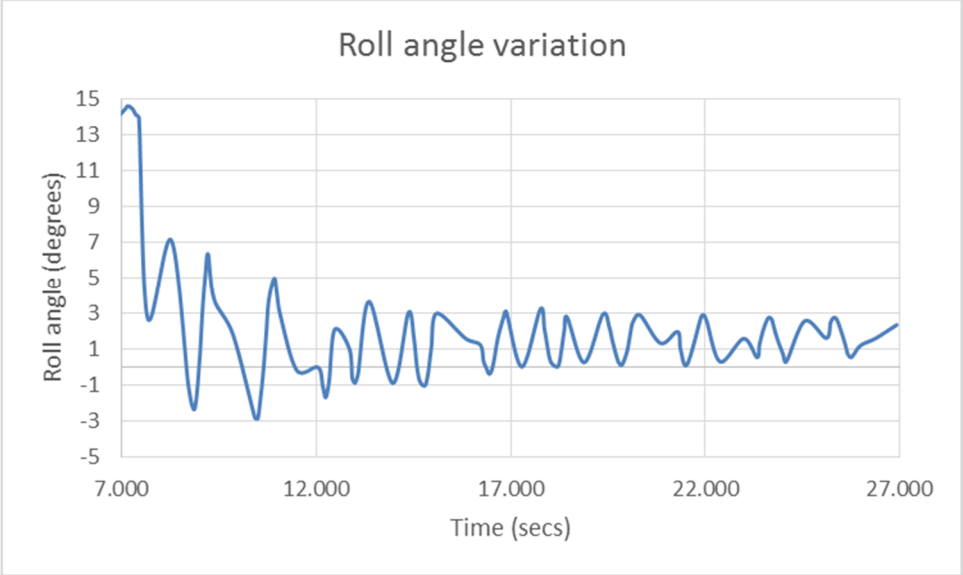

Figure 49. Roll Angle variation without IST effect of 15 inch Float

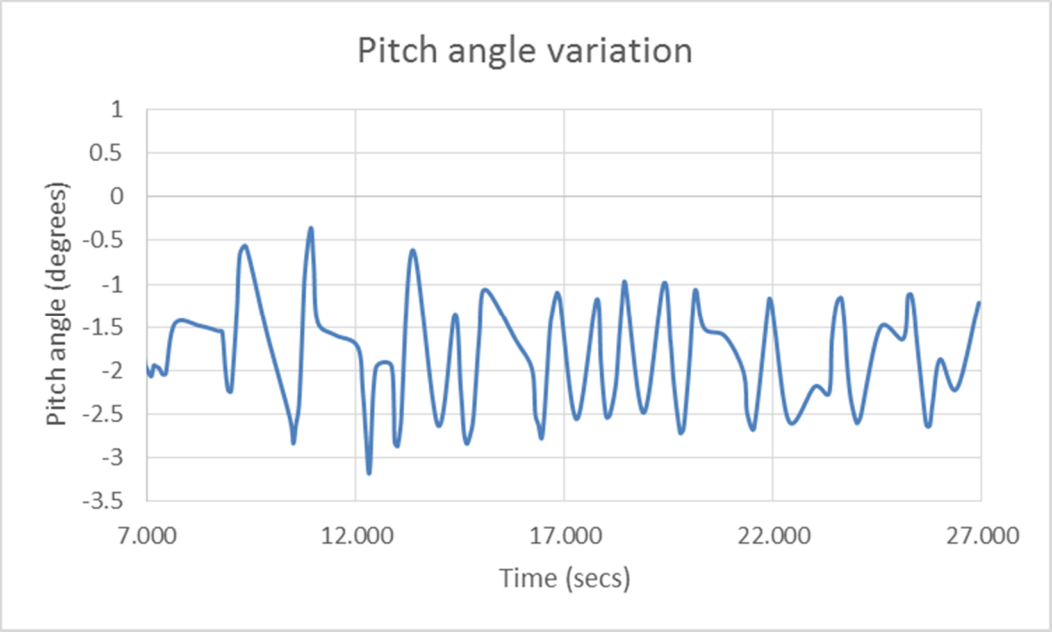

Figure 50. Pitch Angle variation without IST effect of 15 inch Float

The pitch motion recorded simultaneously is shown in Figure 50. It is observed that initially, when the float is heeled in the roll direction, there is no pitch variation. So there was no component of initial heel angle provided to the pitch direction. But eventually variations in pitch angle build up due to pitch roll coupling. And it is also observed that there is no much damping effect in the pitch direction. Though the amplitude of variation is less, it still continues to remain so.

The variation of the angular velocity to the angular displacement, in both pitch and roll motions, are plotted in a phase plane, as shown in Figure 51 and Figure 52 respectively. It is observed that the stable point of the plot is not crowded, indicating that the system is not highly stable.

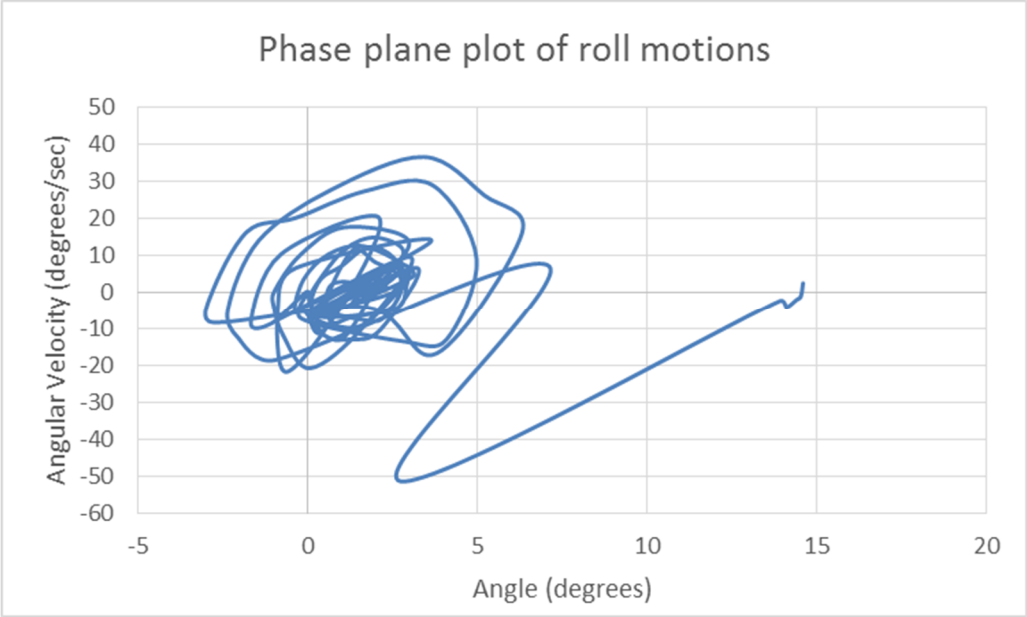

Figure 51. Phase plane plot of Roll motions without IST effect of 15 inch Float

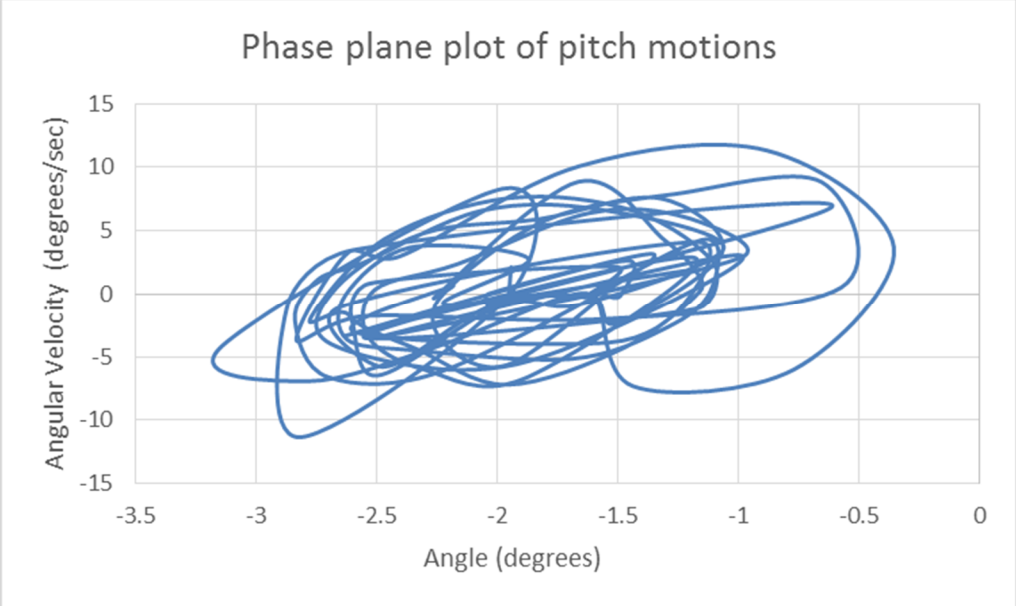

Figure 52.Phase plane plot of Pitch motions without IST effect of 15 inch Float

The float was later filled with water, thereby activating the IST effect, as shown in Figure 53 . The SSF was heeled initially to a roll angle and let the float oscillate freely, as

shown in Figure 54. Simultaneously the variation in the pitch action is also captured, as shown in Figure 55.

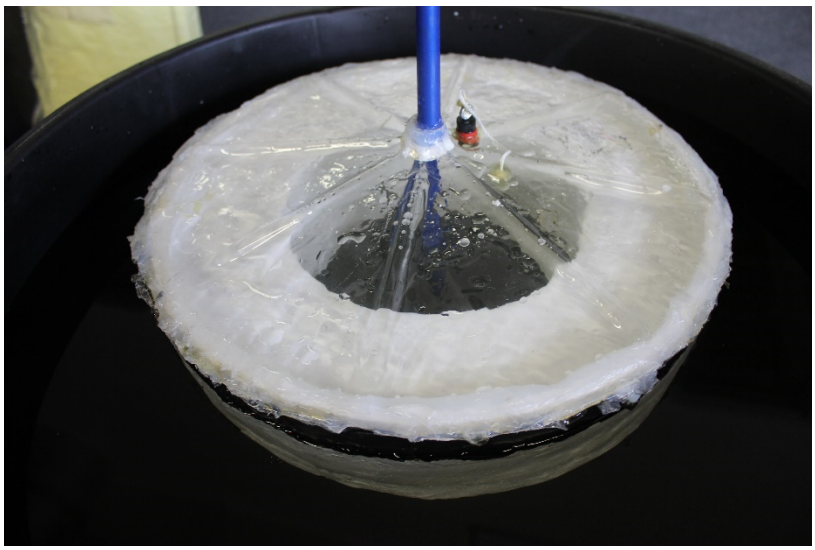

Figure 53. SSF with IST effect Activated

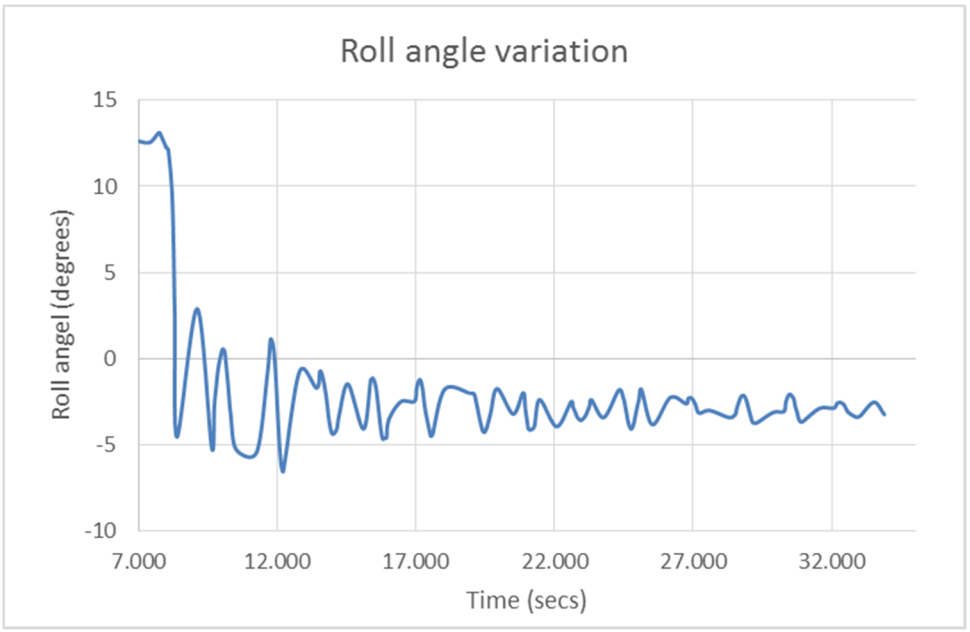

Figure 54. Roll Angle variation with IST effect of 15 inch Float

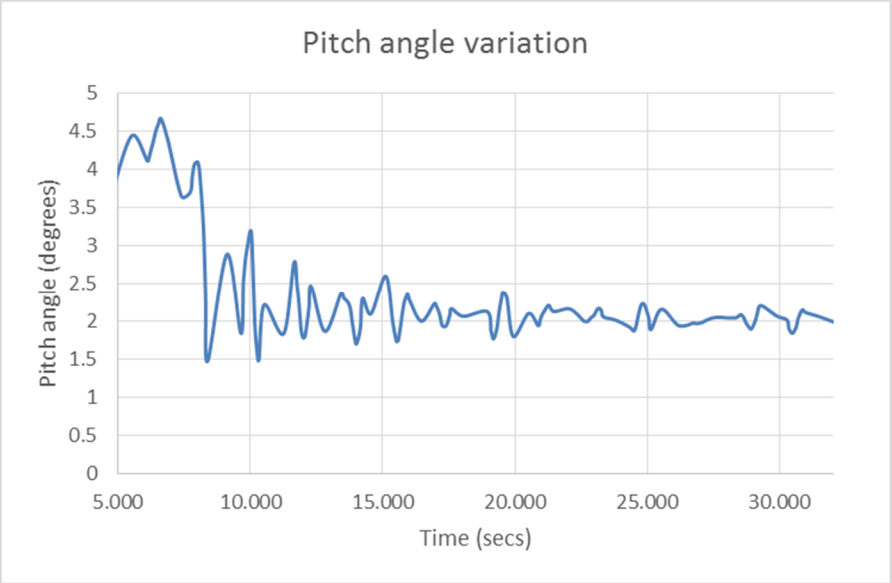

Figure 55. Pitch Angle variation with IST effect of 15 inch Float

It is observed that the amplitude of oscillations reduces from 12.5 degrees to 2.6 degrees, in a very short span of time 2-3 seconds. And it almost reaches the stable position in 25-30seconds. This is due to the damping effect provided by the suction stabilization. The variation of the angular velocity to the angular displacement, in both pitch and roll motions, are plotted in a phase plane, as shown in Figure 56 and in Figure 57 respectively. It is observed that the stable point is more crowed compared to the ones without IST effect.

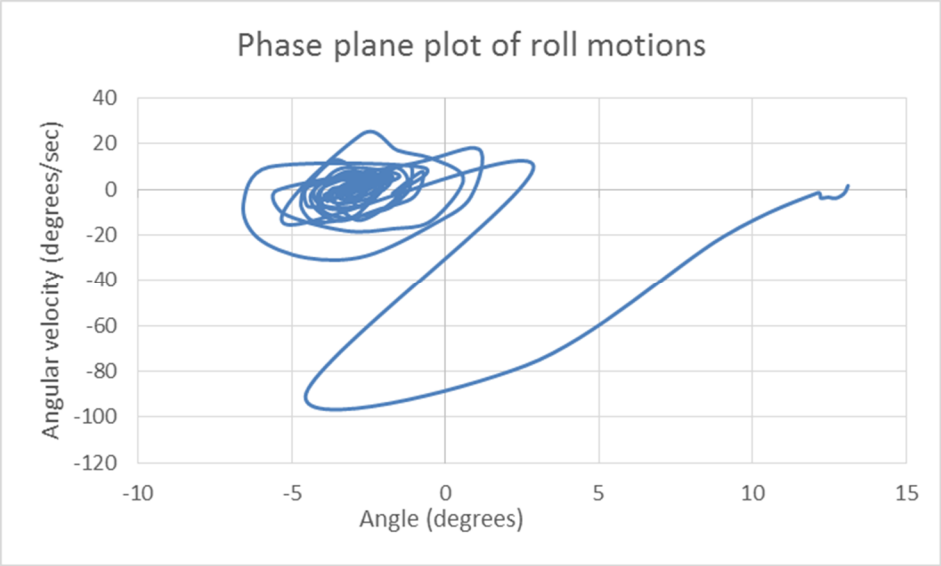

Figure 56. Phase plane plot of Roll motions with IST effect of 15 inch Float

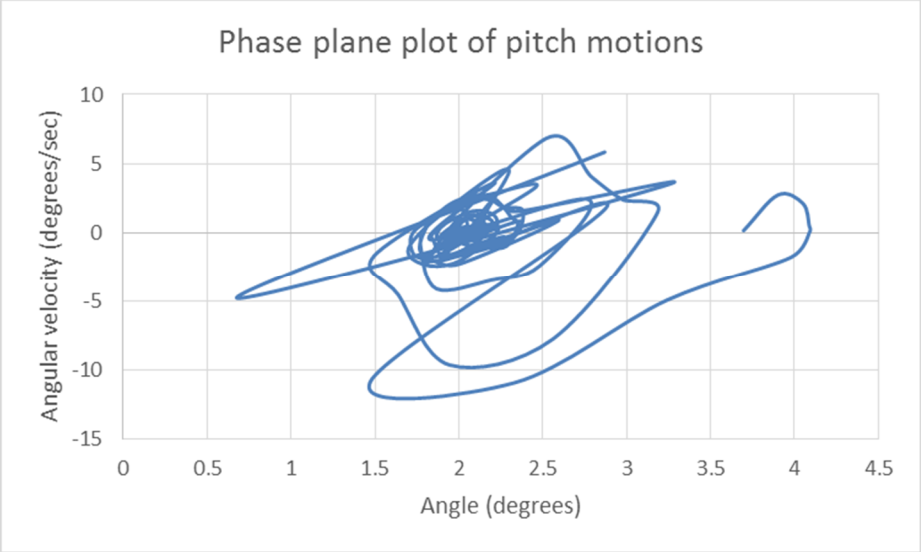

Figure 57. Phase plane plot of Pitch motions with IST effect of 15 inch Float

The same tests were conducted on the 32 inch diameter float and the motion of the float in roll and pitch direction are depicted in Figure 58 and Figure 59.

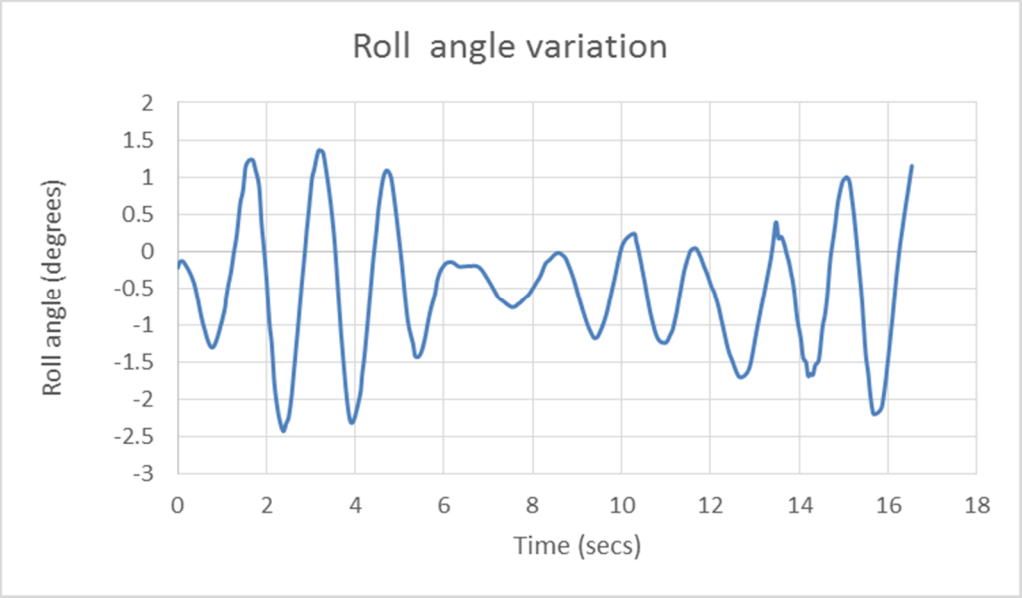

Figure 58. Roll Angle variation without IST effect of 32 inch Float

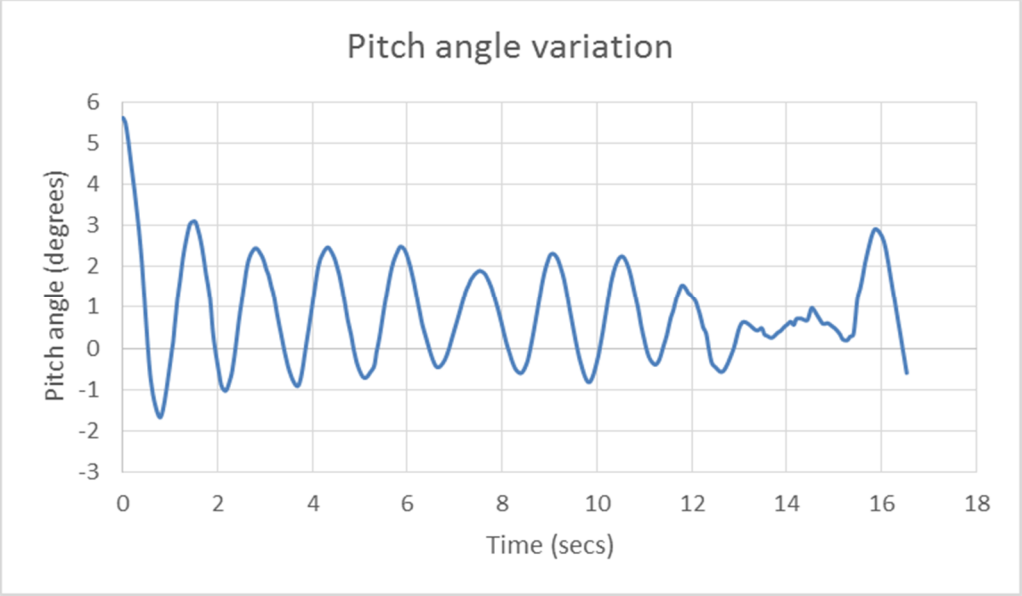

Figure 59. Pitch Angle variation without IST effect of 32 inch Float

It is observed that the initial heel angle is given in the pitch direction and the float dampens to some extent, due to the geometry of the float, but still keep varying in amplitude for a long time.

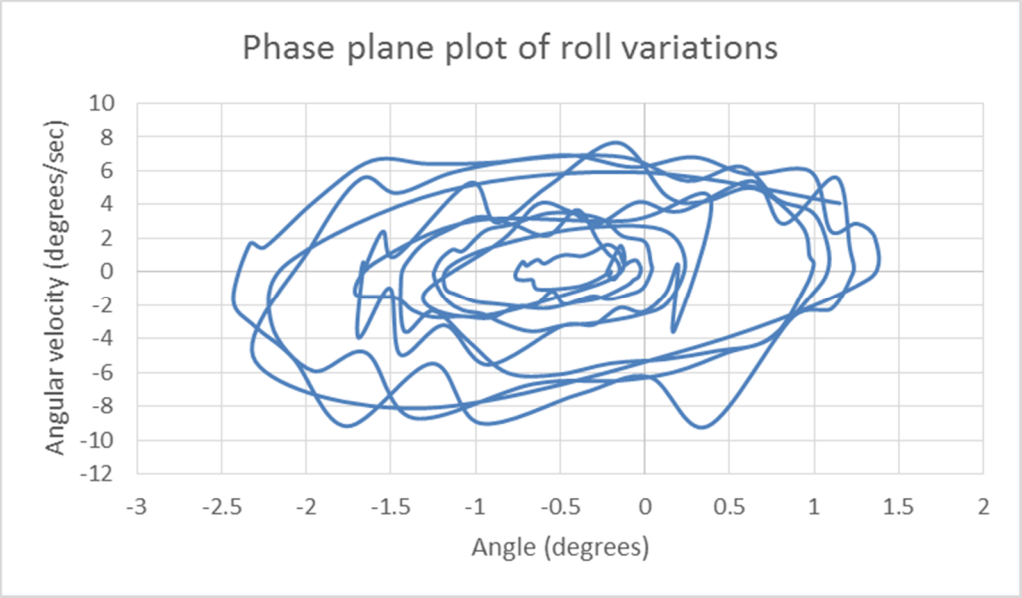

Figure 60. Phase plane plot of Roll motions without IST effect of 32 inch Float

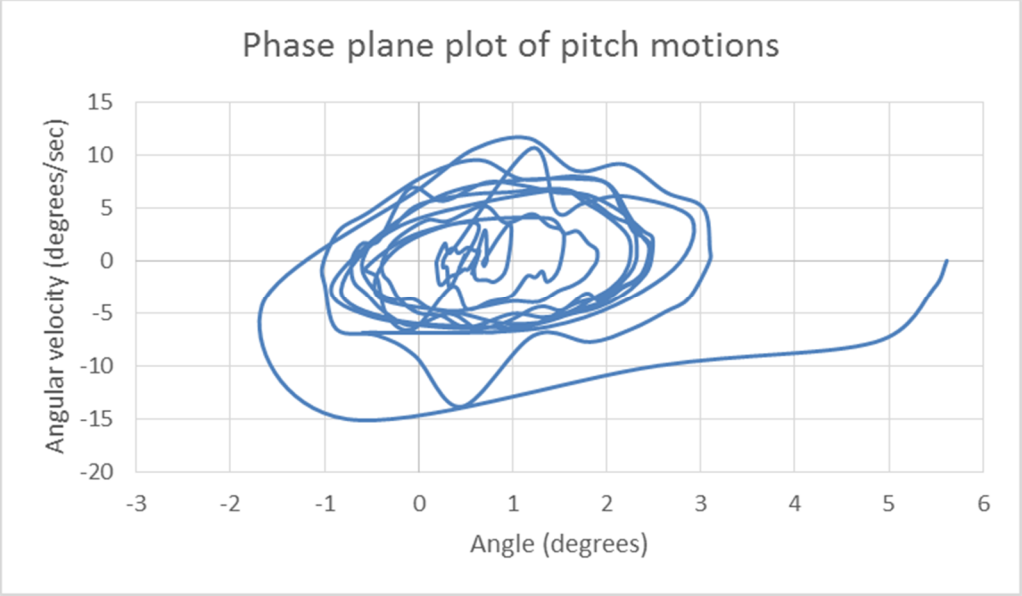

Figure 61. Phase plane plot of Pitch motions without IST effect of 32 inch Float

The phase plane plot in Figure 60 and Figure 61, indicates that the curve is not too dense near to the stable point, thereby indicating, the float is not stabilized in either direction.

The IST effect in the 32 inch diameter float was activated and the same was motions were observed. The graphs in Figure 62 and Figure 63 depicts the roll and pitch angle variation for the same.

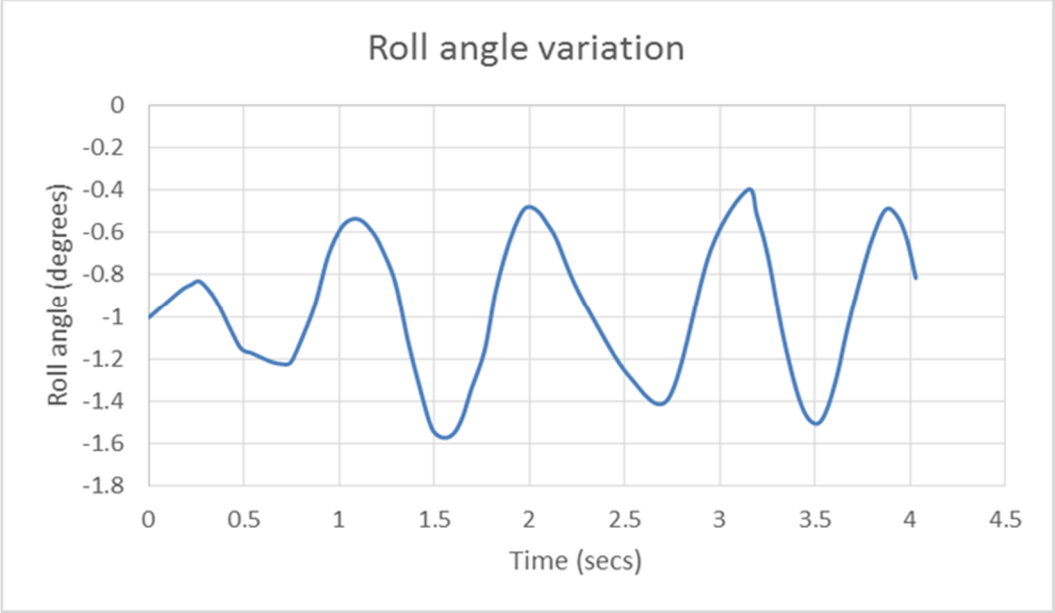

Figure 62. Roll Angle variation with IST effect of 32 inch Float

It is observed that the initial heel angle is provided in the pitch direction and it dampens of completely in 2-2.5 seconds. Since there is no mass on top of the float, the IST effect is so strong that it stabilizes the 32 inch diameter float even faster as compared to the 15 inch diameter float. This proves that the float with more water plane area provides more stability. At the same time the variation in roll direction is bounded and is of very low amplitude.

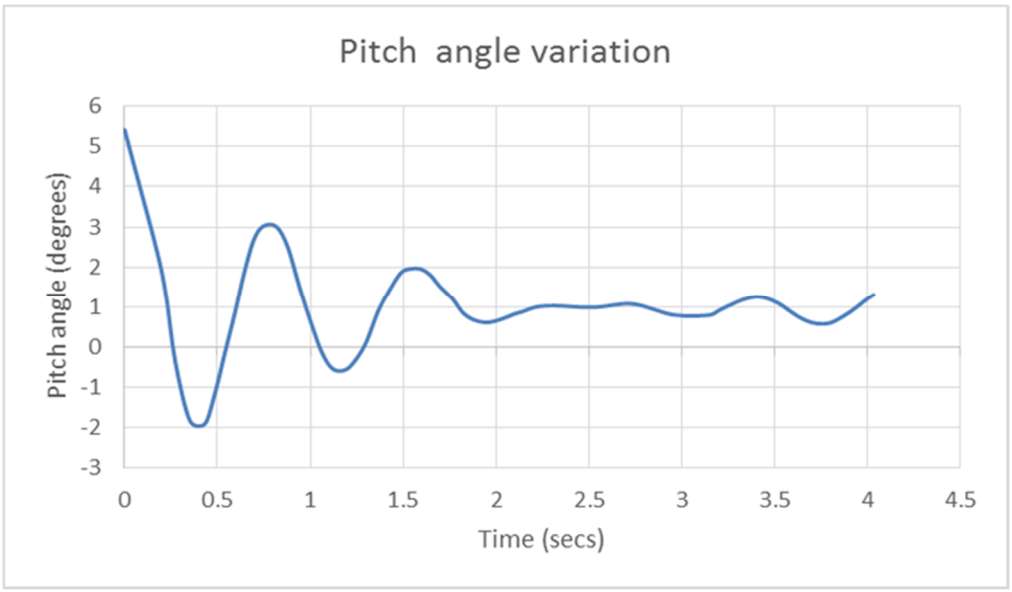

Figure 63. Pitch Angle variation with IST effect of 32 inch Float

The phase plane plots in Figure 64 and Figure 65 indicate that the float comes to a stable position much faster than that in case of a 15 inch diameter float.

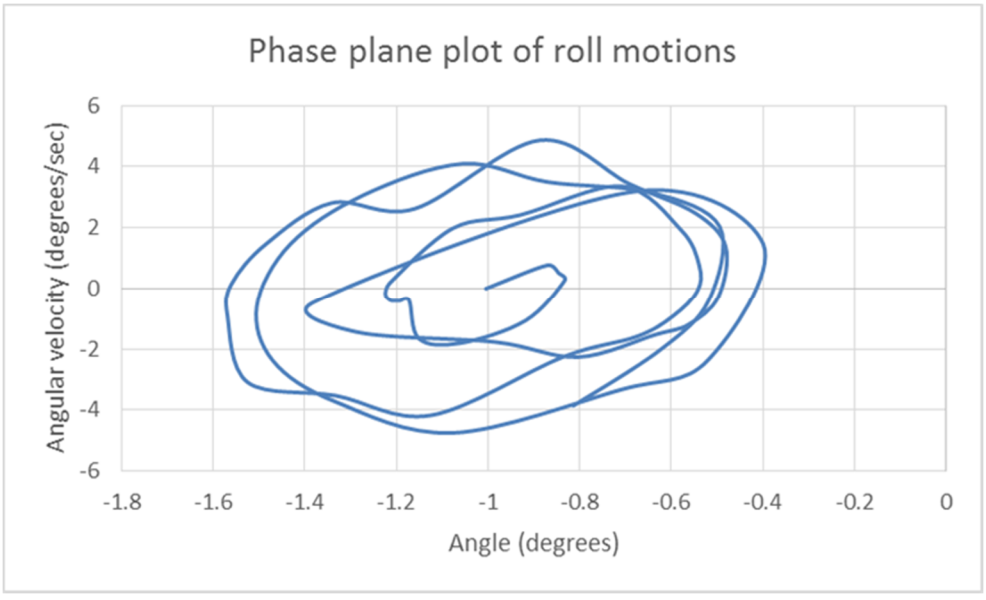

Figure 64. Phase plane plot of Roll motions with IST effect of 32 inch Float

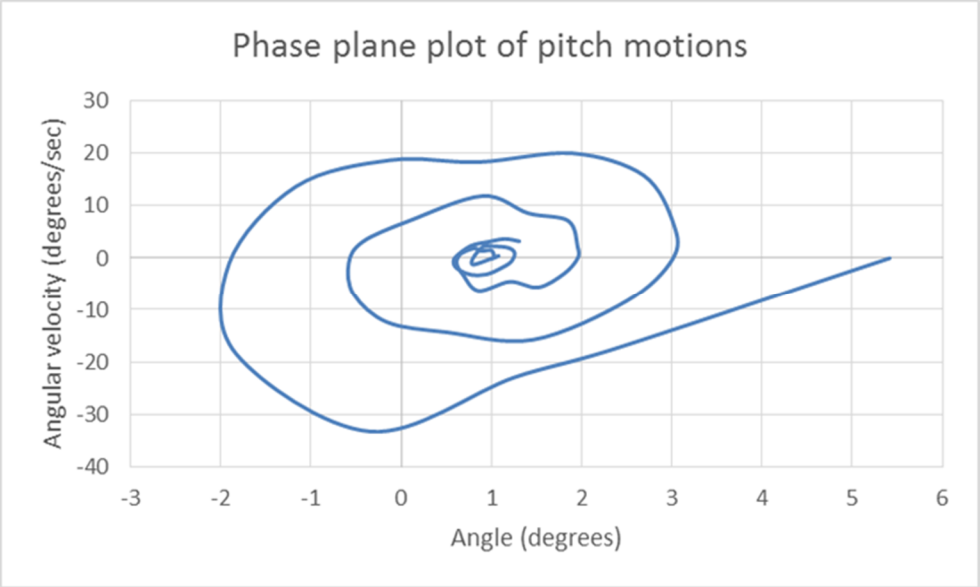

Figure 65. Phase plane plot of Pitch motions with IST effect of 32 inch Float

The same float of 32 inch diameter was tested with a 4 feet long patio umbrella on top of it. The umbrella provides more inertia and increases the roll and pitch motions due to the load of the umbrella. The roll and pitch motions are shown in Figure 66 and Figure 67. It is observed that the though the initial angle is provided in the pitch direction, the amplitude of motion is dampened in both roll and pitch direction. When the umbrella was mounted on the float, the 32 inch float capsized due to the absence of the IST effect. So there are no results for the condition of normal float with umbrella.

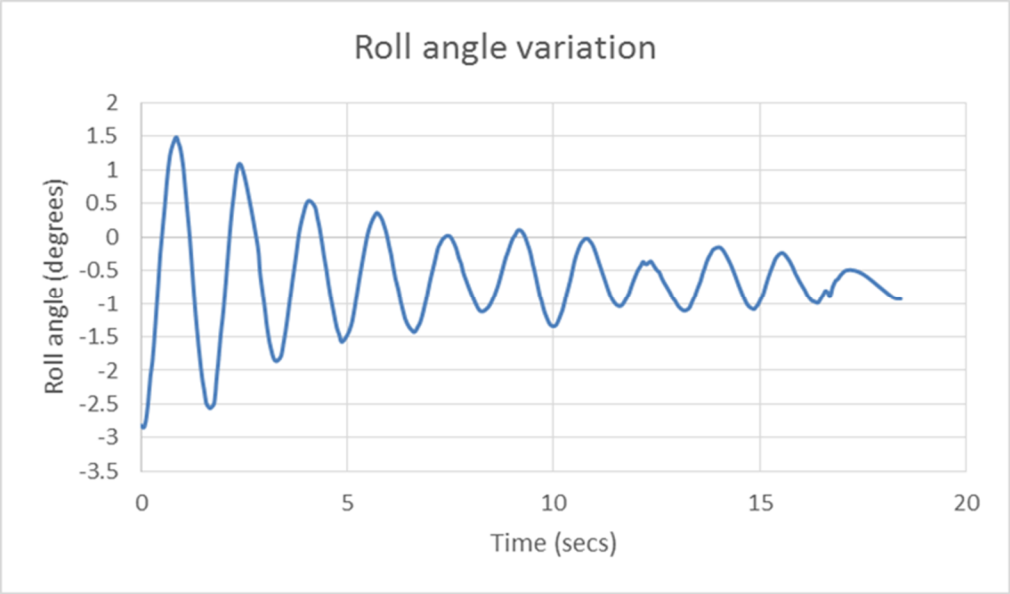

Figure 66. Roll Angle variation with Umbrella and IST effect of 32 inch Float

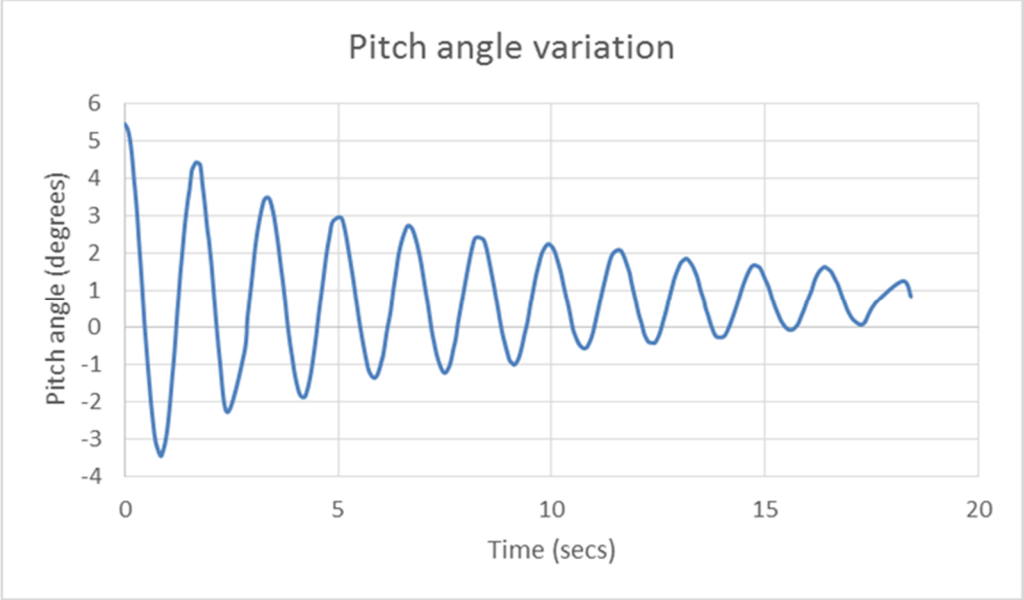

Figure 67. Pitch Angle variation with Umbrella and IST effect of 32 inch Float

The phase plane plot are shown in Figure 68 and Figure 69, where it is observed that the stable position is denser. This indicates the effect of suction stabilization is stabilizing the float.

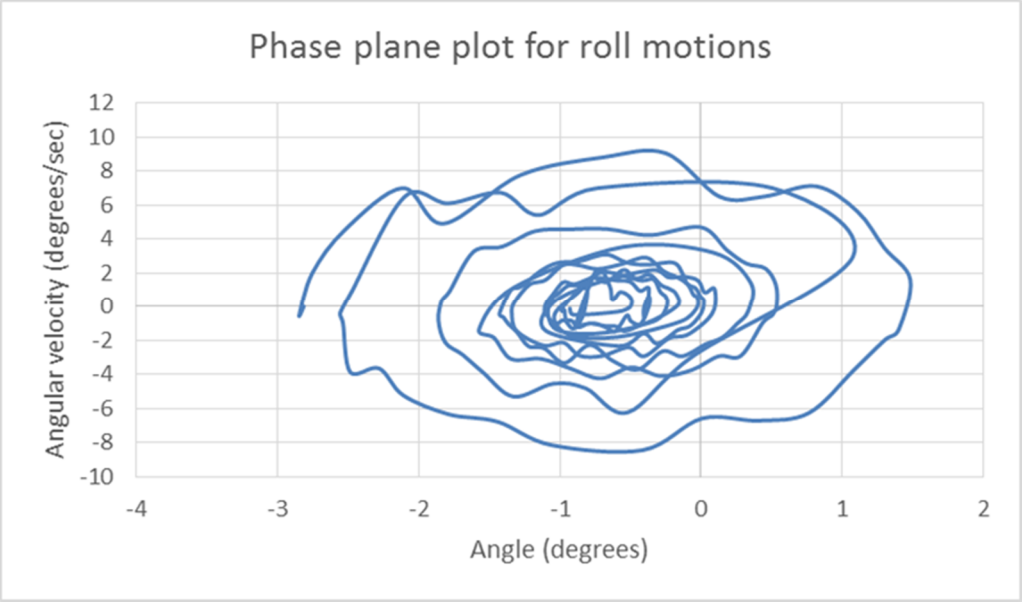

Figure 68. Phase plane plot of Roll motions with Umbrella and IST effect of 32 inch Float

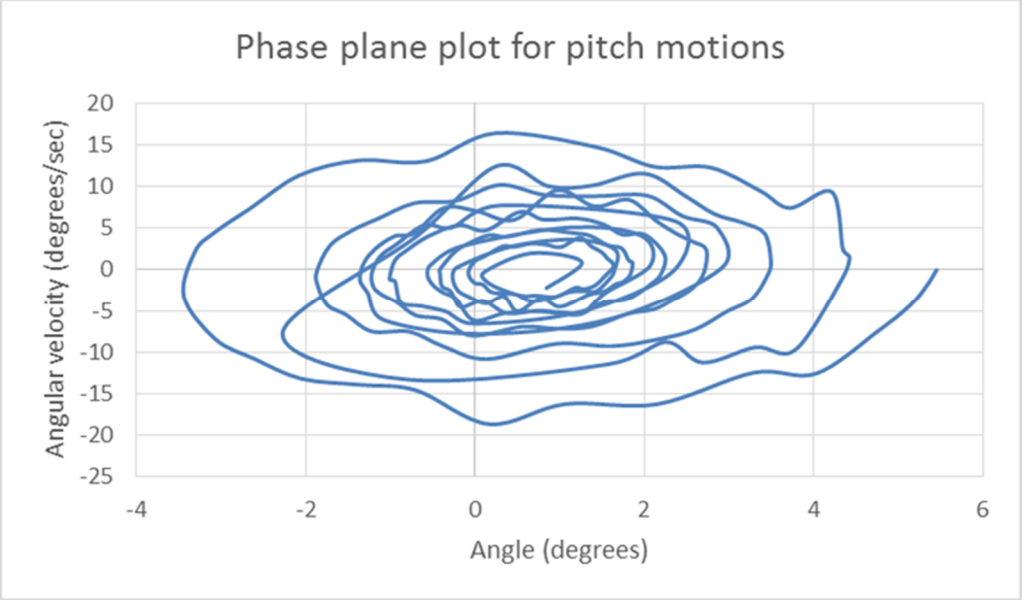

Figure 69. Phase plane plot of Pitch motions with Umbrella and IST effect of 32 inch Float

The 362 inch float was tested with wave actions incident on the float and the resulting motion in heave, roll and pitch direction is shown in Figure 70. The heave motions are accounted by the acceleration of the float in the z-direction. It is observed that the when the float is provided with the heave motion, not much changes are observed in the roll and pitch motions at the same instant. But it is observed that after sometime pitch motions and later roll motions are developed. This proves that there is a coupling between these motions and can result in a condition of parametric roll resonance.

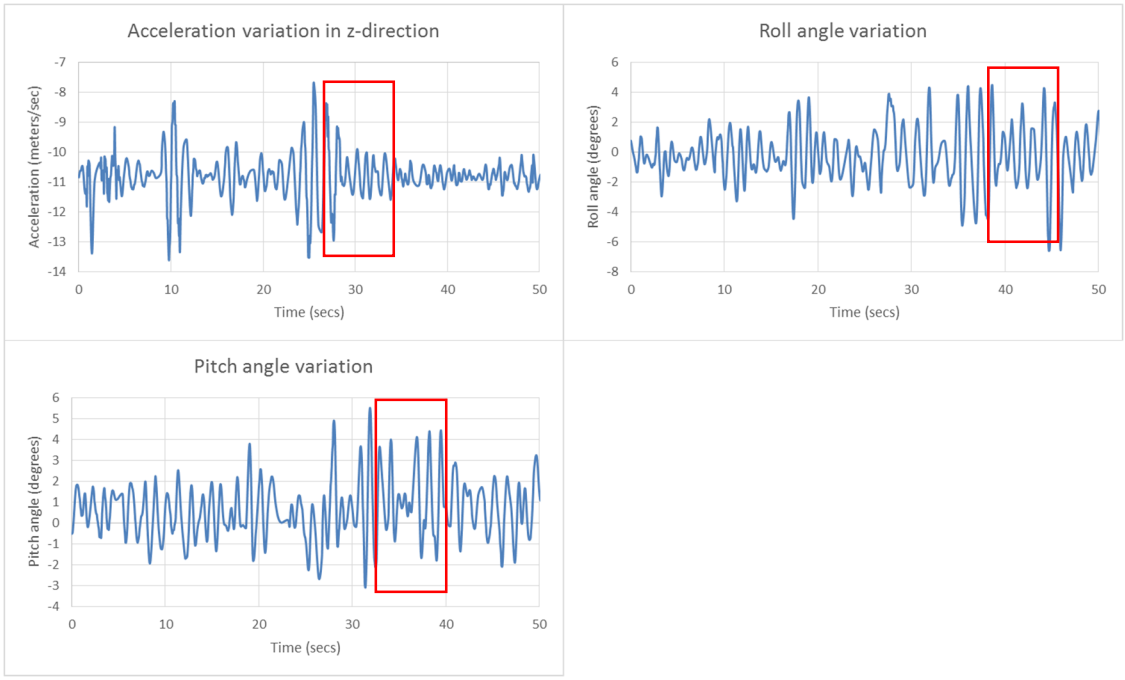

Figure 70. Heave Roll Pitch Coupling on 32 inch Float without Umbrella

The same experiment on 32 inch float with wave action is done with an umbrella mounted on top it and the results are shown in Figure 71. Similar results are observed depicting the coupling in heave, roll and pitch motions.

Figure 71. Heave Roll Pitch Coupling on 32 inch Float with Umbrella

Chapter 7
CONCLUSIONS AND DISCUSSION

The concept of suction stabilized floats proved to stabilize a floating platform. The IST effect dampens the roll motion considerably with no active controls on the system. This concept can proved to be helpful in stability of offshore wind turbines, both analytically and experimentally. The stability of the float can be further improved by adding a skirt around the float, preferably at the water plane section. This would increase the cross sectional area of the water plane area utilized in the moment of area calculations for determining the metacentric height.

The idea of SSF for other applications such as offshore oil and gas platforms, where the design is modified, as shown in Figure 72. Since the platform need to sustain the dynamic forces, due to the working of equipment for oil and gas extraction, it needs to be made of materials like carbon steel, steel etc. And to maintain the buoyancy of such float, an air chamber is required, which differentiates the design.

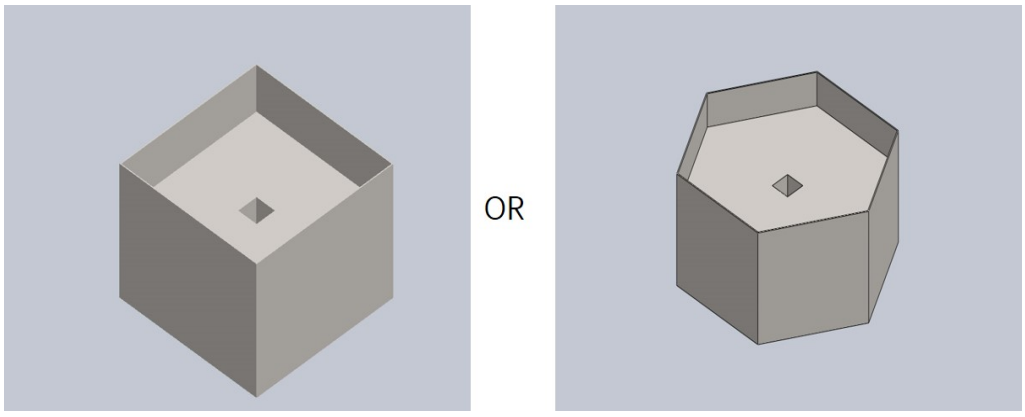

Figure 72 SSF Units for Offshore Oil and Gas Platforms

Multiple such units can be attached together, as shown in Figure 73. Such an assembly can be installed at the current mounting locations of oil and gas platforms on

subsea structures such as tripods and semi-submersibles. And if the current technologies for supporting such platforms are replaced with the concept of suction stabilization, there is huge profit from the amount of material utilized for subsea structures, as shown in Table 1. A detailed explanation of the numbers are shown in Appendix-E. It is observed that there is $1/10^{th}$ to $1/100^{th}$ reduction in the supporting structure weight and also up to $1/5^{th}$ in mounting area.

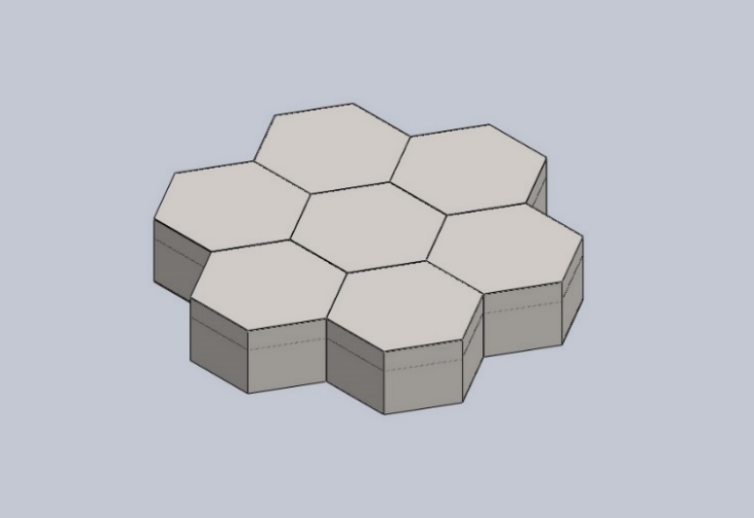

Figure 73 Assembly of SSF Units to form a Platform

Applications	Topside Weight (M.T.)	Supporting Structure & its weight (M.T.)	Mounting Area of topside (m^2)	Number of SSF units required	Total weight SSF (M.T.)	SSF area (m^2)
Fixed Oil & Gas Platforms	12,500	Jacket 23,000	1296	500	1,125	1,459.5
Semi-Submersible Platforms	18,000	Hull 14,000	7216	720	1,620	2,095.2
Jack-up Drill Rigs	13,000	Truss legs 253	5710.52	520	1,170	1,513
Spar Buoy Drill Rigs	1,250	Spar structure 13,000	660.52	50	112.5	145.5

Table 1. Advantages of Utilizing SSF for Current technologies in Offshore Platforms

The assembly of such units can also be helpful in making a floating platform for LNG production facilities or even shifting of cargos along with some active controls for further control on stability. The concept of suction stabilized floats can also be conceptualized for shoes, which would help man walk on water. A primitive sketch and the explanation of the idea is given in Appendix-F. The suggestions for future on the same are also discussed in the same.

REFERENCES

A.H.Nayfeh. (1979). *Nonlinear oscillations.* Canada: John Wiley & Sons.

ABS. (2004). *Assessment of Parametric Roll Resonance in the Design of container carriers.*

Biran, A. (2003). *Ship Hydrostatic and Stability.* Oxford: Butterworth-Heinemann (Elsevier).

Butterfield S., J. J. (2006). Coupled Dynamics Modeling of Floating Wind Turbine Systems. *Offshore Technological Conference No. NREL/CP-500-39481.*

Butterfield S., J. J. (2007). Engineering Challenges for Floating Offshore Wind Turbines. *Offshore Technological Conference No. NREL/CP-500-38116.*

Cheung, K. L. (2000). Hydrodynamic Response of a Pneumatic Floating Platform. *Ocean Engineering. 27, 1407-1444*, 1.

Holden, C. (2011). *Modeling and Control of Paramteric Roll Resonance.* Norwegian University of Science and Technology.

Jonkman, J. (2009). Dynamics of Offshore Floating Wind Turbines-Model development and verification. *Wiley Interscience*.

Kassteen, B. (2010). *Parametric Roll Resonance and Energy Transfer.* Eindhoven.

Kliava, J. M. (2010). Metacenter and Ship Stability. *American Journal of Physics. 78, 738-747*.

Montomery, J. (2011, September 23). *Suction Stabilized Floats.* Phoenix, USA: Patent application 13/242489.

P.N. Modi, S. S. (1995). *Hydraulics and Fluid Mechanics.* Delhi: Standard Book House.

Perunovic, V. (2011). Influence of the GZ Calculation Method on Parametric Roll Prediction. *Ocean Engineering. 38, 295-303*, 1-2.

R.A. Ibrahim, I. G. (2009, June). Modeling of Ship Roll Dynamics and Its Coupling with Heave and Pitch. *Mathematical Problems in Engineering*. Detroit, MI, USA: Hindawi Publishing Corporation.

Radoslav Naberjog, A. T. (1993). Autoparametric Resonance in an Externally Excited System. *Pergamon*.

Redkar, S. (2012, December 21). Suction Stabilisation Float-Progress Report. Mesa, Arizona.

Tondl A., T. R. (2000). *Autoparametric Resonance in Mechanical Systems.* Cambridge, UK: Cambridge University Press.

Tondl A., T. R. (2000). *Autoparametric Resonance in Mechanical Systems.* Cambridge, UK: Cambridge University Press.

Utsonomiya T., W. C. (2010). Hydrodynamic Forces on a Rolling. *Ocean Engineering 32, 219-232.*

Vendrell, L. (2013). *Hydrostatic Ananlysis for Suction Stabilized Floats.* Mesa, USA.

Wilson, J. (2003). *Dynamics of Offshore Structures.* Hoboken: John Wiley & Sons, Inc.

APPENDIX-A

EQUATIONS OF MOTION FOR HEAVE-ROLL MODEL FOR SHIPS

The position vector of the mass m_1, in the vertical plane, can be expressed as

$$r_{m1} = \begin{bmatrix} z \\ 0 \end{bmatrix} = \begin{bmatrix} z + \alpha \cos \omega t \\ 0 \end{bmatrix} \tag{A.1}$$

And the velocity and acceleration vector can be expressed as

$$\dot{r}_{m1} = \begin{bmatrix} \dot{z} \\ 0 \end{bmatrix} = \begin{bmatrix} \dot{z} - \alpha\omega \sin \omega t \\ 0 \end{bmatrix} \tag{A.2}$$

$$\ddot{r}_{m1} = \begin{bmatrix} \ddot{z} \\ 0 \end{bmatrix} = \begin{bmatrix} \ddot{z} - \alpha\omega^2 \cos \omega t \\ 0 \end{bmatrix} \tag{A.3}$$

The position vector of mass m_2, can be expressed as

$$r_{m2} = \begin{bmatrix} z - l\cos(\varphi) \\ l\sin(\varphi) \end{bmatrix} \tag{A.4}$$

The velocity vector of mass m_2, can be given as

$$\dot{r}_{m2} = \begin{bmatrix} \dot{z} + l\dot{\varphi}\sin(\varphi) \\ l\dot{\varphi}\cos(\varphi) \end{bmatrix} \tag{A.5}$$

The total kinetic energy of the system can be expressed as

$$T = \frac{1}{2} m_1 \dot{z}^2 + \frac{1}{2} m_2 \{\dot{z} + l\dot{\varphi}\sin(\varphi)\}^2 + \frac{1}{2} m_2 \{l\dot{\varphi}\cos(\varphi)\}^2 \tag{A.6}$$

The total potential energy of the system can be expressed as

$$V = m_2 g l(1 - \cos(\varphi)) + \frac{1}{2} k z^2 \tag{A.7}$$

For the given system, Lagrange's equation of motion can be given as (Tondl A., Autoparametric Resonance in Mechanical Systems, 2000)

$$(m_1 + m_2)(\ddot{z} - \alpha\omega^2 \cos(\omega t)) + b\dot{z} + kz + m_2 l\{\ddot{\varphi}\sin(\varphi) + \dot{\varphi}^2 \cos(\varphi)\} = 0 \quad \text{(A.8)}$$

$$m_2 l^2 \ddot{\varphi} + c\dot{\varphi} + m_2 gl \sin(\varphi) + m_2 l\{\ddot{z} - \alpha\omega^2 \cos(\omega t)\}\sin(\varphi) = 0 \quad \text{(A.9)}$$

The above equations can be converted to a dimensionless form, by introducing a new variable, called time constant given as $\tau = \left(\sqrt{\frac{g}{l}}\right)t$ which can be written as

$$\ddot{w} + K\dot{w} + q^2 w + \mu\{\ddot{\varphi}\sin(\varphi) + \dot{\varphi}^2 \cos(\varphi)\} = a\eta^2 \cos(\eta\tau) \quad \text{(A.10)}$$

$$\ddot{\varphi} + K_0\dot{\varphi} + \sin(\varphi) + \{\ddot{w} - a\eta^2 \cos(\eta\tau)\}\sin(\varphi) = 0 \quad \text{(A.11)}$$

Where

$$w = \frac{z}{l}, \omega_0 = \sqrt{\frac{g}{l}}, K = \frac{b}{\omega_0(m_1 + m_2)}, q^2 = \frac{k}{\omega_0{}^2(m_1 + m_2)}, \mu = \frac{m_2}{(m_1 + m_2)}, K_0 = \frac{c}{\omega_0 m_2 l^2},$$

$\eta = \frac{\omega}{\omega_0}$ and $a = \frac{\alpha}{l}$.

Now consider the following assumptions

$$\begin{aligned} x_1 &= w \\ x_2 &= \dot{w} \\ x_3 &= \varphi \\ x_4 &= \dot{\varphi} \end{aligned} \quad \text{(A.12)}$$

Now the state equations become as follows

$$
\begin{aligned}
\dot{x}_1 &= x_2 \\
\dot{x}_2 &= \frac{a\eta^2 \mu \sin^2 x_3 \cos\eta\tau - K_0 \mu x_4 \sin x_3 - a\eta^2 \cos\eta\tau + \mu x_4{}^2 \cos x_3 - \mu \sin^2 x_3 + q^2 x_1 + K x_2}{\mu \sin^2 x_3 - 1} \\
\dot{x}_3 &= x_4 \\
\dot{x}_4 &= -\frac{\mu x_4{}^2 \cos x_3 \sin x_3 + K x_2 \sin x_3 - \sin x_3 + q^2 x_1 \sin x_3 - K_0 x_4}{\mu \sin^2 x_3 - 1}
\end{aligned}
\tag{A.13}
$$

APPENDIX-B

EQUATIONS OF MOTION FOR HEAVE-ROLL MODEL FOR SSF

The position vector of the mass m_1, in the vertical plane, can be expressed as

$$r_{m1} = \begin{bmatrix} z \\ 0 \end{bmatrix} = \begin{bmatrix} z + \alpha \cos \omega t \\ 0 \end{bmatrix} \tag{B.1}$$

And the velocity and acceleration vector can be expressed as

$$\dot{r}_{m1} = \begin{bmatrix} \dot{z} \\ 0 \end{bmatrix} = \begin{bmatrix} \dot{z} - \alpha\omega \sin \omega t \\ 0 \end{bmatrix} \tag{B.2}$$

$$\ddot{r}_{m1} = \begin{bmatrix} \ddot{z} \\ 0 \end{bmatrix} = \begin{bmatrix} \ddot{z} - \alpha\omega^2 \cos \omega t \\ 0 \end{bmatrix} \tag{B.3}$$

The position vector of mass m_2, can be expressed as

$$r_{m2} = \begin{bmatrix} z - l\cos(\phi) \\ l\sin(\phi) \end{bmatrix} \tag{B.4}$$

The velocity vector of mass m_2, can be given as

$$\dot{r}_{m2} = \begin{bmatrix} \dot{z} + l\dot{\phi}\sin(\phi) \\ l\dot{\phi}\cos(\phi) \end{bmatrix} \tag{B.5}$$

The total kinetic energy of the system can be expressed as

$$T = \frac{1}{2} m_1 \dot{z}^2 + \frac{1}{2} m_2 \{\dot{z} + l\dot{\phi}\sin(\phi)\}^2 + \frac{1}{2} m_2 \{l\dot{\phi}\cos(\phi)\}^2 \tag{B.6}$$

The total potential energy of the system can be expressed as

$$V = m_2 gl(1 - \cos(\phi)) + \frac{1}{2} kz^2 + \frac{1}{2} k_t \phi^2 \tag{B.7}$$

For the given system, Lagrange's equation of motion can be given as

$$(m_1 + m_2)(\ddot{z} - \alpha\omega^2 \cos(\omega t)) + b\dot{z} + kz + m_2 l\{\ddot{\phi}\sin(\phi) + \dot{\phi}^2 \cos(\phi)\} = 0 \qquad \text{(B.8)}$$

$$m_2 l^2 \ddot{\phi} + c\dot{\phi} + m_2 gl \sin(\phi) + m_2 l\{\ddot{z} - \alpha\omega^2 \cos(\omega t)\}\sin(\phi) = 0 \qquad \text{(B.9)}$$

The above equations can be converted to a dimensionless form, by introducing a new variable, called time constant given as $\tau = \left(\sqrt{\frac{g}{l}}\right)t$ which can be written as

$$\ddot{x} + \bar{B}\dot{x} + q^2 x + \mu\{\ddot{\phi}\sin(\phi) + \dot{\phi}^2 \cos(\phi)\} = a\eta^2 \cos(\eta\tau) \qquad \text{(B.10)}$$

$$\ddot{\phi} + \bar{C}\dot{\phi} + \sin(\phi) + q_t^2\phi + \{\ddot{x} - a\eta^2 \cos(\eta\tau)\}\sin(\phi) = 0 \qquad \text{(B.11)}$$

Where $x = \frac{z}{l}, \omega_0 = \sqrt{\frac{g}{l}}, \bar{B} = \frac{b}{\omega_0(m_1 + m_2)}, q^2 = \frac{k}{\omega_0^2(m_1 + m_2)}, \mu = \frac{m_2}{(m_1 + m_2)}, \bar{C} = \frac{c}{\omega_0 m_2 l^2}$,

$\eta = \frac{\omega}{\omega_0}, q_t^2 = \frac{k_t}{\omega_0^2 m_2 l^2}$ and $a = \frac{\alpha}{l}$.

Now consider the following assumptions

$$\begin{aligned} y_1 &= x \\ y_2 &= \dot{x} \\ y_3 &= \phi \\ y_4 &= \dot{\phi} \end{aligned} \qquad \text{(B.12)}$$

Now the state equations become as follows

$$
\begin{aligned}
\dot{y}_1 &= y_2 \\
\dot{y}_2 &= \frac{a\eta^2 \mu \sin^2 y_3 \cos\eta\tau - \bar{C}\mu y_4 \mathrm{siny}_3 - a\eta^2 \cos\eta\tau + \mu y_4{}^2 \cos y_3 - \mu \sin^2 y_3 + q^2 y_1 + \bar{B} y_2}{\mu \sin^2 y_3 - 1} \\
\dot{y}_3 &= y_4 \\
\dot{y}_4 &= -\frac{\mu y_4{}^2 \cos y_3 \sin y_3 + \bar{B} y_2 \sin y_3 - \sin y_3 + q^2 y_1 \sin y_3 - \bar{C} y_4 - q_t^2 y_3}{\mu \sin^2 y_3 - 1}
\end{aligned}
\tag{B.13}
$$

APPENDIX-C

EQUATIONS OF MOTION FOR DETAILED MODEL OF SSF

The position vector of the mass m_1, in the vertical plane, can be expressed as

$$r_{m1} = \begin{bmatrix} z \\ 0 \end{bmatrix} = \begin{bmatrix} z + a\cos\omega t \\ 0 \end{bmatrix} \tag{C.1}$$

And the velocity and acceleration vector can be expressed as

$$\dot{r}_{m1} = \begin{bmatrix} \dot{z} \\ 0 \end{bmatrix} = \begin{bmatrix} \dot{z} - a\omega\sin\omega t \\ 0 \end{bmatrix} \tag{C.2}$$

$$\ddot{r}_{m1} = \begin{bmatrix} \ddot{z} \\ 0 \end{bmatrix} = \begin{bmatrix} \ddot{z} - a\omega^2\cos\omega t \\ 0 \end{bmatrix} \tag{C.3}$$

The position vector of mass m_2, can be expressed as

$$r_{m2} = \begin{bmatrix} z + 0.7R\theta \\ 0.58R \end{bmatrix} \tag{C.4}$$

The velocity vector of mass m_2, can be given as

$$\dot{r}_{m2} = \begin{bmatrix} \dot{z} + 0.7R\dot{\theta} \\ 0 \end{bmatrix} \tag{C.5}$$

The total kinetic energy of the system can be expressed as

$$T = \frac{1}{2}m_1\dot{z}^2 + \frac{1}{2}m_2\{\dot{z} + 0.7R\dot{\theta}\}^2 + \frac{1}{2}I\dot{\theta}^2 \tag{C.6}$$

The total potential energy of the system can be expressed as

$$V = m_2 g(z + 0.7R\theta) + \frac{1}{2}kz^2 \tag{C.7}$$

For the given system the Lagrange's equations of motion are given as

$$m_1\ddot{z} - m_1 a\omega^2 \cos\omega t + \frac{2}{3}R^3\rho\theta\ddot{z} - \frac{2}{3}R^3\rho\theta a\omega^2 \cos\omega t + \frac{2}{3}R^3\rho\dot{\theta}\dot{z} - \frac{2}{3}R^3\rho\dot{\theta}a\omega \sin\omega t + \frac{2}{3}\times 0.7R^4\rho\theta\ddot{\theta} + \frac{2}{3}0.7R^4\rho\dot{\theta}^2 + kz + ka\cos\omega t + \frac{2}{3}R^3\rho g\theta + b\dot{z} = 0 \quad \text{(C.8)}$$

$$\frac{2}{3}\times 0.7^2R^5\rho\theta\ddot{\theta} + \frac{1}{3}\times 0.7^2R^5\rho\dot{\theta}^2 + \frac{2}{3}\times 0.7R^4\rho\theta\ddot{z} - \frac{2}{3}\times 0.7R^4\rho\theta a\omega^2\cos\omega t + I\ddot{\theta} - \frac{1}{3}R^3\rho\dot{z}^2 - \frac{1}{3}R^3\rho a^2\omega^2\sin^2\omega t + \frac{2}{3}\rho R^3\dot{z}a\omega\sin\omega t + \frac{2}{3}\rho R^3gz + \frac{2}{3}\rho R^3ga\cos\omega t + \frac{4}{3}\times 0.7R^4\rho g\theta + c\dot{\theta} = 0 \quad \text{(C.9)}$$

The above equations are in the non-linear form. After linearizing the above equations we get

$$m_1\ddot{z} - m_1 a\omega^2\cos\omega t - \frac{2}{3}R^3\rho\theta a\omega^2\cos\omega t - \frac{2}{3}R^3\rho\dot{\theta}a\omega\sin\omega t + kz + ka\cos\omega t + \frac{2}{3}R^3\rho g\theta + b\dot{z} = 0 \quad \text{(C.10)}$$

$$-\frac{2}{3}\times 0.7R^4\rho\theta a\omega^2\cos\omega t + I\ddot{\theta} - \frac{1}{3}R^3\rho a^2\omega^2\sin^2\omega t + \frac{2}{3}\rho R^3\dot{z}a\omega\sin\omega t + \frac{2}{3}\rho R^3gz + \frac{2}{3}\rho R^3ga\cos\omega t + \frac{4}{3}\times 0.7R^4\rho g\theta + c\dot{\theta} = 0 \quad \text{(C.11)}$$

By dividing Eq. (C.10), throughout by m_1, and Eq. (C.11), throughout by I and converting the equations in the state space form we get

$$\frac{d}{dt}\begin{Bmatrix} z \\ \dot{z} \\ \theta \\ \dot{\theta} \end{Bmatrix} = \begin{bmatrix} 0 & 1 & 0 & 0 \\ \frac{-k}{m_1} & \frac{-b}{m_1} & \frac{-2}{3m_1}R^3\rho g & 0 \\ 0 & 0 & 0 & 1 \\ \frac{-2}{3I}R^3\rho g & 0 & \frac{-4}{3I}\times 0.7R^4\rho g & \frac{-c}{I} \end{bmatrix} \begin{Bmatrix} z \\ \dot{z} \\ \theta \\ \dot{\theta} \end{Bmatrix} + \begin{bmatrix} 0 \\ a\omega^2\cos\omega t - \frac{k}{m_1}a\cos\omega t \\ 0 \\ \frac{1}{3}R^3\rho^2 a\omega^2\sin^2\omega t - \frac{2}{3}R^3\rho g a\cos\omega t \end{bmatrix} +$$

$$\begin{bmatrix} 0 & 0 & 0 & 0 \\ 0 & 0 & \frac{2}{3m_1}R^3\rho a\omega^2\cos\omega t & \frac{2}{3m_1}R^3\rho a\omega\sin\omega t \\ 0 & 0 & 0 & 0 \\ 0 & \frac{-2}{3I}R^3\rho a\omega\sin\omega t & \frac{2}{3I}\times 0.7R^4\rho a\omega^2\cos\omega t & 0 \end{bmatrix} \begin{Bmatrix} z \\ \dot{z} \\ \theta \\ \dot{\theta} \end{Bmatrix}$$

(C.12)

It can be expressed in a much simpler by making the following substitutions

$$X = \begin{Bmatrix} z \\ \dot{z} \\ \theta \\ \dot{\theta} \end{Bmatrix}, A_0 = \begin{bmatrix} 0 & 1 & 0 & 0 \\ \frac{-k}{m_1} & \frac{-b}{m_1} & \frac{-2}{3m_1}R^3\rho g & 0 \\ 0 & 0 & 0 & 1 \\ \frac{-2}{3I}R^3\rho g & 0 & \frac{-4}{3I}\times 0.7R^4\rho g & \frac{-c}{I} \end{bmatrix}, F(t) = \begin{bmatrix} 0 \\ a\omega^2\cos\omega t - \frac{k}{m_1}a\cos\omega t \\ 0 \\ \frac{1}{3}R^3\rho^2 a\omega^2\sin^2\omega t - \frac{2}{3}R^3\rho g a\cos\omega t \end{bmatrix}$$

and $A(t) = \begin{bmatrix} 0 & 0 & 0 & 0 \\ 0 & 0 & \frac{2}{3m_1}R^3\rho a\omega^2\cos\omega t & \frac{2}{3m_1}R^3\rho a\omega\sin\omega t \\ 0 & 0 & 0 & 0 \\ 0 & \frac{-2}{3I}R^3\rho a\omega\sin\omega t & \frac{2}{3I}\times 0.7R^4\rho a\omega^2\cos\omega t & 0 \end{bmatrix}$

Therefore Eq. (C.12) becomes

$$\dot{X} = \{A_0 + A(t)\}X + F(t) \qquad \text{(C.13)}$$

APPENDIX-D

EQUATIONS OF MOTION FOR TURBINE MODEL WITH SSF

The position vector of the center of gravity of the turbine structure in horizontal plane is given by

$$r_G = \begin{bmatrix} x + h_G\theta \\ 0 \end{bmatrix} \tag{D.1}$$

And the velocity and acceleration vector can be expressed as

$$\dot{r}_G = \begin{bmatrix} \dot{x} + h_G\dot{\theta} \\ 0 \end{bmatrix} \tag{D.2}$$

$$\ddot{r}_G = \begin{bmatrix} \ddot{x} + h_G\ddot{\theta} \\ 0 \end{bmatrix} \tag{D.3}$$

The total kinetic energy of the system can be expressed as

$$T = \frac{1}{2}m(\dot{x} + h_G\dot{\theta})^2 + \frac{1}{2}J_G\dot{\theta}^2 \tag{D.4}$$

The total potential energy of the system can be expressed as

$$V = \frac{1}{2}k_1x^2 + \frac{1}{2}k_0\theta^2 - mgh_G(1-\cos\theta) + mgh_B(1-\cos\theta) \tag{D.5}$$

For the given system the Lagrange's equations of motion are given as

$$m\ddot{x} + mh_G\ddot{\theta} + c_1\dot{x} + k_1x = F \tag{D.6}$$

$$mh_G\ddot{x} + (J_G + mh_G^2)\ddot{\theta} + c_0\dot{\theta} + (k_0 - mgh_G + mgh_B)\theta = h_0F + Mc \tag{D.7}$$

But by using parallel axis theorem, we get

$$J_O = J_G + mh_G^2 \tag{D.8}$$

By using Eq. (D.8) in Eq. (D.6) and Eq. (D.7) and modifying them into the state space form, we get

$$\begin{bmatrix} m & 0 \\ 0 & J_G \end{bmatrix}\begin{bmatrix} \ddot{x} \\ \ddot{\theta} \end{bmatrix}+\begin{bmatrix} \frac{J_O}{J_G}c_1 & -\frac{mh_G}{J_G}c_0 \\ -h_G c_1 & c_0 \end{bmatrix}\begin{bmatrix} \dot{x} \\ \dot{\theta} \end{bmatrix}+\begin{bmatrix} \frac{J_O}{J_G}k_1 & -\frac{mh_G}{J_G}(k_O - mgh_G + mgh_{B)} \\ -h_G k_1 & (k_O - mgh_G + mgh_B) \end{bmatrix}\begin{bmatrix} x \\ \theta \end{bmatrix}$$
$$=\begin{bmatrix} \left\{1-\frac{mh_G}{J_G}(h_O - h_G)\right\}F - \frac{mh_G}{J_G}M_C \\ M_C + (h_O + h_G)F \end{bmatrix} \qquad \text{(D.9)}$$

APPENDIX-E

APPLICATION OF SSF FOR OIL & GAS PLATFORMS

The single unit used in this application is a hexagonal section SSF, as shown in Figure 74. The whole unit is made of 10 millimeter thick carbon steel (CS) plates. So that the structure can withstand the forces due to the working of equipment on the topside of the platform. But to create the buoyancy, an air chamber is provided in the unit. The properties used for calculations are given in Table 2.

Properties	**Value**	**Units**
Density of CS plate, ρ_{CS}	7800	Kg/m^3
Density of sea water, ρ_{SW}	1024.15	Kg/m^3

Table 2. Properties used for Calculations

Using these properties, different parameters are calculated as shown in Table 3.

Parameter	**Symbol**	**Value**	**Units**
Total volume of steel used in the SSF unit	V_{CS}	0.17	m^3
Total volume of water inside SSF unit	V_{SW}	0.912	m^3
Total mass of steel used in the SSF unit	M_{CS}	1316.7	kg
Total mass of water inside SSF unit	M_{SW}	934.025	kg
Total mass of SSF unit with water inside	M_{Total}	2250.73	kg
Volume of air chamber	V_{air}	2.4816	m^3
Volume of SSF unit below inner chamber	η	2.6025	m^3
Area of the water plane section of SSF	A_b	2.919	m^2

Table 3. Different Parameters of SSF Unit calculated

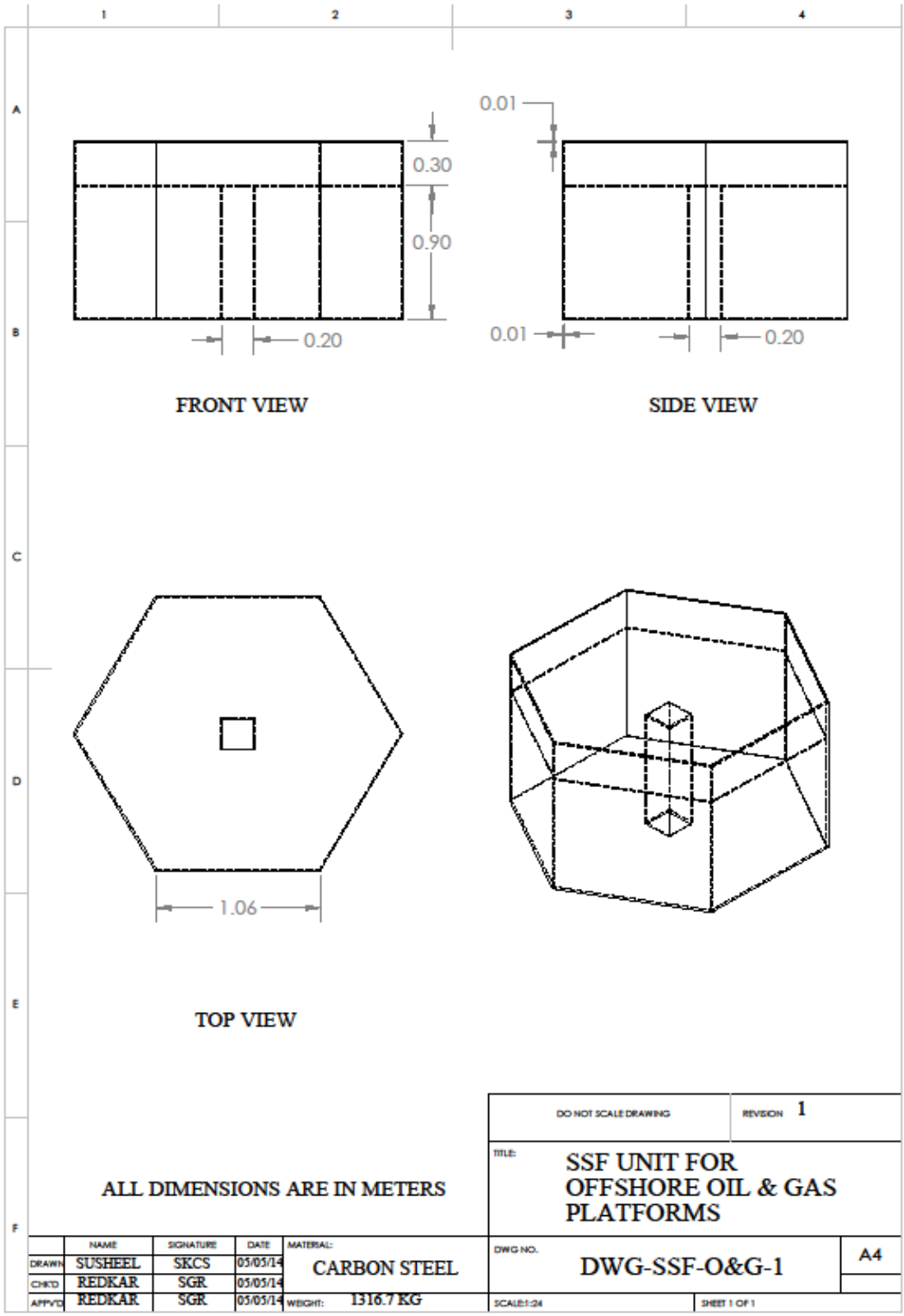

Figure 74. SSF Unit for Offshore Oil & Gas Platforms

The total volume of water displaced (V_{dis}) due to the total mass of the SSF unit and the water inside it, is given by

$$V_{dis} = \frac{M_{Total}}{\rho_{SW}} = \frac{2250.73}{1024.15} = 2.197 m^3 \tag{D.10}$$

The water plane interface is assumed to be at the inner chamber of the SSF, which is above the height of ε = 0.90 meters, for draught calculations. But since the cross sectional area of the SSF is the same through the height of the, it does not affect the performance of the SSF, even if it lower that the mentioned height. The equation for the draught of the SSF is given by (Vendrell, 2013)

$$T = \left[\frac{V_{dis} - \eta}{A_b}\right] + \varepsilon = \left[\frac{2.197 - 2.6025}{2.919}\right] + 0.90 = 0.76m \tag{D.11}$$

But the water plane area can go up to the height of T = 1.2 meters. So substituting this value to Eq. (E.2) and finding the value of the water displaced gives us

$$T = 1.2 = \left[\frac{V_{dis} - 2.6025}{2.919}\right] + 0.90 \Rightarrow V_{dis} = 3.4782 m^3 \tag{D.12}$$

Therefore equivalent mass of CS for this displaced volume of water is given

$$Meq = 3.4782 \times 7800 = 27.129 \text{tons} \tag{D.13}$$

By deducting the total weight of the SSF unit from *Meq*, we get approximately extra 25 tons of CS capacity of each SSF, with which it can perform as a supporting structure for oil and gas platforms.

Considering a fixed bottom type oil and gas platform, which has a topside weight of 12,500 tons. But the supporting jacket structure for such a platform weighs 23,000 tons. If the supporting structure was to be replaced by multiple SSF units, 500 such units would support the same topside weight, which would make use of only 1,125 tons of CS. Similar comparisons are done for semi submersibles, jack-up drill rigs and spar buoy and results are shown in Table 1.

APPENDIX-F

WALKING ON WATER

The concept of SSF can be utilized for shoes, which would help men walk on water. The primitive idea is that the shoe must be buoyant enough to float itself and also the weight of the human body. The shoe should be light too, which would allow the person to move more easily through water and its flow.

Let us consider a man weighing 100 kilograms need to walk on water and if he transfers all his weight on one leg, then the shoe must be designed in such a way that it can keep itself floating and also with it the man wearing those shoes too. A rough model is shown in Figure 75.

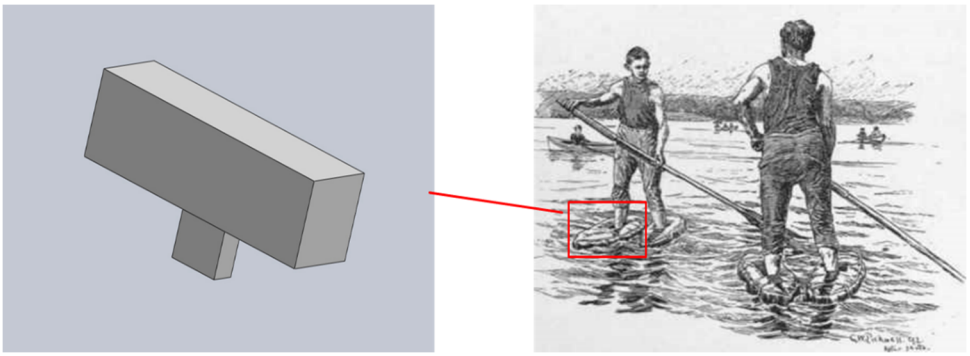

Figure 75. SSF for Walking on Water application

This modified form of SSF is designed considering a mass of 100 kilogram action on top of it at a distance of 1 meter from the center of rotation. The volume of water displaced by the given weight of the man can be calculated as

$$W_{man} = W_{buoyant} \Rightarrow M_{man} \times g = \rho_w \times g \times V_{dis} \qquad \text{(F.1)}$$

where W_{man} is the weight of the man, $W_{buoyant}$ is the weight of the displaced water, M_{man} is the mass of the man, g is the acceleration due to gravity, ρ_w is the density of water and

V_{dis} is the volume of water displaced. Considering the density of water to be 1000 kg/m^3 and by substituting the values we get

$$100 \times 9.81 = 1000 \times 9.81 \times V_{dis} \Rightarrow V_{dis} = 0.1m^3 \qquad \text{(F.2)}$$

So by trying to include this volume of water column inside the shoe, the structure resulted in a rectangular section SSF, as shown in Figure 75. A detailed view of the same, when it is heeled due to the walking action, is shown in Figure 76.

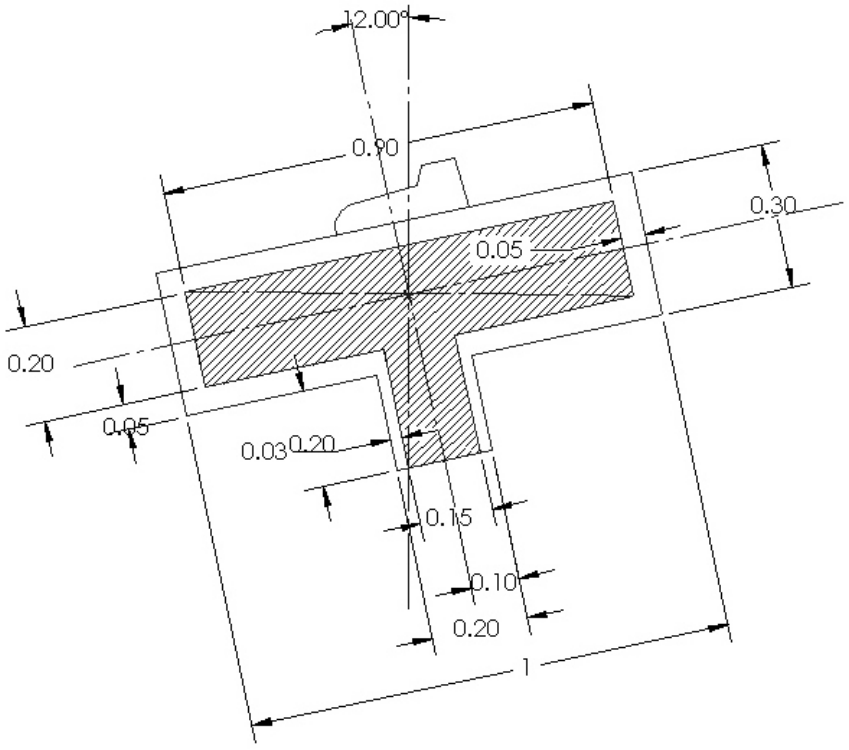

Figure 76. SSF Shoe when Heeled to one direction

The details of the dimension of the same are shown in Figure 77. The shoe is made of a rigid foam material of density of 0.006414 lbs/in^3. Different parameters are calculated, as in the case of oil and gas platforms in Appendix-E and shown in Table 1.

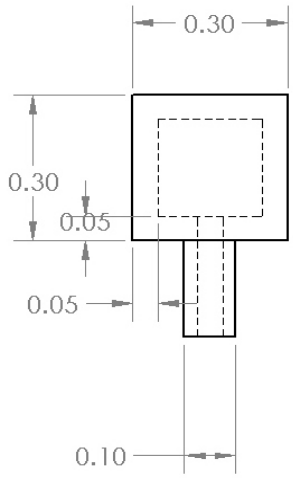

Figure 77. Side View of SSF Shoe

Parameter	Symbol	Value	Units
Mass of SSF body	M_{SSF}	9.96	kg
Mass of water inside SSF body	M_w	37.815	kg
Total mass of SSF unit	M_{total}	47.835	kg
Volume of water displaced due SSF and man	V_{Tdis}	0.147835	m^3
Area of SSF at water plane section	A_b	0.3	m^2
Draught level of SSF alone	T	0.403	m
Draught level of SSF with man on top	T_{total}	0.48	m

Table 4. Parameters Calculated for SSF Shoe

So the shoe can still float and function as a SSF unit with the man still standing on top of it, because the draught level is still within the size of the SSF unit. As discussed in Chapter-3, the wedge formation creates a moment in the opposite direction to the heeling moment due to the walking action. By considering the water plane to be at the mid-section of the height of the inner chamber of the shoe, the volume of the wedge section of the fluid due to the suction stabilization is given by

$$V_{wedge} = \frac{1}{2} \times \frac{b}{2} \times \frac{b}{2} \sin\phi \times l \tag{F.3}$$

Where b = 0.9 meters and l = 0.2 meters. The maximum heel angle is observed to be 12 degrees. The moment due to the wedge section about the center of rotation can be given as

$$M_{wedge} = V_{wedge} \times \rho_w \times g \times \frac{1}{2}\left(\frac{2b}{3}\right) \tag{F.4}$$

By substituting the values in Eq. (F.4), we get

$$M_{wedge} = 41.302\text{N-m} \tag{F.5}$$

At the same time the moment due to the weight of the human body can be calculated as

$$M_{man} = 100 \times 1 \times \tan\phi \times \text{g} = 208.51\text{N} - \text{m} \tag{F.6}$$

So the moment due to the human action is much greater than the righting moment provided by the IST effect in the shoe. In order to improve the performance of the shoe, other add-on techniques are required. The righting moment can be increased by adding a skirt around the shoe, which would limit the roll action, but there is limit to increase the skirt area. Another possible way to improve the performance is by providing air blower on both ends of the longitudinal section of the shoe. This can be activated in the opposite direction to the roll motion, which would provide additional thrust to the shoe in a direction opposite to the heeling. The idea of air blowers can be replaced by utilizing a ball screw mechanism on the top of the shoe, which would again act as an anti-roll ballast mass.